A THREE DIMENSIONAL HETEROGENEOUS COARSE MESH TRANSPORT METHOD FOR REACTOR CALCULATIONS

A Thesis
Presented to
The Academic Faculty

by

Benoit Forget

In Partial Fulfillment
of the Requirements for the Degree
Doctor of Philosophy in the
School of Mechanical Engineering

Georgia Institute of Technology
August 2006

A THREE DIMENSIONAL HETEROGENEOUS COARSE MESH TRANSPORT METHOD FOR REACTOR CALCULATIONS

Approved by:

Dr. Farzad Rahnema, Advisor
School of Mechanical Engineering
Georgia Institute of Technology

Dr. Weston M. Stacey
School of Mechanical Engineering
Georgia Institute of Technology

Dr. C.-K. Chris Wang
School of Mechanical Engineering
Georgia Institute of Technology

Dr. Thomas D. Morley
School of Mathematics
Georgia Institute of Technology

Dr. Jean Koclas
Department of Engineering Physics
École Polytechnique de Montréal

Date Approved: May 12th, 2006

ACKNOWLEDGEMENTS

I would like to gratefully acknowledge my advisor, Dr. Farzad Rahnema, for his invaluable help throughout the last three years at Georgia Tech. His passion and devotion for his work motivated me to always work harder and his support, guidance and friendship made me feel at home from the first day I started.

Sincere appreciation is also extended to Dr. Weston Stacey, Dr. Chris Wang, Dr. Tom Morley and Dr. Jean Koclas for their willingness to serve on my thesis committee and for their reviewing efforts. Special recognition goes to Dr. Scott Mosher whose work inspired this thesis and whose kindness made us friends. I am also extremely grateful to Dr. David Griesheimer for the valuable help offered with some important aspects of this thesis.

I would also like to thank my parents, Robert and Louise, and my brother, François, for their continuous support. Knowing how proud they were of me no matter what I did was always motivation enough for me to keep going. A great deal of gratitude also goes out to my friends Jean-François, David, Jean-Olivier, Karine, Marc, Jessica and my uncles Vianney and Robert for their frequent visits and for making me realize that I wasn't forgotten.

Many thanks to all the great friends I've made here in Atlanta starting with my girlfriend, Erin, who's made this whole experience worth it. Many thanks also to my fellow Canadians living abroad, to my roommate Zach, my golfing buddy Chris and all the rest of you that I have made my stay so enjoyable.

Special thanks also go out to everyone that I had the pleasure to work or interact with at the Neely Nuclear Research Center and to all the staff of the Mechanical engineering department.

Finally, I would like to gratefully acknowledge the support of the Department of Energy's Nuclear Engineering Research Initiative and Nuclear Engineering Education Research programs. I would also like to extend gratitude to the Natural Science and Engineering Research Council of Canada and to the George W.Woodruff school of Mechanical Engineering for their financial support.

TABLE OF CONTENTS

LIST OF TABLES

LIST OF FIGURES

SUMMARY

Current advancements in nuclear reactor core design are pushing reactor cores towards greater heterogeneity in an attempt to make nuclear power more sustainable in terms of fuel utilization and long-term disposal needs. These new designs are now being limited by the accuracy of the core simulators/methods. Increasing attention has been given to full core transport as the flux module in future core simulators. However, the current transport methods, due to their significant memory and computational time requirements, are not practical for whole core calculations. While most researchers are working on developing new acceleration and phase space parallelization techniques for the current fine mesh transport methods, this dissertation focuses on the development of a practical heterogeneous coarse mesh transport method.

In this thesis, a heterogeneous coarse mesh transport method is extended from two to three dimensions in Cartesian geometry and new techniques are developed to improve the computational efficiency. The high efficiency is achieved by decoupling the problem into a series of fixed source calculations in smaller sub-volume elements (*e.g.* coarse meshes). This decoupling leads to shifting the computation time to *a priori* calculations of response functions in unique sub-volumes in the system. Therefore, the method is well suited for large problems with repeated geometry such as those found in nuclear reactor cores. Response functions can be generated with any suitable 3-D fine-mesh (deterministic or stochastic) code. A stochastic method is selected in this dissertation due to its high fidelity, continuous energy and arbitrary geometry capabilities. Previous work in two dimensions used discrete polynomial expansions that are well suited for treating discrete variables used in pure deterministic transport methods. We use continuous Legendre polynomial expansions since stochastic methods treat the phase space variables continuously.

The coarse mesh method was initially implemented in two dimensions and tested on benchmark problems of varying size and type. In all cases, low order surface current expansions were sufficient to obtain accurate core eigenvalue and pin power distribution results. The three dimension implementation was tested on the C5G7 MOX benchmark problem. Once again, the results proved to be very accurate with low order expansions.

CHAPTER 1

INTRODUCTION

1.1 Overview and Motivations

The calculation of the neutron flux or fission density distribution in a large heterogeneous eigenvalue problem has been traditionally accomplished using low-order methods, such as diffusion theory, that treat large-scale systems composed of homogeneous coarse-meshes (Lawrence, 1986). In reactor applications, a coarse-mesh typically corresponds to a single fuel assembly that is characterized by homogeneous cross-sections and flux discontinuity factors (Smith, 1986). The homogenized parameters are generated from a high-order fine-mesh calculation of the heterogeneous assembly. In large part, the accuracy of this approach is limited by the extent to which the boundary condition used in the fine-mesh calculation (typically full specular reflection) accurately represents the true relationship between the fluxes entering and exiting the coarse-mesh in the global system.

The motivation for the two-phase approach just described is to avoid the computational expense of generating global fine-mesh solutions. The ever-increasing processing speed and memory capacity of computers have motivated the development of many high-order methods aimed at tackling large transport problems. A great deal of research has been dedicated to developing techniques for accelerating existing fine-mesh methods, as well as schemes that take advantage of parallel processing systems. Much less attention has been dedicated to developing high-order coarse-mesh methods that avoid homogenization. Such methods have the potential of offering an accurate means for solving large heterogeneous problems without consuming the vast computational resources required to generate fine-mesh solutions.

Several transport methods have been developed in which an individual coarse-mesh is characterized by a set of response functions (Villarino and Stamm'ler, 1984; Rathkopf and Martin, 1986; Moriwaki *et al.*, 1999; Ilas and Rahnema, 2003). The response functions are computed as fine-mesh solutions to fixed source problems with in-volume sources and/or incident flux boundary conditions. An estimate of the global flux distribution is constructed from a linear superposition of the individual responses. In this way, the approximations associated with homogenization schemes are avoided. These methods have been shown to provide extremely accurate results for highly-heterogeneous 1-D problems.

The major obstacle to extending these methods to higher-dimensional geometries is the sheer number of response functions required to characterize a coarse-mesh in such problems. Recently, Mosher and Rahnema (2005) generalized the response expansion of Ilas and Rahnema (2003) to facilitate a practical extension of the method to 2-D. This new method admits a broad class of functions that are responses to an orthogonal set of incident flux boundary conditions. Certain sets of functions are extremely efficient in that they allow the response expansion to be truncated at a low order while maintaining an accurate characterization of the integrated response, which vastly increases computational efficiency. This represents a significant step toward developing an accurate and efficient coarse-mesh method for higher-dimensional problems. The extension of the coarse mesh transport method to 3-D is a necessity for whole core reactor calculations.

1.2 Literature Review

The literature review is divided into three main sections. The first section reviews the current state-of-the-art method used in reactor calculations. The second section reviews methods relevant to the coarse mesh transport method, while the third section deals with the available benchmark problems found in the literature.

1.2.1 Nodal Diffusion Method/GET

The nodal diffusion method is the current state-of-the-art methodology for whole core three dimensional calculations (Lawrence, 1986). This method is essentially a two-step approach: 1) single bundle infinite lattice transport calculations, followed by, 2) whole core three dimensional nodal diffusion calculations. The single bundle calculations are used to compute few energy group node homogenized parameters for use in the nodal diffusion calculations.

1.2.1.1 Generalized Equivalence Theory

The accuracy of the nodal diffusion method relies heavily on the homogenization techniques used. The most advance method is called the generalized equivalence theory (GET) that goes beyond simple spatial homogenization based on reaction rates preservation as shown in the following equation.

$$\hat{\Sigma}_{\alpha g} = \frac{\int_{V_i} \Sigma_{\alpha g}(r)\Phi_g(r)}{\int_{V_i} \hat{\Phi}_g(r)} \tag{1.1}$$

where $\Sigma_{\alpha g}$ is the macroscopic cross-section of reaction type α within energy group g, Φ_g is the neutron flux in group g and the symbol "^" indicates that the parameters are homogenized. The GET also introduces additional homogenization parameters called "discontinuity factors" (Smith, 1986) defined by

$$f_g^{kl} = \frac{\Phi_g^{kl}}{\hat{\Phi}_g^{kl}} \tag{1.2}$$

This expression allows the heterogeneous flux to be continuous across a node interface, denoted by the superscript *kl*, by letting the homogenous flux be discontinuous. The addition of discontinuity factors has the added benefit of preserving the nodal leakage rates.

1.2.1.2 Nodal Diffusion Method

In the nodal diffusion method, the reactor is subdivided in non-overlapping nodes that usually correspond to fuel assemblies for which it is assumed that homogenized parameters defined in the previous section are known. The diffusion equations are then integrated over each node and the transverse integration procedure is used to compute the surface currents of the node in each direction. This procedure reduces the three dimensional equation to three one dimensional equations by integrating the three dimensional equation in each of the two transverse directions. The one-dimensional nodal fluxes are then approximated by polynomials or obtained analytically with different assumed shapes of the transverse leakages. The equations are then solved iteratively and the multidimensional flux solution is constructed from the one-dimensional solutions.

1.2.1.3 Accuracy

Smith (1980) as shown that using GET in nodal diffusion calculations reproduces exactly node average reaction rates, node leakage rate and system eigenvalue when using the reference lattice cell solution to evaluate his homogenized parameters and discontinuity factors. However, when performing a core calculation, the reference solution is certainly not known *a priori*. The parameters of equations (1.1) and (1.2) are approximated from the single bundle infinite lattice calculation. By using the infinite lattice fluxes, the parameters lose the effect produced by neighboring nodes of different composition making the nodal diffusion method unsuitable for very heterogeneous problems.

1.2.1.4 Pin Power Reconstruction

In reactor calculations, predicting the power of each individual pin is most often desired. The difficulty with the nodal diffusion method is that the solution provides only nodal averaged fluxes and reaction rates. Reconstruction techniques must be used to

relate the node averaged solution to the heterogeneities of the true problem. The simplest technique is to compute form factors from the single bundle infinite lattice calculations that modulate the smooth nodal flux shape to the heterogeneous assembly flux shape. This method is quite inaccurate for heterogeneous cores. An alternative is to perform single bundle calculations using boundary conditions obtained from the nodal solution and compute the form factors. This approach is quite accurate but becomes quite expensive when pin powers for many assemblies are sought. A less expensive approach of flux reconstruction is to match assembly flux shapes to polynomial flux shapes whose coefficients are determined by forcing conservation of node averaged, surface averaged and corner point fluxes obtained from the nodal solution.

1.2.2 Nodal Transport Methods

This section reviews methods considered similar to the heterogeneous coarse mesh transport method, mainly the interface current method and the response matrix method. These two methods were explored in the early 1970's (Leonard, 1975) for lattice calculations but eventually gave way to fine-mesh deterministic methods as computer power became more accessible. Both methods used the spatially flat cosine current approximation extensively.

1.2.1.1 Interface Current Method

In the interface current method, the domain is divided into a number of cells. A simplified model is then used to describe the transfer between these cells, the most common one being the cosine current approximation. The solution within a single sub-region can be computed with any method, such as discrete-ordinates, Monte Carlo or spherical harmonics (Leonard, 1975), it is however more common to derive this method in terms of the collision probability method (Sanchez and McCormick, 1982).

1.2.1.1.1 Theory

For a system comprised of *N* regions within which the flux is assumed constant, the multigroup integral transport equation, as done by Pryor and Graves (1973), can be written as:

$$V_n \sigma_{tr,n}^g \phi^g(n) = \sum_{n'=1}^{N} P_{VV}^g(n,n') S^g(n') \tag{1.3}$$

where V_n is the volume of region *n*, *g* is the energy group indicator, $\sigma_{tr,n}^g$ is the macroscopic transport cross-section of region *n*, $\phi^g(n)$ is the average neutron flux in region *m*, $P_{VV}^g(n,n')$ is the neutron first flight collision probability from region *n'* to region *n* and $S^g(n')$ is the neutron source in region *n* given by:

$$S^g(n') = V_{n'} \sum_{g'} \left(\sigma_{s,g'\to g} + \frac{\chi_{g'\to g}}{k} \upsilon \sigma_{f,g'} \right) \phi^{g'}(n') + S_{n'}^g \tag{1.4}$$

In the above equation, σ_s is the scattering cross-section, χ is the fission energy spectrum, υ is the mean number of fission neutrons produced and σ_f is the fission cross-section. The external source in region *n'* is represented by $S_{n'}^g$. The parameter *k* represents the multiplication factor of the system and is 1 in the presence of an external source.

The interface current method divides the domain into a collection of contiguous cells. The domain is thus divided into *M* coarse meshes each composed of R_m regions. The R_m regions of all *M* meshes correspond to the *N* regions of the large problem, which is shown by the following equivalence.

$$V = \sum_{n=1}^{N} V_n = \sum_{m=1}^{M} V_m = \sum_{m=1}^{M} \sum_{r=1}^{R_m} V_{m,r} \tag{1.5}$$

By assuming a phase space shape for the currents entering mesh *m*, such as the flat cosine-current approximation, the coupling in equation (1.3) can then be reduced to:

$$V_{m,r} \sigma_{tr,m,r}^g \phi_m^g(r) = \sum_{r'=1}^{R_m} P_{VV}^g(r,r') S_m^g(r') + \sum_{s\in\partial m} P_{VS}^g(r,s) J_{IN,m}^g(s) \tag{1.6}$$

where $V_{m,r}$ is the volume of region *r* in mesh *m*, $P_{VS}(r,s)$ is the neutron first flight collision probability from face *s* to region *r*, where the sum is over all surfaces (∂m) of mesh *m* and $J_{IN,m}(s)$ is the current entering mesh *m* from surface *s*. An expression for evaluating the outgoing current, $J_{OUT,m}(s)$, from mesh *m* can also be written.

$$J^g_{OUT,m}(s) = \sum_{r'=1}^{R_m} P^g_{SV}(s,r') S^g_m(r') + \sum_{s' \in \partial m} P^g_{SS}(s,s') J^g_{IN,m}(s') \tag{1.7}$$

where $P_{SV}(s,r')$ is the probability that a neutron originating in region *r'* will pass through surface *s* without making a collision and $P_{SS}(s,s')$ is the probability that a neutron entering through surface *s'* will exit mesh *m* through surface *s* without having made a collision.

Once all first-flight collision probabilities are computed, the large system can be solved by a straightforward mesh-by-mesh iterative procedure over the scalar fluxes and interface currents. In the case the system is critical (no external source), the eigenvalue (*k*) that appears in equation (1.4) can be solved by factoring out *k* from the solution of these equations.

$$\phi^g(n) = \phi^g_0(n) + \frac{1}{k}\phi^g_1(n) + \frac{1}{k^2}\phi^g_2(n) + \ldots \tag{1.8}$$

and

$$J^g_{OUT}(s) = J^g_{OUT,0}(s) + \frac{1}{k}J^g_{OUT,1}(s) + \frac{1}{k^2}J^g_{OUT,2}(s) + \ldots \tag{1.9}$$

where ϕ^g_i and $J^g_{OUT,i}$ are the flux and currents for the ith neutron generation, respectively. The 0th generation flux and current are the solution to equations (1.6) and (1.7) with no fission sources, while all other generations are the solution to the same equations with a fission source but with no incoming current.

1.2.1.2 Response Matrix Method

In the response matrix method (Leonard, 1975; Lewis and Miller, 1993), the system that needs to be solved is also divided into a number of local subunits. Very similarly, each of these subunits is solved locally by a transport or diffusion method to obtain the response of outgoing neutron current to any given input. The unknowns are thus the interface currents of each subunit. Once these are known, any other quantity of interest may be evaluated within each subunit (e.g. reaction rates). The response matrix equations can be obtained from the interface current derivation previously described. To facilitate this demonstration, the interface current equations are rewritten in matrix form.

$$V\Sigma_{tr}\Phi = P_{VV}F + P_{VS}J_{IN} \tag{1.10}$$

and

$$J_{OUT} = P_{SV}F + P_{SS}J_{IN} \tag{1.11}$$

with

$$F = V\Sigma_s\Phi + \frac{V\Sigma_f\Phi}{k} + S \tag{1.12}$$

where Φ and $J_{IN/OUT}$ are the flux and current vectors for all meshes and energy group, respectively, V is the volume matrix, Σ_{tr} is the transport cross-section matrix, Σ_s is the scattering matrix, Σ_f is the fission matrix that includes the mean number of neutrons produced by fission and the energy spectrum of the fission neutrons, P_{VV} is the volume to volume first flight collision probability matrix, P_{VS} is the volume to surface without collision probability matrix, P_{SS} is the surface to surface without collision probability matrix, P_{SV} is the surface to volume first flight collision probability matrix and k is the system multiplication factor. Once again, it should be noted that the parameter k of equation (1.12) only appears when solving a critical system, implying that the source

vector S is set to zero. The source term, F, of equation (1.12) is replaced in equation (1.10), then the flux, Φ, is solved for in the ensuing equation.

$$\Phi = \left(V\Sigma_{tr} - P_{VV}V\Sigma_s - \frac{P_{VV}V\Sigma_f}{k} \right)^{-1} \cdot P_{VS}J_{IN} + \left(V\Sigma_T - P_{VV}V\Sigma_s - \frac{P_{VV}V\Sigma_f}{k} \right)^{-1} \cdot P_{VV}S \tag{1.13}$$

The term for the flux is then used in equation (1.11) to obtain the common response matrix equation.

$$J_{OUT} = R(k)J_{IN} + \widetilde{S} \tag{1.14}$$

where R is the response matrix corresponding to

$$R(k) = P_{SS} + P_{SV}V\left(\Sigma_s + \frac{\Sigma_f}{k} \right) \cdot \left(V\Sigma_{tr} - P_{VV}V\left(\Sigma_s + \frac{\Sigma_f}{k} \right) \right)^{-1} \cdot P_{VS} \tag{1.15}$$

The external source is expressed as

$$\widetilde{S} = P_{SV}V\left(\Sigma_s + \Sigma_f \right) \cdot \left(V\Sigma_{tr} - P_{VV}V\left(\Sigma_s + \frac{\Sigma_f}{k} \right) \right)^{-1} \cdot P_{VV}S \tag{1.16}$$

To solve this system in its matrix form, another relation is introduced that connects the currents leaving one mesh to the currents entering the neighboring mesh. This relation is expressed in terms of the connectivity matrix C that also includes the system boundary conditions.

$$J_{IN} = CJ_{OUT} \tag{1.17}$$

1.2.1.2.1 Criticality Calculation

Replacing this relation in equation (1.14), for a critical system ($S = 0$), yields an eigenvalue equation

$$J_{OUT} = \lambda R(k)CJ_{OUT} \tag{1.18}$$

where λ is known as the current eigenvalue (Pryor and Graves, 1973). This system can be solved by using standard numerical methods. The matrix *R(k)* is computed for a certain value of *k*, the system multiplication factor, which is adjusted until the current eigenvalue is equal to unity (Pryor and Graves, 1973). As done in the interface current method, the multiplication factor *k* can be factored out of the response matrix.

$$R(k) = R_0 + \frac{1}{k} R_1 + \frac{1}{k^2} R_2 + \ldots \tag{1.19}$$

where the matrices R_i are independent of the parameter *k* and can thus be precomputed for each unique mesh.

1.2.1.2.2 External Source

Replacing equation (1.17) in equation (1.14), with an external source ($S \neq 0$ and $k = 1$), the following relation is obtained:

$$J_{OUT} = RCJ_{OUT} + \widetilde{S} \tag{1.20}$$

or

$$J_{OUT} = (I - RC)^{-1} \cdot \widetilde{S} \tag{1.21}$$

where *I* is the identity matrix. This equation system can be solved by direct Gauss elimination if the system is fairly small or iteratively for larger problems.

1.2.1.3 Cosine Current Approximation

This approximation is based on the assumption that the flux is isotropic in the two angular half spaces at each region interface (Mohanakrishnan, 1981). The cosine current approximation has proven to work quite well for heavy water reactors (Honeck, 1971; Forget *et al*, 2004b) as well as for tightly coupled light water reactors (Leonard *et al*, 1971; Forget *et al*, 2004a; Forget *et al*, 2004c). However, this optimistic representation of the interface currents can become quite inaccurate in some circumstances, especially in two or three dimensions. Leonard (1975) illustrated this setback of the cosine current

approximation by assuming a system of constant mesh size a in which very few scattering events occur, $\Sigma_s a << 1$, as represented in Figure 1.1.

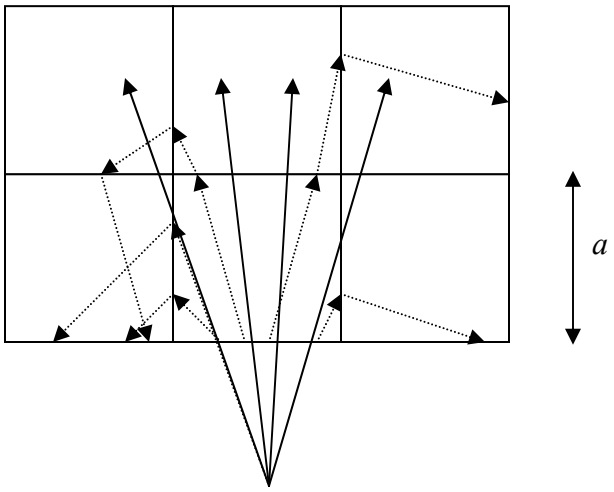

Figure 1.1: Reflection of Cosine-Current Approximation

For illustration purposes, neutrons produced from the source point are entering the boundary only on the south face of the middle mesh. The actual neutron flight paths are illustrated by the solid lines, while the cosine redistributed flight paths are represented by the dashed lines. In the true flight path, a negligible fraction of neutrons will be reflected through the originating boundary, however, with the cosine current approximation, too many neutrons are reflected and not nearly enough are transmitted. If the mesh size goes to zero, the cosine current approximation makes the neutrons isotropically reflected at their entry point regardless of the material properties or the entering angular distribution. The neutrons are thus refracted when one uses the cosine current approximation.

The errors due to cosine current approximation can thus be reduced over all energy groups by using a mesh size as large as fast neutron mean free path. However, another very common approximation is to assume that the spatial distribution of the interface current is uniformly distributed (spatially flat). This approximation requires

meshes as small as the thermal neutron mean free path. Obviously, these conflicting requirements cannot be met. As an alternative, higher order angular or spatial modes must be considered.

1.2.1.4 Higher Order Modes

Anderson and Honeck (1973) developed an interface-current technique in two-dimension that expanded the angular component of the half-space angular fluxes in a P_N series (Legendre polynomial expansion). This gave a more accurate representation of the interface currents as compared to the cosine current approximation. This method is still limited by the flat-current approximation and couples only homogeneous regions but shows improvement in the angular treatment.

Mueller and Wagner (1972) developed a three-dimensional interface current method that expanded the collision probabilities along the spatial variables in a P_N series. In this method, the expansion is limited to first order and the P_1 component is chosen proportional to the gradient of the source in the direction of travel of the neutrons. This ratio is approximated by the ratios of in and out-currents at opposite sides of the cell. This method showed great improvement over diffusion theory but still uses cosine-current distribution, which limits the accuracy of the angular component. This method considered (coupled) homogeneous regions only.

Griesheimer and Martin (2003) developed a Monte Carlo based angular flux response function method that discarded the use of cosine-current approximation in favor of a double Legendre polynomial expansion of the cosine of the polar angle. The 1-D results accurately predicted the magnitude and angular distribution of the neutron current at the interfaces. The method however was not used or extended for solving the transport equation in a reactor core.

1.2.1.5 Additional Literature Review

This section covers additional methods closely related to the heterogeneous coarse mesh transport method. The last sub-section dealing with the variational heterogeneous coarse mesh transport method is reviewed in greater detail because it is the basis for the work developed in this thesis.

1.2.1.5.1 Use of Monte Carlo in Response Matrix Method

Pryor and Graves (1973) proposed a homogeneous response matrix method for treating 2-D reactor configurations. Their method was based on integral transport methods through the use of collision probabilities which required a great deal of region subdivision to obtain accurate results. More subdivision invariably meant more computational time. To overcome this they performed a Monte Carlo calculation for the 0^{th} generation of neutrons (neutrons that do not come from fission) in each homogeneous node and combined it with the collision probability calculations for the neutrons born from fission. This method showed good computational efficiency and accuracy, but it is once again limited by the cosine-current angular distribution and also by the flat flux approximation along each segment.

McDaniel (1975) also derived a two-dimensional response matrix method that used Monte Carlo calculations. A Monte Carlo code was used to compute the water response matrix. Six different types of responses were computed using a Monte Carlo process: reflection, side transmission, transmission, rod return, water escape and rod capture. The rest of the system response matrices were computed from the collision probability method. This method also showed great promise but is also limited by the same constraint as the previous ones: cosine-current and flat-current approximation. The method was also based on homogeneous nodes, which greatly limits its application and practicability in reactor calculations. Most of these methods were developed for solving lattice (fuel assembly) problems.

Moriwaki, Ishii, Maruyama and Aoyama (1999) developed a direct method of calculating response matrices using a Monte Carlo technique. The response matrix is decomposed in sub-matrices representing the transmission probability, the neighbor-induced production probability, the self-induced production probability and the escape probability. Reasonable accuracy was achieved for simplified 2-D BWR benchmarks, but the use of flat-flux approximation and cosine-current distribution limits the practicality of this method to more realistic problems.

1.2.1.5.2 Heterogeneous Response Matrix Methods

Villarino and Stamm'ler (1984) developed a 1-D heterogeneous coarse mesh method based on the interface current method, which they referred to as the Heterogeneous Response Method (HRM). Each cell's response was computed from collision probabilities and was coupled with neighboring cells through the cosine-current approximation. The 1-D results were very promising.

Rathkopf and Martin (1986) developed a finite element response matrix method for the solution of the neutron transport equation. This method computes response matrices for a heterogeneous coarse mesh by means of the finite element method in both space and angle. The one dimensional results were very promising and found to be more efficient than the conventional finite element method. Better efficiency was said to be obtained for the two-dimensional extension. No results were found in the literature.

1.2.1.5.3 Asymptotic Methods

Zhang *et al*. (1995 and 1997) developed a multiple-scale asymptotic expansion method which, starting from either the diffusion or transport equation, results in a systematic homogenization theory and a self-consistent local flux reconstruction procedure. The two spatial scales employed are similar to those previously used by Larsen (1975 and 1976) in a multi-scale approach for heterogeneous media comprised of

exactly periodic pin cells. The method developed by Zhang *et al*. (1997) is based on the assumption that the core is an array of near-periodic fuel assemblies. Results presented by Zhang *et al.* show significant improvement over generalized equivalence theory, which is the current state-of-the-art homogenization technique for core calculations. Despite the encouraging results, there are two significant drawbacks to the multi-scale method as described by the authors. First, the authors state that the iterative solution procedure will diverge without very tight convergence criteria (10^{-10} to 10^{-12}) for the forward and adjoint eigenvalue and auxiliary fixed source calculations. Second, the method is currently restricted to the one-group approximation, which is not sufficient for modern reactor calculations. The authors (Zhang *et al.*, 1995 and 1997) believe that it is possible to extend their method to multigroup equations by building on the ideas presented by Pomraning (1990).

1.2.1.5.4 Subelement Variational Nodal Method

Palmiotti *et al* (1995) developed a code called VARIANT that solved the multigroup even-parity transport equation using a variational nodal method. The original method solved large systems using transport theory over homogenized nodes that are coupled together by odd-parity Lagrange multipliers. Despite the use of high-order angular approximations, doubt remained in the accuracy of the results caused by the homogenization procedures and the subsequent dehomogenization needed to reconstruct fuel pin powers. Smith *et al* (2003) proposed the subelement variational nodal method that permits the coupling of heterogeneous nodes in two-dimensions. The nodes of the test problems consisted of a single fuel pin cell with no fuel-coolant homogenization. Possibilities of using larger nodes (e.g. several pin cells) are mentioned as a way of achieving large gains in computational efficiency by building the response matrix on parallel computers. It was also concluded that very high order spherical harmonic approximations were required to obtain accurate eigenvalue and pin power solutions.

1.2.1.5.5 Heterogenenous Coarse Mesh Transport

A variational heterogeneous coarse-mesh transport method (Ilas, 2001; Ilas and Rahnema, 2003) was previously developed and implemented for one-dimensional discrete ordinates problems. The method is based on a coarse-mesh response formulation in which the fission source distribution is treated implicitly. This is accomplished by considering a fission term in the fixed source equations used to calculate response functions. Consequently, only responses to incident fluxes are required. This leads to a significant improvement in overall efficiency over similar methods that require both incident flux and in-volume source responses. In addition, this formulation makes no approximation regarding the shape of the fission source distribution, which is necessary with methods that employ in-volume responses.

As part of a NERI project (Rahnema, 2002), the 1-D method was extended to two-dimensional Cartesian geometry by Mosher and Rahnema (Mosher and Rahnema, 2003; Mosher, 2004; Mosher and Rahnema, 2005). A broad class of functions were identified that can be used to characterize the response of a coarse-mesh to an arbitrary incident flux distribution. For example, the surface Green's functions that were employed in the original 1-D method are a special case of the general class. By truncating the response expansion at a low order, the scope of the pre-computations (*i.e.*, response function calculations) is greatly reduced. However, not all sets of response functions will lead to highly accurate coarse-mesh calculations with low order truncation.

This new coarse-mesh method was implemented in 1-D and 2-D geometry using a finite-difference, multigroup, discrete ordinates response function generator. An efficient set of response functions was generated using orthogonal boundary conditions constructed from the Discrete Legendre Polynomials (Neuman, 1974; Mosher, 2004; Mosher and Rahnema, 2003). Several simplified one and two-dimensional heterogeneous light water reactor benchmark problems were studied. Relatively low-order response expansions were used to generate highly accurate results using both the variational and

non-variational methods. However, the variational technique requires adjoint response functions which double the pre-computational effort. The expansion order was found to have a far more significant impact on the accuracy of the results than the type of method. The variational techniques provide better accuracy, but at substantially higher computational costs. It was also found that the flexibility and accuracy of the coarse mesh method were highly dependant on the fine mesh method used to generate the response functions and on the choice of orthogonal boundary condition.

1.2.3 Benchmark review

This section covers the most relevant and available benchmark problems in 2-D and 3-D commonly used to assess code performance in nuclear reactor analysis. Only the first benchmark is described thoroughly because it is the only one considered to be a reasonable test for the heterogeneous coarse mesh transport method. The others are presented mainly as a review of existing problems and to emphasize the need for more complex test cases.

1.2.3.1 2D/3D MOX Fuel Assembly Benchmark

This is a very recent benchmark problem sponsored by the OECD/NEA Expert Group on 3-D Radiation Transport Benchmarks. The emphasis of this problem is on transport calculations without spatial homogenization. It offers a 2-D and 3-D problem (Lewis, 2003). The 3-D problem is extended to include configurations with inserted control rods (Lewis, 2005). The benchmark problem is composed of four PWR fuel assemblies (2 sets of two identical fuel assemblies) each with 264 fuels pins, 24 guide tubes (or control rods) and one fission chamber explicitly represented. The two uranium oxide (UO_2) assemblies have only one type of fuel and the mixed oxide (MOX) assembly is composed of fuel rods with three different enrichments. A seven group cross-section library is given for each material. In the 2-D configuration, presented in Figure 1.2, each

fuel assembly measures 21.42 cm per side. Specular reflective boundary conditions are used on the left and top boundaries. A vacuum boundary condition is assumed on the other external boundaries. The fuel pin pitch is 1.26 cm and the radius of the fuel pin is 0.54 cm. In Figure 1.2, the upper left and lower right fuel assemblies are UO_2 and the other two are MOX.

In the 3-D configurations, the fuel assemblies are surrounded on three sides by a reflector region with vacuum boundary conditions, while the other three sides have specular reflective boundary conditions. In the original 3-D case, as shown in Figure 1.3, the height of the core including the water reflector is 192.78 cm. Figure 1.3 is a simplified illustration of the benchmark. The fuel assemblies of the 3-D case are identical as the ones shown in Figure 1.2.

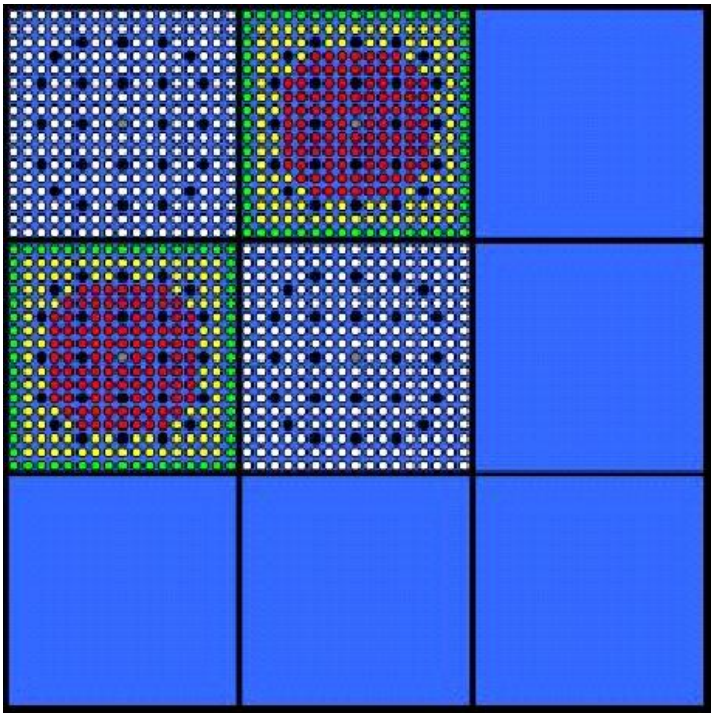

Figure 1.2: 2-D C5G7 MOX Benchmark

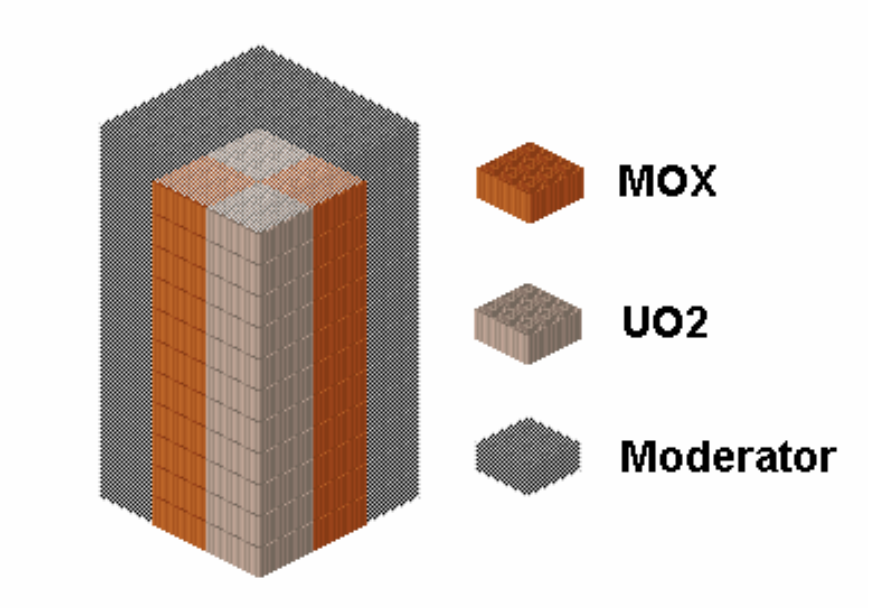

Figure 1.3: 3-D C5G7 MOX Benchmark

In the extended 3-D cases, the height of the geometry is reduced to 64.26 cm to reduce the memory requirements and computational times needed to solve the benchmark. The presence of control rods is also added as an additional element of complexity for the problems. In the first configuration, named *Unrodded*, control rod clusters (composed of 24 control rods) are inserted in the water reflector above the fuel assemblies as indicated by Figure 1.4.

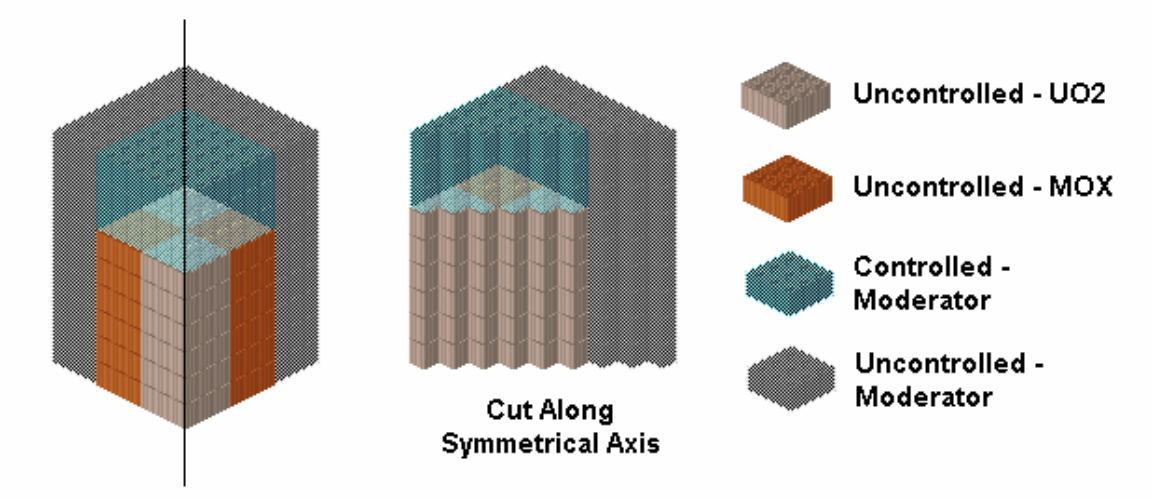

Figure 1.4: *Unrodded* Configuration of the 3-D Extended Case C5G7 Benchmark

In the second configuration, named *Rodded A*, a control rod cluster is inserted 1/3 of the way into the corner UO_2 fuel assembly as illustrated in Figure 1.5.

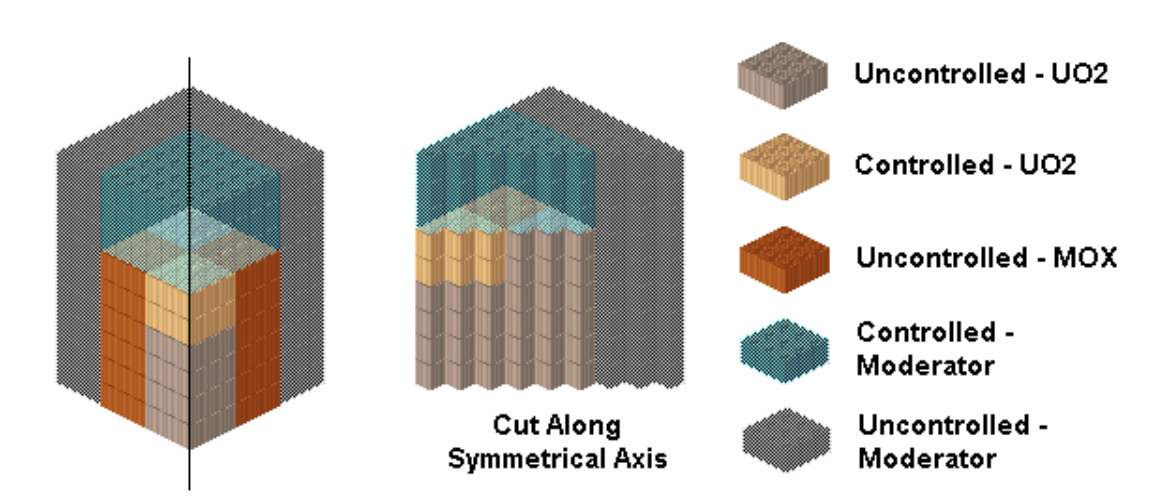

Figure 1.5: *Rodded A* Configuration of the 3-D Extended Case C5G7 Benchmark

The last configuration, *Rodded B*, offers even more complexity. One control rod cluster is inserted 2/3 of the way in the corner UO_2 assembly and control rod clusters are inserted 1/3 of the way in both MOX fuel assemblies as shown in Figure 1.6.

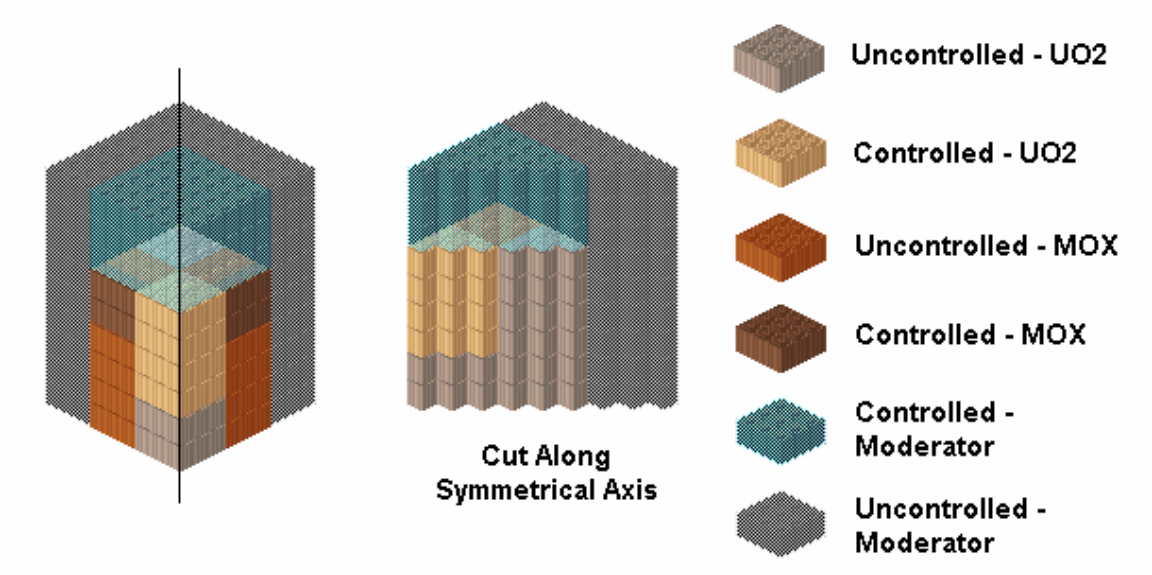

Figure 1.6: *Rodded B* Configuration of the 3-D Extended Case C5G7 Benchmark

1.2.3.2 The Henry-Worley Benchmark Problem

The Henry-Worley benchmark problem (Smith, 1980) is an idealized 2-D BWR representation of 25 fuel assemblies of 8 cm widths with an 8 cm reflector region surrounding the core. The fuel pins are modeled as being homogenous within the pin cell. The only strong heterogeneity in the problem is the presence of the control blades.

1.2.3.3 The CISE BWR Benchmark Problem

The CISE 2-D benchmark problem (Smith, 1980) is also an idealized version of a BWR but presents a little more heterogeneity, representative of an actual BWR, than the previous benchmark. It consists of 208 fuel assemblies of 15 cm widths surrounded by a

15 cm water reflector. The fuel pins are once again homogenized within the fuel cell but all control blades and water gaps are treated explicitly.

1.2.3.4 The HAFAS BWR Benchmark Problem

The HAFAS problem (Smith, 1980) presents most of the heterogeneities present in an actual BWR reactor. It consists of 308 fuel assemblies of 15.31 cm widths surrounded by a 15.31 cm water reflector. The fuel pins are presented explicitly and the fuel enrichment is also modeled. The presence of 16 control blades and assemblies with different void conditions (0%, 40%, 70%) also add to the complexity of this problem.

1.2.3.5 Other benchmarks

There exists other two-dimensional and three dimensional benchmarks for evaluating transport theory models such as the 2D/3D IAEA benchmark problem (Misfeldt, 1975) or the 3D Neutron Transport benchmark problem (Takeda and Ikeda, 1991). However these benchmarks do not offer a great deal of complexity and are not useful for evaluating a whole core transport method.

1.3 Objectives

The goal of this thesis is to develop an efficient three-dimensional whole core neutronics method/tool which is based solely on transport theory, does not de-couple the transport phenomena between coarse meshes (e.g., assemblies), does not rely on homogenization or discontinuity factors, contains an accurate self-contained flux reconstruction procedure and does not restrict the size of the coarse meshes. This method will thus eliminate the errors associated with spatial homogenization and diffusion theory. The new method must be a flexible tool for a variety of reactor designs and spectra. It must also be substantially faster than fine mesh transport method. Another goal of this thesis is to develop new and realistic numerical benchmark problems for evaluating transport methods.

1.4 Organization

The coarse mesh transport method is developed in Chapter 2. This includes the description of (1) a general formulation for treating eigenvalue and external source problems simultaneously (2) the main approximations made in solving the transport equation and (3) the concept of a response function. Two different techniques for evaluating the eigenvalue are also presented. Chapter 3 describes a special case of the method in which the response functions are generated from Monte Carlo calculations. All the aspects related to choosing Monte Carlo methods (*e.g.* sampling, uncertainties, tallying …) are explained in this chapter. Segmentation and spectral mapping are introduced as ways of enhancing the phase space approximation. The computer code COMET (Coarse Mesh Transport) that was developed for this research is also briefly presented. Even thought the main objective is to perform three dimensional transport calculations, a great deal of work was initially performed in two dimensions to fully develop the method. Chapter 4 contains two-dimensional results obtained in a variety of benchmark problems based on different reactor types (*e.g.* PWR, BWR and CANDU). In Chapter 5, the three dimensional results are presented, while Chapter 6 offers concluding remarks and recommendations for future work. Detailed information related to Chapters 4 and 5 are found in Appendices A and B. These include the description of the benchmark problems, cross-sections (or atom densities), if available, and additional results.

CHAPTER 2

METHODOLOGY

In this section, a general method for solving large heterogeneous problems is described. The general ideas of this method for eigenvalue calculations were previously introduced by Mosher and Rahnema (2005). The following is a more general description allowing both source and eigenvalue problems to be solved. It also offers a new eigenvalue evaluation technique and introduces the node coupling through partial angular currents.

2.1 Domain Decomposition

The decomposition starts by assuming a large heterogeneous system of volume V for which the angular flux distribution of neutral particles is sought. This can be obtained by solving the transport equation expressed here in its general form.

$$\begin{aligned}\hat{\Omega}.\nabla\psi\left(\vec{r},\hat{\Omega},E\right)+\sigma_t\left(\vec{r},E\right)\psi\left(\vec{r},\hat{\Omega},E\right)-\int_0^\infty dE'\int_{4\pi}d\Omega'\,\sigma_s\left(\vec{r},\hat{\Omega}',E'\to\hat{\Omega},E\right)\psi\left(\vec{r},\hat{\Omega}',E'\right)\\ =\frac{1}{4\pi}\chi\left(\vec{r},E\right)\int_0^\infty dE\int_{4\pi}d\Omega\,\frac{\nu\sigma_f\left(\vec{r},E'\right)}{k}\psi\left(\vec{r},\hat{\Omega}',E'\right)+Q\left(\vec{r},\hat{\Omega},E\right)\end{aligned} \tag{2.1}$$

with an arbitrary boundary condition

$$\psi\left(\vec{r}_b,\hat{\Omega},E\right)=B\,\psi\left(\vec{r}_b,\hat{\Omega}',E'\right)\ \text{where}\ \vec{n}.\hat{\Omega}<0\ \text{and}\ \vec{n}.\hat{\Omega}'>0\ \text{and}\ \vec{r}_b\in\partial V \tag{2.2}$$

where ψ is the angular flux distribution of the system, Q is the source term and k is the system eigenvalue (only present if $Q = 0$, otherwise equals one). This eigenvalue is the largest positive eigenvalue of equation (2.1) and corresponds to the fundamental mode of the transport equation. This largest eigenvalue is defined physically as the ratio of neutrons in successive generations, where a fission reaction is the event separating generations. The external boundary of the system is denoted by ∂V , the normal vector

$\vec{n}$ is chosen as the outward unit vector with respect to ∂V, and B is the general boundary condition operator obtained from the redistribution kernel as defined by Gheorghiu and Rahnema (1998). The phase-space variables are defined by $\left(\vec{r},\hat{\Omega},E\right)$ for the space, angle and energy respectively. The macroscopic cross-sections are denoted by σ with subscripts *t, s* and *f* representing the total cross-section, the scattering cross-section and the fission cross-section, respectively. The fission spectrum is denoted by the function χ.

The system is decomposed in a set of N non-overlapping sub-volume elements V_i (*e.g.* coarse mesh), within which, the angular flux distribution can be expressed by the following relation.

$$\begin{aligned}\hat{\Omega}.\nabla\psi_i\left(\vec{r},\hat{\Omega},E\right)+\sigma_t\left(\vec{r},E\right)\psi_i\left(\vec{r},\hat{\Omega},E\right)-\int_0^\infty dE'\int_{4\pi}d\Omega'\,\sigma_s\left(\vec{r},\hat{\Omega}',E'\to\hat{\Omega},E\right)\psi_i\left(\vec{r},\hat{\Omega}',E'\right)\\ =\frac{1}{4\pi}\chi\left(\vec{r},E\right)\int_0^\infty dE\int_{4\pi}d\Omega\,\frac{\nu\sigma_f\left(\vec{r},E'\right)}{k}\psi_i\left(\vec{r},\hat{\Omega}',E'\right)+Q_i\left(\vec{r},\hat{\Omega},E\right)\end{aligned} \tag{2.3}$$

with the following boundary condition

$$\psi_i\left(\vec{r}_{ij},\hat{\Omega}_i,E\right)=\psi_j\left(\vec{r}_{ij},\hat{\Omega}_j,E\right) \tag{2.4}$$

where $\vec{r}_{ij}\in\left\{V_i\cap V_j\right\}$ for all V_j bounding V_i and $\left|\vec{n}_i\cdot\hat{\Omega}_i\right|=\left|\vec{n}_j\cdot\hat{\Omega}_j\right|$ with $\vec{n}_i.\hat{\Omega}_i<0$ and $\vec{n}_j.\hat{\Omega}_j>0$. Also, ψ_i is the angular flux within the sub-volume element V_i and V_j represents all the sub-volume elements sharing a common boundary with V_i. It should also be noted that k is still the system eigenvalue and that Q_i is the source within volume element V_i. Equation (2.3) has a unique solution in a vacuum as long as coarse mesh i remains sub-critical (Bell and Glasstone, 1970). In some cases (codes), it is more convenient to use a boundary condition that is in terms of angular current rather than angular flux. Multiply Equation (2.4) by $\left|\vec{n}_i\cdot\hat{\Omega}_i\right|$ and use $\left|\vec{n}_i\cdot\hat{\Omega}_i\right|=\left|\vec{n}_j\cdot\hat{\Omega}_j\right|$, then the boundary condition (2.4) becomes

$$\left|\vec{n}_i \cdot \hat{\Omega}_i\right| \psi_i\left(\vec{r}_{ij}, \hat{\Omega}_i, E\right) = \left|\vec{n}_j \cdot \hat{\Omega}_j\right| \psi_i\left(\vec{r}_{ij}, \hat{\Omega}_j, E\right) \Leftrightarrow J_i\left(\vec{r}_{ij}, \hat{\Omega}_i, E\right) = J_j\left(\vec{r}_{ij}, \hat{\Omega}_j, E\right), \quad \vec{n}_i . \hat{\Omega}_i < 0 \text{ and } \vec{n}_j . \hat{\Omega}_j > 0 \tag{2.5}$$

In the above equation, J_i is the angular partial current of V_i and J_i is the angular partial current of V_j. This new formulation of the sub-volume element boundary condition makes this approach more suitable to the Monte Carlo adaptation of the method introduced in the next section.

In the particular case where V_i shares a boundary with the system, the boundary condition takes the following form:

$$\psi_i\left(\vec{r}_{ib}, \hat{\Omega}_i, E\right) = B\,\psi_i\left(\vec{r}_{ib}, \hat{\Omega}'_i, E'\right) \tag{2.6}$$

where $\vec{r}_{ib} \in \{V_i \cap \partial V\}$ and $\left|\vec{n}_i \cdot \hat{\Omega}_i\right| = \left|\vec{n}_i \cdot \hat{\Omega}'_i\right|$ with $\vec{n}_i . \hat{\Omega}_i < 0$ and $\vec{n}_i . \hat{\Omega}'_i > 0$. Following the same procedure for deriving Eq. (2.5), Eq. (2.6) can be reformulated in terms of the angular current as

$$\psi_i\left(\vec{r}_{ib}, \hat{\Omega}_i, E\right) = B \frac{\left|\vec{n}_i \cdot \hat{\Omega}'_i\right| \psi_i\left(\vec{r}_{ib}, \hat{\Omega}'_i, E\right)}{\left|\vec{n}_i \cdot \hat{\Omega}'_i\right|} \Leftrightarrow J_i\left(\vec{r}_{ib}, \hat{\Omega}_i, E'\right) = B\,J_i\left(\vec{r}_{ib}, \hat{\Omega}'_i, E'\right) \tag{2.7}$$

2.1.1 Eigenvalue/External Source Calculations

Upon applying the decomposition of the previous section, a series of N fixed source problems, as shown in equation (2.3), are obtained which are entirely equivalent to solving the problem of equation (2.1). The immediate benefits of such decomposition might not appear obvious at first hand. However, solving the transport equation directly on large heterogeneous systems (*e.g.* nuclear reactor) is a very difficult task. Most computational methods quickly run into memory and processor limitations and as a result end up simplifying the problem through spatial and spectral homogenization. On the other hand such methods have proven to be very accurate and efficient on smaller fixed source or eigenvalue problems (*e.g.* fuel assembly). Thus, combining the efficiency and

accuracy of current methods on small fixed source problems with the domain decomposition could lead to efficient and accurate solutions of large heterogeneous systems. When performing eigenvalue calculations, a two level iterative process is introduced: 1) inner iterations on the angular flux (or current) on the boundaries of the sub-volume elements, and 2) outer iterations on the system eigenvalue. For fixed source calculations, the outer iteration disappears

2.2 Considerations for Eigenvalue Mode

This section deals with issues relevant only to eigenvalue calculations. Even thought fixed source problems are not considered in this thesis, similar considerations are discussed in Section 2.3.

2.2.1 Implicit Treatment of the Fission Source

The implicit treatment of the fission source (Ilas and Rahnema, 2003; Mosher and Rahnema, 2005) is the main difference between the coarse mesh transport method and conventional response matrix or interface currents methods. In the previous methods, described in Section 1.2.2, the fission source is treated explicitly, thus requiring surface to surface, surface to volume (where fission may occur), volume to surface and volume to volume first-flight collision probabilities. They also require an approximation in terms of the number of neutron generations that are tracked. The coarse mesh transport method treats the fission source implicitly meaning that the neutron transport equation is solved over a coarse mesh in which the fission source is scaled by the core eigenvalue, as shown in equations (2.3) and (2.4). In this case, only surface to surface calculations need to be performed. Outer iterations are thus performed directly on the eigenvalue instead of the fission source. This leads to a significant improvement in terms of overall efficiency. In addition, this formulation makes no approximation regarding the shape of the fission source distribution and with the number of neutron generations, which is necessary with

methods that employ in-volume responses. However, with the implicit source treatment, the magnitude of the source has to be controlled by the incident flux in the local fixed source calculation, thus requiring an external normalization in order to converge on the global system solution.

2.2.2 Inner Iterations

The process starts with an initial guess of k and a normalized uniform incoming angular flux (or current) estimate on the surface $\vec{r}_{ij} \in \{V_i \cap V_j\}$ e.g., the initial guess is given by

$$\psi_i^{-/+}\left(\vec{r}_{ij}, \hat{\Omega}, E\right) = \frac{1}{D} \tag{2.8}$$

The choice of the normalization factor (D) is arbitrary and thus remains unspecified for the time being.

Starting from the initial guess, equation (2.3) is evaluated on V_i and the corresponding solution will give us information that we can transmit to neighboring sub-volume elements. For example, if the local fixed source problem is evaluated on V_j prior to V_i, then an immediate update to the boundary conditions of the V_i sub-volume element can be performed in accordance to equation (2.4). Once all the volume elements have been solved, the surface angular fluxes (or currents) are renormalized as done in equation (2.9). Both incoming and outgoing angular fluxes of all volume elements are normalized using the same normalization factor.

$$\tilde{\psi}_i^l\left(\vec{r}_{ij}, \hat{\Omega}, E\right) = \frac{\psi_i^l\left(\vec{r}_{ij}, \hat{\Omega}, E\right)}{D^l} \tag{2.9}$$

where ψ_i^l is the unnormalized angular flux of inner iteration l and $\tilde{\psi}_i^l$ is the normalized angular flux of that same inner iteration. Also, D^l is the normalization factor evaluated with the unnormalized angular fluxes.

The surface angular fluxes are then compared to the previous estimate to verify if convergence is achieved to a pre-defined criterion ε_{ψ}.

$$\left| \frac{\tilde{\psi}^{l}}{\tilde{\psi}^{l-1}} - 1 \right| < \varepsilon_{\psi} \tag{2.10}$$

where *l* represents the inner iteration number. The above equation ensures the convergence of the global flux, however this choice is not unique. One may choose any other quantity of interest that is related to the solution.

The process for updating local boundary conditions of equation (9) yields discontinuities in the angular flux (or current) on every coarse mesh interface and therefore does not satisfy the global boundary condition unless the normalization factor (*D*) equals unity, which will only happen when the system eigenvalue is fully converged. The discontinuities are present since the initial guess of the eignvlaue deviates from the system eigenvalue. They disappear as convergence in the eigenvalue and the flux is achieved.

Asymmetry in a symmetric solution may be observed if care in sweeping scheme is not exercised. An arbitrary sweeping scheme when a symmetrical solution is expected may lead to small deviations from symmetry that are proportional to the convergence criteria. Mosher (2004) illustrated the use of symmetrical sweeping schemes to avoid such inconsistencies, but this requires some user input. A more classical and user-independent approach, described in Section 2.2.4, is to use checkerboard sweeping patterns which will always lead to satisfactory results.

2.2.3 Outer Iterations

Upon the convergence of the inner iteration, two methods are used to evaluate the new system eigenvalue. These are: the neutron balance method and the discontinuous normalization method. The former was introduced by Mosher and Rahnema (2004), while the latter is an original concept developed in this thesis.

2.2.3.1 Neutron Balance Method

Mosher and Rahnema (2004) presented the following formula to evaluate *k*.

$$k = \frac{\iiint F\psi \, d\vec{r} d\hat{\Omega} dE}{\iiint A\psi \, d\vec{r} d\hat{\Omega} dE + L} \tag{2.11}$$

where the fission operator *F* is defined by

$$F\psi = \frac{1}{4\pi k} \chi(\vec{r}, E) \int_0^\infty dE \int_{4\pi} d\vec{\Omega}' \nu\sigma_f(\vec{r}, E') \psi(\vec{r}, \hat{\Omega}', E') \tag{2.12}$$

In the above equation *A* is the absorption operator

$$A\psi = \sigma_t(\vec{r}, E)\psi(\vec{r}, \hat{\Omega}, E) - \int_0^\infty dE' \int_{4\pi} d\hat{\Omega}' \, \sigma_s(\vec{r}, \hat{\Omega}', E' \to \hat{\Omega}, E) \psi(\vec{r}, \hat{\Omega}', E') \tag{2.13}$$

and *L*, the net leakage from the global system boundary, is defined as

$$L = \iiint \left| \vec{n} \cdot \hat{\Omega} \right| \psi(\vec{r}, \hat{\Omega}, E) dS d\hat{\Omega} dE \tag{2.14}$$

The convergence is achieved when the difference between the last two iterates is less than a predefined value ε_k. i.e.,

$$\left| k^u - k^{u-1} \right| < \varepsilon_k \tag{2.15}$$

where *u* is the outer iteration index. .

2.2.3.1.1 Algorithm

Figure 2.1 describes the algorithm used to evaluate the angular fluxes and the eigenvalue using the neutron balance method.

This simple algorithm shows explicitly the two levels of iterations: an outer iteration on the eigenvalue and an inner iteration on the surface angular fluxes. The algorithm also introduces the possibility of pre-computing the response functions to form a database. Ilas and Rahnema (2003) showed that excellent accuracy is obtained by pre-computing a database as a function of eigenvalue chosen on a 10% grid. The initial

guess, k_0, of the eigenvalue is usually set to one if the global system represents an operating (critical) reactor. However, if a prior knowledge indicates that the system eigenvalue differs from one (*e.g.* sub-critical reactors), a different initial guess can be used.

Algorithm Neutron Balance Method
$k = k_0$! initial guess of eigenvalue
Initialize angular fluxes by equation (2.8)
DO WHILE *k* isn't converged
    Obtain response functions for given *k*
        - Perform fixed source calculations for given *k*
        - Interpolation from a database
    DO WHILE ψ isn't converged
        Sweep on the surface angular fluxes
        Normalize angular fluxes by equation (2.9)
    END DO
    Evaluate new eigenvalue with equation (2.10)
END DO

Figure 2.1: Algorithm for the Neutron Balance Method

2.2.3.2 Discontinuous Normalization Method

A new method for evaluating the system eigenvalue is presented. This method (Forget and Rahnema, 2005c) requires a smaller number of parameters and therefore makes the overall coarse mesh method more efficient than when the neutron balance method (NBM) is used. The NBM method requires the precomputation of the fission and absorption and terms (F and A), which make the fixed source calculations less efficient in addition to increasing the total amount of response function data. The new method is based on the knowledge that the normalization factor (D) will approach unity once the solution is converged. In an attempt to accelerate convergence the normalization constant is evaluated at two distinct guesses of k. From this information, linear interpolation is used to find the corresponding value of k for a normalization constant equal to 1. Convergence is achieved when the following criterion is met

$$\left|D^u - 1\right| < \varepsilon_k \tag{2.16}$$

Clearly, the new method for evaluating the eigenvalue is most effective when the normalization constant varies somewhat linearly with *1/k*. It is thus important to indicate in which cases this constraint holds. We must first introduce a definition of our normalization factor:

$$D = \sum_i \psi_i^+ \left(\vec{r}_{ij}, \hat{\Omega}, E\right) \tag{2.17}$$

Equation (2.17) corresponds to the summation of all outgoing surface angular fluxes. Introducing this definition in equation (2.9) will normalize the outgoing currents to unity. By linearity of the transport equation we can decompose the normalization factor to a sum of local (coarse mesh) normalization factor.

$$D = \sum_{i=1}^{CM} D_i \tag{2.18}$$

where D_i is the local normalization factor and the summation is performed over all coarse meshes (*CM*). We are now left with showing the relation that exits between the normalization factor and *k*.

2.2.3.2.1 Demonstration

Once the global problem is decomposed, the coarse mesh becomes a fixed source transport problem. We will thus rewrite equation (2.3) in more details for the cases of $k = k_1$ and $k = k_2$ over coarse mesh *i* with the assumption that neutrons are born isotropically from fission. The values of k_1 and k_2 are chosen such that coarse mesh *i* remains sub-critical in a vacuum, thus allowing for a unique solution (Bell and Glasstone, 1970).

$$\begin{aligned} &\hat{\Omega}.\nabla \psi_{i,1}\left(\vec{r}, \hat{\Omega}, E\right) + \sigma_t\left(\vec{r}, E\right)\psi_{i,1}\left(\vec{r}, \hat{\Omega}, E\right) \\ &\qquad - \int_0^\infty dE' \int_{4\pi} d\hat{\Omega}'\, \sigma_s\left(\vec{r}, \hat{\Omega}', E' \to \hat{\Omega}, E\right)\psi_{i,1}\left(\vec{r}, \hat{\Omega}', E'\right) \\ &\qquad\qquad = \frac{1}{4\pi k_1}\chi\left(\vec{r}, E\right)\int_0^\infty dE \int_{4\pi} d\vec{\Omega}'\, v\sigma_f\left(\vec{r}, E'\right)\psi_{i,1}\left(\vec{r}, \hat{\Omega}', E'\right) \end{aligned} \tag{2.19}$$

with the following boundary condition

$$\psi_{i,1}\left(\vec{r}_{ij},\hat{\Omega},E\right)=\psi_{j}\left(\vec{r}_{ij},\hat{\Omega},E\right) \text{ where } \vec{r}_{ij}\in\left\{V_i\cap V_j\right\} \text{ for all } V_j \text{ bounding } V_i \qquad (2.20)$$

and for $k = k_2$

$$\begin{aligned}\hat{\Omega}.\nabla\psi_{i,2}\left(\vec{r},\hat{\Omega},E\right)+\sigma_t\left(\vec{r},E\right)\psi_{i,2}\left(\vec{r},\hat{\Omega},E\right)&\\ -\int_0^{\infty}dE'\int_{4\pi}d\hat{\Omega}'\,\sigma_s\left(\vec{r},\hat{\Omega}',E'\to\hat{\Omega},E\right)\psi_{i,2}\left(\vec{r},\hat{\Omega}',E'\right)&\\ =\frac{1}{4\pi k_2}\chi\left(\vec{r},E\right)\int_0^{\infty}dE\int_{4\pi}d\hat{\Omega}'\,\nu\sigma_f\left(\vec{r},E'\right)\psi_{i,2}\left(\vec{r},\hat{\Omega}',E'\right)&\end{aligned} \qquad (2.21)$$

with the following boundary condition

$$\psi_{i,2}\left(\vec{r}_{ij},\hat{\Omega},E\right)=\psi_{j}\left(\vec{r}_{ij},\hat{\Omega},E\right) \text{ where } \vec{r}_{ij}\in\left\{V_i\cap V_j\right\} \text{ for all } V_j \text{ bounding } V_i \qquad (2.22)$$

For the sake of simplicity, the following additional assumptions are made:

1) one-group approximation in energy
2) the angular variation of the scattering cross-section $\sigma_s\left(\vec{r},\hat{\Omega}'\to\hat{\Omega}\right)$ depends only on the scattering angle $\sigma_s\left(\vec{r},\hat{\Omega}\cdot\hat{\Omega}'\right)$.

Change the sign of the angular variables in equation (2.21) to get

$$\begin{aligned}-\hat{\Omega}.\nabla\psi_{i,2}\left(\vec{r},-\hat{\Omega}\right)+\sigma_t\left(\vec{r}\right)\psi_{i,2}\left(\vec{r},-\hat{\Omega}\right)-\int_{4\pi}d\Omega'\,\sigma_s\left(\vec{r},\hat{\Omega}\cdot\hat{\Omega}'\right)\psi_{i,2}\left(\vec{r},-\hat{\Omega}'\right)&\\ =\frac{1}{4\pi k_2}\chi\left(\vec{r}\right)\int_{4\pi}d\hat{\Omega}'\,\nu\sigma_f\left(\vec{r}\right)\psi_{i,2}\left(\vec{r},-\hat{\Omega}'\right)&\end{aligned} \qquad (2.23)$$

This equation is now multiplied by $\psi_{i,1}\left(\vec{r},\hat{\Omega}\right)$ and equation (2.19) by $\psi_{i,2}\left(\vec{r},-\hat{\Omega}\right)$.

$$\begin{aligned}-\psi_{i,1}\left(\vec{r},\hat{\Omega}\right)\hat{\Omega}.\nabla\psi_{i,2}\left(\vec{r},-\hat{\Omega}\right)+\sigma_t\left(\vec{r}\right)\psi_{i,2}\left(\vec{r},-\hat{\Omega}\right)\psi_{i,1}\left(\vec{r},\hat{\Omega}\right)&\\ -\psi_{i,1}\left(\vec{r},\hat{\Omega}\right)\int_{4\pi}d\Omega'\,\sigma_s\left(\vec{r},\hat{\Omega}\cdot\hat{\Omega}'\right)\psi_{i,2}\left(\vec{r},-\hat{\Omega}'\right)&\\ =\frac{1}{4\pi k_2}\chi\left(\vec{r}\right)\psi_{i,1}\left(\vec{r},\hat{\Omega}\right)\int_{4\pi}d\Omega'\,\nu\sigma_f\left(\vec{r}\right)\psi_{i,2}\left(\vec{r},-\hat{\Omega}'\right)&\end{aligned} \qquad (2.24)$$

and

$$\psi_{i,2}\left(\vec{r},-\hat{\Omega}\right)\hat{\Omega}.\nabla\psi_{i,1}\left(\vec{r},\hat{\Omega}\right)+\sigma_t(\vec{r})\psi_{i,1}\left(\vec{r},\hat{\Omega}\right)\psi_{i,2}\left(\vec{r},-\hat{\Omega}\right)$$
$$-\psi_{i,2}\left(\vec{r},-\hat{\Omega}\right)\int_{4\pi}d\Omega'\,\sigma_s\left(\vec{r},\hat{\Omega}\cdot\hat{\Omega}'\right)\psi_{i,1}\left(\vec{r},\hat{\Omega}'\right) \tag{2.25}$$
$$=\frac{1}{4\pi k_1}\chi(\vec{r})\psi_{i,2}\left(\vec{r},-\hat{\Omega}\right)\int_{4\pi}d\Omega'\,\nu\sigma_f(\vec{r})\psi_{i,1}\left(\vec{r},\hat{\Omega}'\right)$$

The two new expressions are then subtracted, (2.25) minus (2.24), and integrated over V_i and all angles.

$$\iint\left(\psi_{i,2}\left(\vec{r},-\hat{\Omega}\right)\hat{\Omega}\cdot\nabla\psi_{i,1}\left(\vec{r},\hat{\Omega}\right)+\psi_{i,1}\left(\vec{r},\hat{\Omega}\right)\hat{\Omega}\cdot\nabla\psi_{i,2}\left(\vec{r},-\hat{\Omega}\right)\right)dVd\hat{\Omega}=$$
$$\iint\left(\begin{array}{l}\psi_{i,2}\left(\vec{r},-\hat{\Omega}\right)\dfrac{\nu\sigma_f(\vec{r})}{k_1}\int\psi_{i,1}\left(\vec{r},\hat{\Omega}'\right)d\hat{\Omega}' \\ \qquad\qquad -\psi_{i,1}\left(\vec{r},\hat{\Omega}\right)\dfrac{\nu\sigma_f(\vec{r})}{k_2}\int\psi_{i,2}\left(\vec{r},-\hat{\Omega}'\right)d\hat{\Omega}'\end{array}\right)dVd\Omega \tag{2.26}$$

The left hand side of equation (2.26) may be rewritten as:

$$\iint\nabla\cdot\hat{\Omega}\,\psi_{i,1}\left(\vec{r},\hat{\Omega}\right)\psi_{i,2}\left(\vec{r},-\hat{\Omega}\right)dVd\hat{\Omega} \tag{2.27}$$

Then, using the divergence theorem, the volume integral becomes a surface integral and equation (2.26) now becomes:

$$\iint_{n.\hat{\Omega}<0}\left|n.\hat{\Omega}\right|\psi_j\left(\vec{r}_{ij},\hat{\Omega}\right)\left(\psi_{i,1}\left(\vec{r},-\hat{\Omega}\right)-\psi_{i,2}\left(\vec{r},-\hat{\Omega}\right)\right)d\hat{\Omega}dA$$
$$=\nu\sigma_f\left(\frac{1}{k_1}-\frac{1}{k_2}\right)\left(\int\phi_{i,1}(\vec{r})\phi_{i,2}(\vec{r})dV\right) \tag{2.28}$$

Where the scalar flux is given by

$$\phi(\vec{r})=\int\psi\left(\vec{r},\hat{\Omega}\right)d\hat{\Omega} \tag{2.29}$$

Setting our fixed source boundary condition ψ_j to unity and performing the integral over the angular half-space, we get:

$$\int_{A_i}\left(J^+_{i,1}(\vec{r})-J^+_{i,2}(\vec{r})\right)dA=\nu\sigma_f\left(\frac{1}{k_1}-\frac{1}{k_2}\right)\left(\int\phi_{i,1}(\vec{r})\phi_{i,2}(\vec{r})dV\right) \tag{2.30}$$

which is equivalent to

$$D_{i,1} - D_{i,2} = \nu\sigma_f \left(\frac{1}{k_1} - \frac{1}{k_2} \right) \left(\int \phi_{i,1}(\vec{r}) \phi_{i,2}(\vec{r}) dV \right) \tag{2.31}$$

This relation indicates that the normalization constant will vary linearly with *1/k* only if $\int \phi_{i,1}(\vec{r}) \phi_{i,2}(\vec{r}) dV$ is constant. This however would be the case if the response function grid in k is not too coarse.

2.2.3.2.2 Algorithm

Figure 2.2 describes the algorithm used to evaluate the angular fluxes and the eigenvalue using the discontinuous normalization method.

This algorithm is slightly more complex than the previous NBM method (Figure 2.1). It requires two initial guesses of the eigenvalue that should preferably be chosen as to bind the expected value. In doing so, the need of using extrapolation is avoided. For each initial guess, sweeping is performed until convergence of the angular fluxes is reached and the normalization factor is evaluated. If in either case this factor differs from unity by more than the convergence criterion ε_k as per equation (2.16), linear interpolation is performed to evaluate a new estimate of *k* that corresponds to a normalization factor of one and convergence of the angular fluxes is obtained through the sweeps. If the correlation between *k* and *D* is almost linear, no outer iterations on *D* will be necessary. As this is hardly ever the case, another linear interpolation is performed between the new *k* estimate and one of the previous points and an iteration process on the normalization factor is repeated. This process is illustrated in Figure 2.3.

Algorithm Discontinuous Normalization Method

Start with two initial guesses of eigenvalue (k_1 and k_2)
They are preferably chosen to bind the converged eigenvalue

$k = k_1$

Initialize angular fluxes by equation (2.8)
Obtain response functions for given k
- Perform fixed source calculations for given k
- Interpolation from a database

DO WHILE ψ isn't converged
    Sweep on the surface angular fluxes
    Normalize angular fluxes by equation (2.9)
END DO
Evaluate normalization factor (D_1) with equation (2.13)
Verify convergence of D_1 with (2.12)
    If convergence is reached **EXIT**

$k = k_2$

Initialize angular fluxes by equation (2.8)
Obtain response functions for given k
- Perform fixed source calculations for given k
- Interpolation from a database

DO WHILE ψ isn't converged
    Sweep on the surface angular fluxes
    Normalize angular fluxes by equation (2.9)
END DO
Evaluate normalization factor (D_2) with equation (2.13)
Verify convergence of D_1 with (2.12)
    If convergence is reached **EXIT**

Initial guess of $D_3 = 0$
DO WHILE D_3 isn't converged according to (2.12)
    By linear interpolation between (k_1,D_1) and (k_2,D_2), evaluate eigenvalue k_3 for a normalization factor $D = 1$
    Obtain response functions for given k
    - Perform fixed source calculations for given k
    - Interpolation from a database

    DO WHILE ψ isn't converged
        Sweep on the surface angular fluxes
        Normalize angular fluxes by equation (2.9)
    END DO
    Evaluate normalization factor (D_3) with equation (2.13)
    IF (D_1 **and** D_3 **less than** 1) **THEN**
        Set $k_1 = k_3$ and $D_1 = D_3$
    ELSE
        Set $k_2 = k_3$ and $D_2 = D_3$
    END IF
END DO

Figure 2.2: Algorithm for the Discontinuous Normalization Method

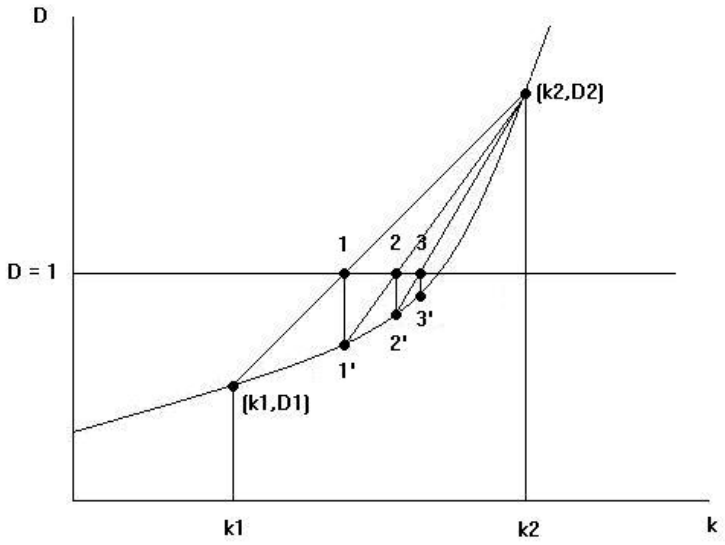

Figure 2.3: Iteration Process of the Discontinuous Normalization Method

Figure 2.3 indicates graphically how convergence is obtained for a situation in which equation (2.31) is not a linear relation between k and D. Interpolating between the two initial guesses gives point 1 which yields a new eigenvalue. Solving the system with this new estimate of the eigenvalue exposes the non-linearity of the system for k and D by introducing the solution at point 1'. Another interpolation is then performed between 1' and (k_2, D_2) from which a new estimate of the eigenvalue is obtained at point 2. The solution of the system to this estimate yields point 2'. This procedure is repeated until convergence of the normalization factor is met. Similarities can be drawn between this method and methods used to find the roots of polynomials. This thus introduces the possibility of developing many different algorithms based on these approaches that might prove considerably faster. For example, a bisection or a Newton approach could be implemented fairly easily.

2.2.3.2.3 Bisection

The bisection method (Burden and Faires, 1997) starts with two initial guesses (k_1 and k_2) that still need to be chosen to bind the expected value. The midpoint of these guesses, k_3, would be evaluated. If, for example, $f(k_1)$ and $f(k_3)$ are both smaller than one and $f(k_2)$ is larger than one, the midpoint between k_2 and k_3 is calculated. The procedure is repeated until convergence. This method is very similar to the one proposed previously without the need of interpolation.

2.2.3.2.4 Newton

In the Newton method (Burden and Faires, 1997), the two initial guesses (k_1 and k_2) are chosen very close to one an other in a way to approximate the tangential slope of the function with this formula:

$$f'(k_{12}) \approx \frac{f(k_1) - f(k_2)}{k_1 - k_2} \tag{2.32}$$

where k_{12} is the midpoint between k_1 and k_2 and f' is the derivative of the function. This method is identical to the previously proposed method with the exception that it is based on extrapolation instead of interpolation.

2.2.4 Sweeping technique

The sweeping technique refers to the procedure through which the information is transferred from one coarse mesh to another. When dealing with approximate methods with iteration process, residual error can accumulate and propagate in a non-symmetrical way to neighboring coarse meshes. To avoid such a problem a symmetric sweeping scheme must be employed. Mosher (2004) introduced such a scheme by analyzing the transfer of information in a symmetrical problem. This requires only a brief analysis of the problem to be solved, but does not eliminate the possibility of pushing the residual error in given symmetrical directions. As an alternative, a simple red-black iteration

scheme is proposed. The method, which has been used extensively in diffusion theory, is based on the checkerboard pattern. Every other coarse mesh is solved (red squares) and then all coarse meshes that were skipped are solved (black squares). This method offers a good compromise between obtaining a perfectly symmetrical solution and a more evenly distributed residual error.

2.3 Considerations for Source Driven Calculations

Source driven calculations are far simpler than eigenvalue calculations. An iteration process over the angular surface fluxes is performed with no need for an outer iteration. This eliminates the presence of discontinuities at the coarse mesh interfaces. There is also no need for normalization of any kind, since the magnitude of the angular fluxes is determined by the magnitude of the source. As done in equation (2.10), the iteration process is terminated when convergence is attained over the surface angular fluxes or any other quantity of interest.

The sweeping through the meshes is preferably done by starting from the meshes with external sources and moving to its neighboring mesh and so on. In doing so, the information carried by the source is transported more rapidly through the meshes from regions of high importance to regions of relatively low importance.

2.4 Concept of a Response Function

Before continuing any further, it is of utmost importance to understand precisely the concept of a response function and how it is evaluated. We define a response function as the solution of a system (*e.g.* the transport equation in a coarse mesh) to an incoming unitary current on one surface with vacuum boundary conditions everywhere as illustrated in Figure 2.4 and written in equation (2.3).

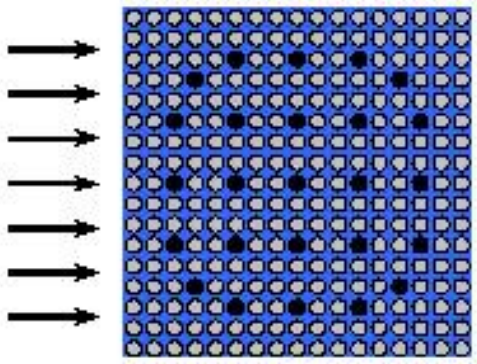

Figure 2.4: Concept of a response function

The response of this system to a particular incoming source can be characterized by any form of the solution (parameters of interest). The most important ones for the coarse mesh method are the outgoing currents on all surfaces. Other quantities of interest may also be computed, such as fission rates in fuel elements or absorption rates. The phase space distribution of the incoming unitary current is where the key approximation lies. The accuracy of the coarse mesh solution depends on how precisely this incoming angular current is representative of the full core problem. Different approximations were reviewed in Chapter 1, but none could truly represent the complexity observed in highly heterogeneous cores.

2.5 Interface Approximation

The method described in the previous section is exact but it is based on the assumption that the surface flux distribution in angle, space and energy of each coarse mesh is known. To resolve this, an approximation is introduced. The local fixed source problem of equation (2.3) is solved with the following boundary condition:

$$\psi_i\left(\vec{r}_{is},\hat{\Omega},E\right) or\ J_i\left(\vec{r}_{is},\hat{\Omega},E\right)=\begin{cases}\Gamma^m\left(\vec{r}_{is},\hat{\Omega},E\right) & where\ r_{is}\in\{V_i\cap\partial V_s\}\\ 0 & elsewhere\end{cases} \tag{2.33}$$

where ∂V_S denotes a sub-region of the boundary of coarse-mesh V_j that shares a boundary with V_i, and Γ^m is the m^{th} member of a set of functions that are orthogonal on the infinite-dimensional half-space. The solution of equation (2.3) with the boundary condition of equation (2.33) yields a result referred to as a response function denoted $R_{is}^m\left(\vec{r},\hat{\Omega},E\right)$. This response function is the actual angular flux solution corresponding to a given boundary condition Γ^m, it thus gives the response of the coarse mesh to this particular boundary condition. Then the solution to the local fixed source problem within coarse-mesh V_i can be constructed as the linear superposition

$$\psi_i(\vec{r},\hat{\Omega},E)=\sum_{m=0}^{\infty}\sum_s c_{is}^m R_{is}^m(\vec{r},\hat{\Omega},E), \tag{2.34}$$

where the coefficients are defined by

$$c_{is}^m=\iiint\psi_i^-\left(\vec{r}_{is},\hat{\Omega},E\right)\Gamma^m d\vec{r}_{is}d\hat{\Omega}dE \tag{2.35}$$

where we recall that ψ_i^- is the incoming partial angular flux of the local fixed source problem and $\vec{r}_{is}$ is the spatial variable along the boundary of V_i and ∂V_S. For computational efficiency, it is desirable to truncate the response expansion at a low order. The accuracy obtained for a given maximum order depends, of course, on the type of response functions used.

CHAPTER 3

MONTE CARLO ADAPTATION

In previous work, Mosher (2004) and Mosher and Rahnema (2005) identified some issues with the discrete-ordinates implementation of the coarse mesh method, mainly that the discrete Legendre polynomials used to expand the angular flux were defined on uniform intervals. However, non-uniform spatial intervals are computationally more efficient than a very fine uniform meshing scheme. The obvious extension would have been to replace the orthogonal set by a more flexible alternative, but this was later dismissed in favor of the Monte Carlo adaptation. When working with a deterministic code to generate response functions, a spatial and angular approximation is introduced making the use of discrete polynomials more suitable. To solve very heterogeneous coarse meshes, a very fine spatial and angular discretization must be used, thus requiring extensive memory to store all the necessary information for later use by the coarse mesh code. As the complexity of the two-dimensional problems grew, the library became quite large making the extension to 3-D impractical.

Using Monte Carlo methods as a response function generator enabled the transition from discrete polynomials to continuous polynomials (Forget and Rahnema, 2005a). In doing so, the uniform interval problem disappeared and the size of the library was reduced greatly by storing only the expansion coefficients of the polynomial set. Monte Carlo methods also possess the advantage of geometric flexibility in modeling complex structures inside the coarse meshes. Another substantial advantage of using Monte Carlo methods is the possibility of performing both multigroup and continuous energy calculations. This work also demonstrates that the coarse-mesh technique introduced previously is robust and flexible with respect to the choice of fine-mesh method used to generate the response functions.

The set of orthogonal continuous polynomials chosen for this work is the Legendre polynomials. The choice was made in part by their widespread use in the nuclear industry. However, any other set of orthogonal continuous polynomials, such as the Chebyshev or the Jacobi polynomials, could have been used. The impact of orthogonal set type is believed to be small enough.

3.1 Reference System

Before describing the source sampling and tallying technique using a continuous Legendre polynomial expansion, it is important to discuss the reference system chosen to represent the spatial and angular variables. Each face of a coarse mesh has its own independent reference system. At this point, all expansions are performed on flat surfaces. Our interest thus lies in the half-space angular current. Figure 3.1 illustrates a particle crossing a surface with a given direction for the reference system implemented and compares it to the one that was readily available in the Monte Carlo code MCNP (Briemeister, 1997) that is used to generate the response functions. This change was necessary because MCNP did not offer possibilities for tallying variations in the azimuthal angle. The angular half-space is defined by a variation of the cosine of the polar angle in the [-1, 1] domain and a variation of the azimuthal angle in the $[0, \pi]$ interval. Spatially, in a 3-D volume element, the surface expansion has two spatial variables that we will name u and v. Assuming a surface of dimension U x V, the spatial variables u and v are defined over the intervals $[0,U]$ and $[0,V]$, respectively.

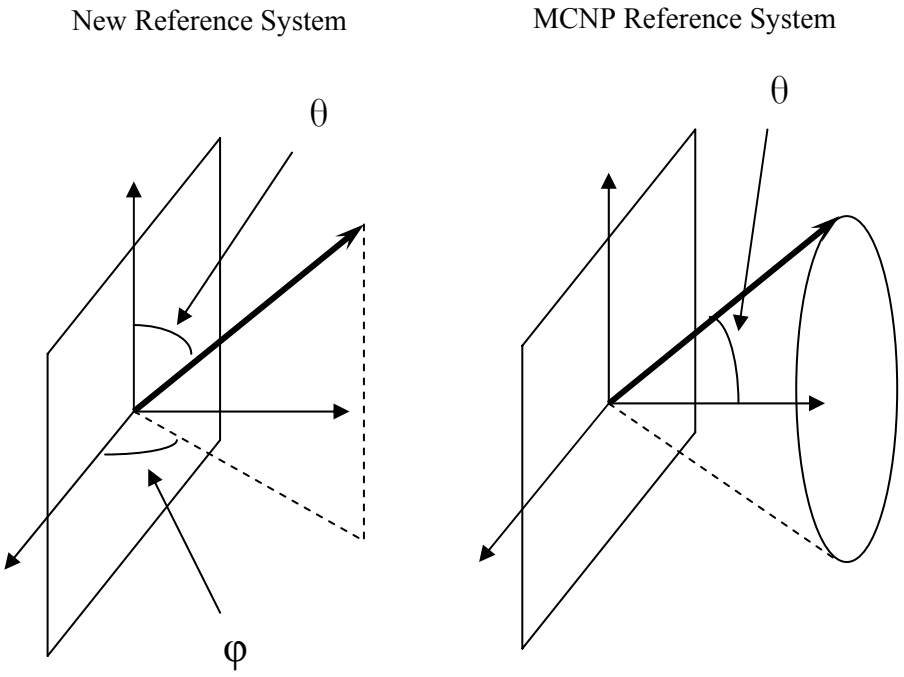

Figure 3.1: Reference System Comparison

The axis system of Figure 3.1 was chosen in a way to minimize the number of response functions and complexity of post-processing for lattices that present some level of symmetry. This is illustrated in Figure 3.2 for the two dimensional case.

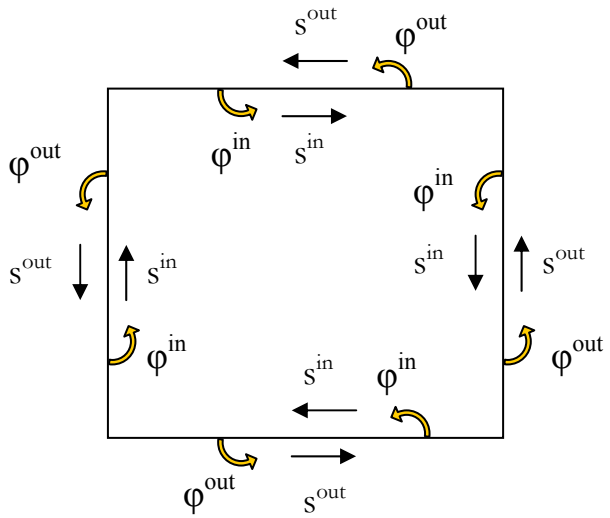

Figure 3.2: Reference system on a 2-D coarse mesh

In Figure 3.2, the *s* variable defines the axis of the spatial variable where the arrow points in the positive direction. The φ variable is the azimuthal angle varying from 0 to π in the direction of the arrow. The "*in*" and "*out*" superscript indicate that the axis system corresponds to an incoming or an outgoing angular current, respectively. The reason for this axis system is better illustrated in Figure 3.3 which presents the coupling between neighboring coarse meshes.

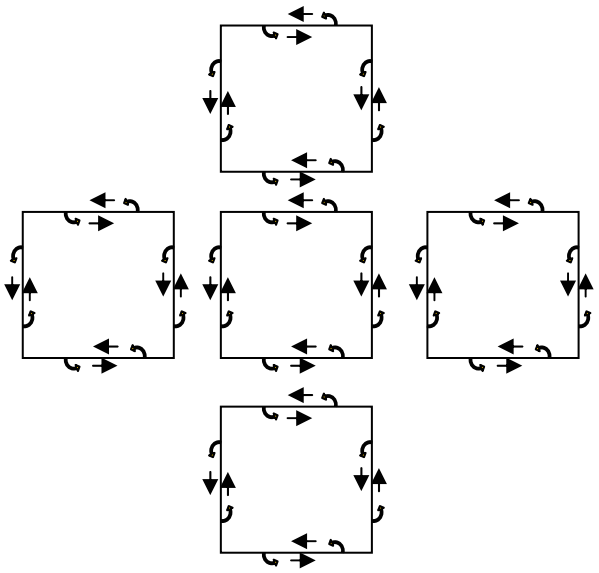

Figure 3.3: Reference System for Sweeping Purposes

The coarse mesh method is based on a deterministic sweeping technique that calculates outgoing currents from a mesh that become the incoming currents of the neighboring mesh. The scheme presented in Figure 3.3 has axes for the outgoing currents that are identical to the neighboring meshes axes for the incoming currents. When coupling scalar currents or currents with a fixed symmetric shape (*e.g.* spatially flat cosine current) such a scheme is not necessary. However, when the coupling is performed on angular currents, such a scheme allows for a more transparent coupling.

3.2 Legendre Polynomials

The Legendre polynomials (Bell and Glasstone, 1970) are defined as a set of polynomials orthogonal over the interval [-1,1] and are given by the following equations:

$$P_0(x) = 1 \tag{3.1}$$

$$P_n(x) = \frac{1}{2^n n!}\frac{d^n}{dx^n}\left(x^2 - 1\right)^n \quad for\ n = 1, 2, ... \tag{3.2}$$

With the exception of P_0, all the Legendre polynomials integrate to 0 over the interval [-1,1]. This can be seen readily in Figure 3.4, which illustrates the first five Legendre polynomials also written in equation (3.3).

$$\begin{aligned} P_0(x) &= 1 \\ P_1(x) &= x \\ P_2(x) &= \left(3x^2 - 1\right)/2 \\ P_3(x) &= \left(5x^3 - 3x\right)/2 \\ P_4(x) &= \left(35x^4 - 30x + 3\right)/8 \end{aligned} \tag{3.3}$$

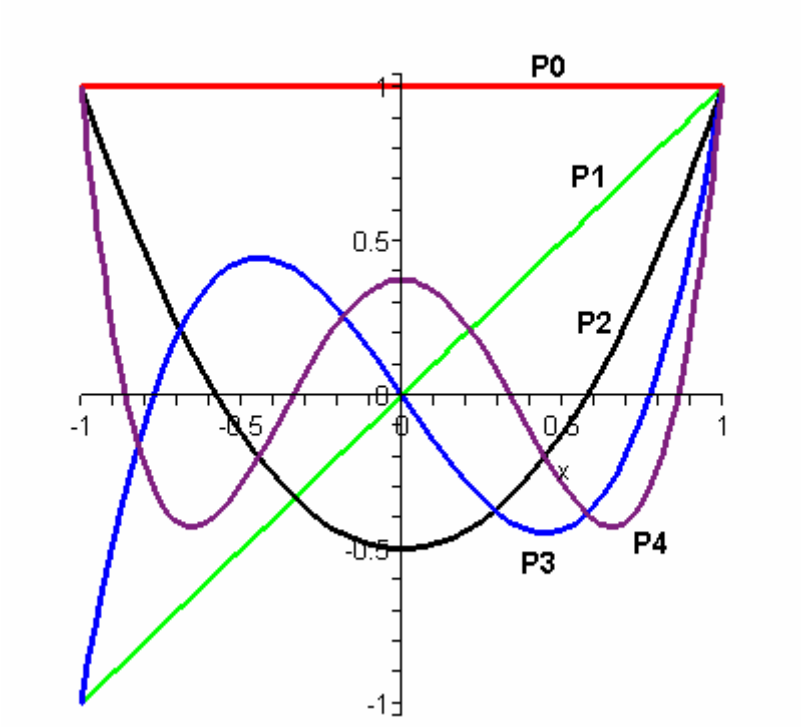

Figure 3.4: First five Legendre polynomials

3.3 Sampling from Legendre polynomials

To sample from the continuous Legendre polynomials (P_n), they must be expressed in terms of a probability density function, *f(x)*, meaning that they must respect the following conditions (Hines *et al*, 2003):

$$1) \qquad \int_{\Re} f(x)dx = 1 \tag{3.4a}$$

$$2) \qquad f(x) \geq 0, \quad \forall x \geq 0 \tag{3.4b}$$

$$3) \qquad If \ A \subseteq \Re, \ then \ P(X \in A) = \int_{A} f(x)dx \tag{3.4c}$$

To facilitate the transition to a probability density function of the Legendre polynomials, the orthogonal set is transferred to the interval [0,1] by a simple change of variable.

$$y = \frac{x+1}{2} \tag{3.5}$$

This special set of Legendre polynomials is commonly referred to as the double Legendre polynomials (DP_n or $P_n^{[0,1]}$). Even with this change, we do not obtain directly probability density functions for all orders. As was done before for the source sampling (Griesheimer *et al*, 2003; Mosher *et al*, 2003), the polynomials were sampled by linear combinations of the Legendre expansions thus avoiding the presence of negative weights associated with expansions orders greater than zero and also complying to the properties of probability distribution functions given by equations (3.4). The resulting probability distribution functions are illustrated in Figure 3.5.

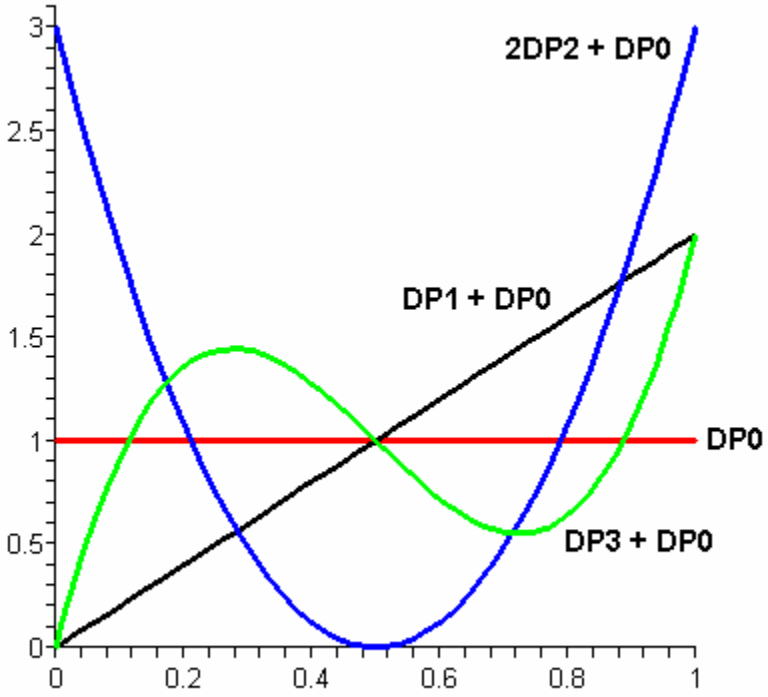

Figure 3.5: Linear Combinations of Double Legendre polynomials.

Griesheimer and Martin (2003) introduced modifications to MCNP4C to sample the polar angle over the interval [0,1] using Double Legendre polynomials for orders up to two. They used this sampling scheme in a 1-D response matrix method. The sampling was performed using the inversion technique. This work was thus extended allowing sampling on arbitrary intervals as well as higher order cases. Analytical solutions for higher orders are cumbersome and sometimes do not exist, thus polynomials with order greater than two were sampled using the rejection technique. It should also be noted that the statistical uncertainty of these distributions is being neglected. It is assumed that enough particles are sampled to represent accurately the expected distributions.

3.4 Surface Source Sampling

The distribution of particles along a given surface is defined by a tensor product of Legendre polynomials orthogonal over given intervals specified by their respective variables and scaled appropriately to become probability density functions. Equation (3.6) indicates the form taken by the unitary angular current on the coarse mesh surface.

$$\Gamma^{g,l,m,n,p,r}(u,v,\mu,\varphi,E) = P_l^{[E_{g-1},E_g]}(E_g)P_m^{[0,U]}(u)P_n^{[0,V]}(v)P_p^{[0,\pi]}(\varphi)P_r^{[-1,1]}(\mu) \qquad (3.6)$$

The expansion order is given by the variables *l, m, n, p* and *r*, which correspond respectively to the expansion in energy over group *g*, space (*u* and *v*) and angle (μ and φ). Sampling each variable according to the procedure introduced in Section 3.3 for orders *l, m, n, p* and *r* will determine the location, direction and velocity of the particle emerging from the given surface. This is repeated for as many particles necessary to obtain reasonable precision of the quantities of interest in the Monte Carlo simulation.

All possible combinations of expansion orders *l, m, n, p* and *r* must be solved. For example, a second order expansion in three variables, noted $\{a,b,c\}$, will require solving 27 independent simulations: {0,0,0}, {0,0,1}, {0,0,2}, {0,1,0}, {0,1,1}, {0,1,2} {0,2,0}, {0,2,1}…

3.5 Tallying

3.5.1 Outgoing Currents

Every time a particle leaves the system, it crosses a surface at a given location (*x,y,z*) with a direction vector (*i,j,k*) and a specific energy (*E*). From these variables, it can be determined easily which surface of the system the particle is exiting from, its location on the surface, its energy and its angular direction as defined in Section 3.1. With this information it is then possible to evaluate the expansion coefficients of the outgoing angular current in response to a specific source.

In Monte Carlo simulations, the surface current tally is a simple count of particles (Briemeister, 1997), of a given weight (W), which cross a given surface within specific bins and is given by equation (3.7).

$$R_{J,g\to g',s\to s'}^{l,m,n,p,r} = \frac{1}{C}\sum_{i=1}^{C} W_{i,g',s'} \tag{3.7}$$

where C is the total number of particles simulated and $R_{J,g\to g',s\to s'}^{l,m,n,p,r}$ is the estimated surface current response of surface *s'* within energy group *g'* to a given incoming current from surface *s* of order *l, m, n, p* and *r* in energy, space (two variables) and angle (two variables) within energy group *g*, respectively. However, the coarse mesh method requires that the tally be performed on the coefficients of the scaled Legendre polynomial expansion as shown in equation (3.8).

$$R_{J,g\to g',s\to s'}^{l\to l',m\to m',n\to n',p\to p',r\to r'} = \frac{1}{C}\sum_{i=1}^{C} P_{l'}^{[E_{g'-1},E_{g'}]}(E_{g'})P_{m'}^{[0,U]}(u)P_{n'}^{[0,V]}(v)P_{p'}^{[0,\pi]}(\varphi)P_{r'}^{[-1,1]}(\mu)W_{i,g',s'}^{l',m',n',p',r'} \tag{3.8}$$

where $R_{J,g\to g',s\to s'}^{l\to l',m\to m',n\to n',p\to p',r\to r'}$ is the estimated surface current response of surface *s'* with orders *l', m', n', p'* and *r'*, within energy group *g'* to a given incoming current from surface *s* of order *l, m, n, p* and *r* in energy, space (two variables) and angle (two variables) within energy group *g*, respectively. When dealing with Monte Carlo methods, uncertainties associated with the mean value of the response functions must also be estimated. This is done by evaluating the variance. Since the true sample mean is not know, an approximation of the true variance, also known as the sample variance (Hines *et al*, 2003), is evaluated according to equation (3.9).

$$S^2 = E[X^2] - \left(E[X]\right)^2 \tag{3.9}$$

where S^2 is the sample variance, E is the expected value and X represents the set of all outcomes, x_i, of the simulation. The estimate of *E[X]* corresponds to the tally of equation

(3.8). The estimate of $E[X^2]$ needs a separate tally in which all values are squared as shown in equation (3.10).

$$E[X^2] = \frac{1}{C}\sum_{i=1}^{C}\left(P_{l'}^{[E_{g'-1},E_{g'}]}(E_{g'})P_{m'}^{[0,U]}(u)P_{n'}^{[0,V]}(v)P_{p'}^{[0,\pi]}(\varphi)P_{r'}^{[-1,1]}(\mu)W_{i,g',s'}^{l',m',n',p',r'}\right)^2 \quad (3.10)$$

The estimated variance of X is given by:

$$S_X^2 = \frac{S^2}{C} \quad (3.11)$$

3.4.2 Other Quantities

As of now, only the outgoing currents were tallied on Legendre polynomials because other quantities showed no need for such expansions. However, the extension of this procedure to other quantities of interest is essentially straightforward. For example, using Legendre expansion, it would be possible to solve for the radial and axial variations of power within each fuel element.

A popular tally amongst other quantities of interest is the reaction rate of a given reaction Z expressed by equation (3.12).

$$R_{Z,g,s}^{l,m,n,p,r} = \frac{1}{C}\sum_{i=1}^{C}\frac{W_i T_i}{V}\sigma_Z \quad (3.12)$$

where $R_{Z,g,s}^{l,m,n,p,r}$ is the estimated Z-reaction rate response to a given incoming current of order *l, m, n, p* and *r* in energy, space (two variables) and angle (two variables) within energy group *g* over surface *s*, respectively. This response function type is evaluated over a volume element V in which particles travel a distance T.

3.6 Concept of a Response Function

In Section 2.4, a response function was defined as being the response to a unitary incoming current of a given (fixed) distribution. After introducing the Legendre boundary expansion of equation (3.6), this concept can now be refined. The response function is known as the response of a mesh to a given tensor product of Legendre

polynomials of given order. Response functions now have to be generated for all combinations of cross terms. The tallying of a response function must also be done on all possible expansion order combinations. The amount of generated data for each response function is thus much larger than when a single fixed phase space distribution (*e.g.* spatially flat cosine-current) is used and the total number of response functions is also increased. Coarse mesh solutions with very high expansion order can quickly require countless amounts of memory, thus making response function reduction techniques very important (see Section 3.10).

3.7 Segmentation

It is clear from equation (3.6) that the energy variable must be treated differently than the other variables. The energy expansion is performed over a given energy range (group). The same concept can be applied to all the other variables in an effort to reduce the expansion orders as shown in equation (3.13).

$$\Gamma_{g,a,b,c,d}^{l,m,n,p,r}(u,v,\mu,\varphi,E) = P_l^{[E_{g-1},E_g]}(E_g)P_m^{[u_{a-1},u_a]}(u)P_n^{[v_{b-1},v_b]}(v)P_p^{[\varphi_{c-1},\varphi_c]}(\varphi)P_r^{[\mu_{d-1},\mu_d]}(\mu) \quad (3.13)$$

The interval of any given variable is reduced to a number of non-overlapping intervals (segments). The expansions are thus performed on smaller intervals allowing each to evolve independently. This becomes quite useful in dealing with (treating) strong flux gradients along a given interval. In nuclear reactor calculations, the angular distribution is generally well behaved over the entire angular interval, which does not really require this type of segmentation. However, the spatial variables will sometimes have very strong gradients along the surfaces making segmentation (allowing discontinuities) desirable.

3.8 Energy Treatment

The derivation of the coarse mesh transport method by Ilas and Rahnema (2003) and subsequently by Mosher and Rahnema (2005) treated the energy variable in the

multigroup (energy bin) formalism. The deterministic response function generator (discrete-ordinates code) solved the fixed source problem of equation (2.3) using cross-sections previously condensed in energy by a lattice code. This procedure was directly translated to the Monte Carlo approach. Fixed source calculations for each group were solved and responses were tallied over all groups (in energy bins). However, the transition from deterministic to stochastic methods to generate response functions offered the additional possibility of using continuous energy data in our calculations. Attempts were made with segmentation and Legendre polynomial expansion, but as the results will show the eigenvalue accuracy suffered. This type of expansion/segmentation is expected to work well with a low-order expansion if the energy variation of the surface current is smooth. Unfortunately, interface currents are not smooth in energy in nuclear reactor calculations, particularly in the thermal and resonance range. Sharp gradients in the current in the resonance range would require impractical high order expansions making the energy expansion less attractive than the current multigroup scheme. As an alternative, a new technique is proposed in the next section.

3.8.1 Spectral Mapping

The spectral mapping approach is based on mapping a predetermined energy spectrum to a 0^{th} order expansion and then performing polynomial expansions based on this mapping, as shown in Figure 3.6. The 0^{th} order represents the initial energy spectrum and the higher orders are shifts to that spectrum.

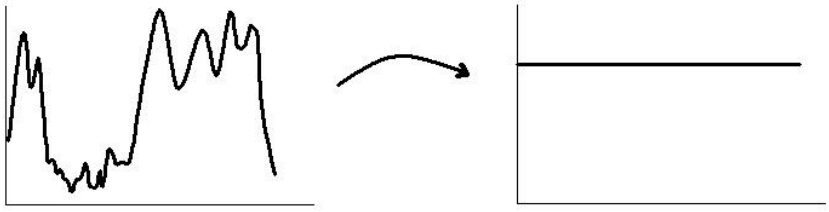

Figure 3.6: Spectral Mapping (0^{th} order)

The initial spectrum must be carefully chosen to obtain good accuracy. This choice is usually made by evaluating the energy spectrum found in a typical coarse mesh (e.g. average burnup) or by averaging over selected meshes. No exact method exists for choosing this spectrum and the methods presented here are mostly based on the experience user.

3.8.1.1 Energy Spectrum

The key step in this method is identifying a suitable spectral map. This can be done by performing infinite lattice calculations on unique coarse meshes and tallying the energy spectrum at the boundaries of the mesh over a fine group energy structure. The fine group structure is chosen in the current literature to be representative of the type of reactor under consideration (*e.g.* HELIOS energy structure for light water reactors (Casal *et al*, 1991)). A leakage correction should be applied to these infinite lattice calculations to simulate more accurately the true core conditions. The normalized energy spectra of all the unique coarse meshes in the core are then averaged to a "reference" spectrum that will be used for the mapping.

3.8.1.2 Source Sampling

The reference energy spectrum is then used to generate probability mass functions from which the surface source will be sampled at different expansion orders. The 0^{th} order expansion corresponds directly to the reference spectrum, while the higher orders correspond to a scaled Legendre polynomial of a given order multiplying the reference spectrum. Once again, the Legendre polynomials are sampled on linear combinations of the 0^{th} order to avoid the presence of negative values and to make normalization to a probability mass function possible. Figure 3.7 illustrates a 1^{st} and 2^{nd} order spectral mapping. The plots on the right hand side indicate how the higher expansion order

influences the reference energy spectrum of Figure 3.6. The probability mass function of the energy variable is then sampled using the rejection technique, while all other variables of the surface source are sampled according to Section 3.4.

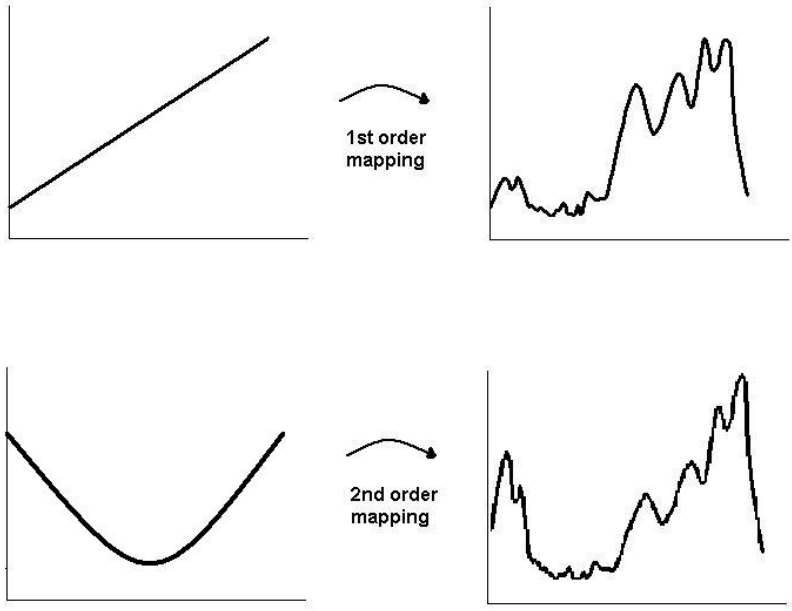

Figure 3.7: Spectral Mapping (1st and 2nd order)

3.8.1.3 Tallying

Tallying the Legendre expansion coefficients on such an energy spectrum is done in a two-step procedure. First, the response functions calculations are performed with the new surface source expansion but with tallies identical to that of equation (3.8). By itself, this procedure is inconsistent because we are not evaluating the expansion coefficients of the reference spectrum but merely evaluating deviations from a flat spectrum. The second step consists of applying a correction factor to these tallies. These correction factors correspond to the expansion coefficients obtained by representing the reference spectrum in terms of a Legendre polynomial expansion as shown in equation (3.14).

$$J(E) \approx \sum_{l=0}^{L} (2l+1) j_l P_l^{[E_{\min}, E_{\max}]}(E) \tag{3.14}$$

where J is the angular current at the boundary of a coarse mesh that serves as the reference spectrum, j is the expansion coefficient of order l and P is the Legendre polynomial scaled over the interval of minimum (E_{min}) to a maximum energy (E_{max}).

3.9 Deterministic Sweeps

Once the response functions for each unique coarse mesh have been computed using the appropriate boundary condition, a deterministic sweeping technique will be used to calculate the outgoing half-space currents from each coarse mesh and any other quantities of interest (*i.e.* fission density in each fuel pin). The coefficients of the exiting current j^+ from coarse mesh V_i are calculated from equations (2.34) and (2.35) which give the following relation

$$j^+_{i,l,m,n,p,r,g,s} = \sum_{s'=1}^{S} \sum_{g=1}^{E} \sum_{l'=0}^{L} \sum_{m'=0}^{M} \sum_{n'=0}^{N} \sum_{p'=0}^{P} \sum_{r'=0}^{R} (2l'+1)(2m'+1)(2n'+1)(2p'+1)(2r'+1) \times R^{l\to l',m\to m',n\to n',p\to p',r\to r'}_{J,i,g\to g',s\to s'} j^-_{i,l',m',n',p',r',g',s'} \tag{3.15}$$

where $R^{l\to l',m\to m',n\to n',p\to p',r\to r'}_{J,i,g\to g',s\to s'}$ is the current response function relating the incoming to the outgoing coefficients of the currents for all expansion orders, surfaces and energy groups in coarse mesh V_i. The summations are performed over all energy groups/bins E and surfaces S for up to the maximum expansion orders in energy (L), spatial (M, N) and angular (P, R) variables, respectively. It is important to note that there is no need to compute (iterate on) the interface currents since the inner iterations can be performed directly on the expansion coefficients. If one wishes to evaluate other quantities of interest (*e.g.* pin fission density, region-wise absorption …) within the volume element V_i, a similar relation can be developed.

$$Z = \sum_{s'=1}^{S} \sum_{g'=1}^{E} \sum_{l'=0}^{L} \sum_{m'=0}^{M} \sum_{n'=0}^{N} \sum_{p'=0}^{P} \sum_{r'=0}^{R} (2l'+1)(2m'+1)(2n'+1)(2p'+1)(2r'+1) \times R^{l',m',n',p',r'}_{Z,i,g',s'} j^-_{i,l',m',n',p',r',g',s'} \tag{3.16}$$

where Z is the quantity of interest and $R_{Z,i,g',s'}^{l',m',n',p',r'}$ is the response of this quantity to a boundary condition of order l' in energy, m' and n' in space, p' in azimuthal angle and r' in polar angle. These quantities can also be used to assess convergence for the inner iterations.

3.9.1 Propagation of Statistical Uncertainty

Using a Monte Carlo method as a response function generator implies dealing with the statistical uncertainty associated with all the quantities provided by the fine mesh code. As was done before in Forget *et al.* (2004a), the propagation of statistical uncertainty was implemented in the coarse mesh code using the following formula to calculate the standard deviations (Bevington, 1969):

$$s_W = \sqrt{\left(\frac{\partial W}{\partial x}\right)^2 s_x^2 + \left(\frac{\partial W}{\partial y}\right)^2 s_y^2 + 2\rho_{xy}^2 \left(\frac{\partial W}{\partial x}\right)\left(\frac{\partial W}{\partial y}\right) + \ldots} \tag{3.17}$$

In this equation W is a function of variables x y, … and ρ_{xy}^2 is the covariance between x and y. We assume that the Monte Carlo results are uncorrelated and as a result all the terms with the covariance data in equation (3.17) are set to zero.

An expression for the standard deviation of each of the exiting current coefficients follows from equations (3.15) and (3.17).

$$s_{J_{i,l,m,n,p,r,g,s}^{+}} = \sqrt{\begin{array}{l}\sum_{s'=1}^{S}\sum_{g=1}^{E}\sum_{l'=0}^{L}\sum_{m'=0}^{M}\sum_{n'=0}^{N}\sum_{p'=0}^{P}\sum_{r'=0}^{R}(2l'+1)(2m'+1)(2n'+1)(2p'+1)(2r'+1) \\ \times\left(\begin{array}{l} R_{J,i,g\to g',s\to s'}^{l\to l',m\to m',n\to n',p\to p',r\to r'^2}\, s^2_{J^{-}_{i,l',m',n',p',r',g',s'}} \\ +\left(j^{-}_{i,l',m',n',p',r',g',s'}\right)^2 s^2_{R^{l\to l',m\to m',n\to n',p\to p',r\to r'}_{J,i,g\to g',s\to s'}}\end{array}\right)\end{array}} \tag{3.18}$$

A similar expression for evaluating the standard deviation of a quantity of interest Z can also be derived from equations (3.16) and (3.17).

$$s_Z = \sqrt{\sum_{s'=1}^{S}\sum_{g'=1}^{E}\sum_{l'=0}^{L}\sum_{m'=0}^{M}\sum_{n'=0}^{N}\sum_{p'=0}^{P}\sum_{r'=0}^{R}(2l'+1)(2m'+1)(2n'+1)(2p'+1)(2r'+1) \times\left(R_{Z,i,g',s'}^{l',m',n',p',r'^2} s^2_{j^-_{i,l',m',n',p',r',g',s'}} + \left(j^-_{i,l',m',n',p',r',g',s'}\right)^2 s^2_{R^{l',m',n',p',r'}_{Z,i,g',s'}}\right)} \quad (3.19)$$

3.10 Acceleration

When performing coarse mesh calculations based on Legendre expansions of the surface angular currents, an acceleration scheme inherent to the method can be developed. Obtaining an accurate solution requires in most cases an expansion order between 2 and 5 in all variables. However, when pre-computing a high order database from the tensor product of Legendre polynomials of equation (3.6), lower order response function subsets are included. This implies that performing a fast low-order calculation is possible because all the information is already there. The solution of this low-order calculation can then be used as the initial guess for the higher order solution. This method tends to reduce the number of inner iteration required to converge the interface partial currents. This procedure can also be done incrementally, meaning that a low-order solution becomes the starting point of a higher order calculation whose solution also becomes the starting point of an even higher order calculation.

3.11 Order Reduction

It is now evident that the coarse mesh method relies heavily on the pre-computation of the so called response functions. More precise solution obviously requires a greater number of fixed source calculations making the pre-computational phase that much longer. The surface angular current expansion expressed in terms of a tensor product of Legendre polynomials requires all of the response function expansion coefficients. Different techniques have been proposed to reduce the number of response functions associated with the polynomial expansion of the phase space.

3.11.1 Multi-Variable Orthogonal Polynomials

The first possibility is to use multi-variable orthogonal polynomials (Suetin, 1999). This would combine two or more variables in a single expansion. A classical choice would be a spherical harmonic expansion in angle, which is often used in transport theory for other resolution techniques. The orthogonal expansion couples the polar angle and the azimuthal angle in a single expansion. This choice was discarded mainly because the order of expansion of the azimuthal angle is somewhat limited by the polar angle expansion order. This makes the spherical harmonic basis set quite impractical in 2-D calculations where high order azimuthal angle expansions are of utmost importance in comparison to the expansion order of the polar angle. This avenue of research has not yet been fully investigated. Many possibilities of coupling the angular variables or the spatial variables exist and should be investigated.

3.11.2 High Order Reduction

Another possibility is to drop high order cross terms. For example, consider the second order polynomial *p(x,y)* written in terms of variables *x* and *y*

$$p(x,y) = ax^2 + by^2 + cxy + dx + ey + f \tag{3.20}$$

where *a, b, c, d, e* and *f* are arbitrary coefficients and $-1 < x, y < 1$. The polynomial *p(x,y)* is clearly a second order function that we will now expand using 2nd order Legendre polynomials in both variables.

$$p(x,y) \approx \sum_{n=1}^{2}\sum_{m=1}^{2}(2n+1)(2m+1)P_n(x)P_m(y)K_{n,m} \tag{3.21}$$

where *n* and *m* are the expansion orders of variables *x* and *y*, and $K_{n,m}$ is obtained from the orthogonality relation

$$K_{n,m} = \frac{1}{4}\int_{-1}^{1}\int_{-1}^{1} p(x,y)P_n(x)P_m(y)dxdy \tag{3.22}$$

Equation (3.21) can now be rewritten in the following form

$$p(x,y) \approx a'x^2y^2 + b'x^2y + c'xy^2 + d'x^2 + e'xy + f'y^2 + g'x + h'y + i' \tag{3.23}$$

where *a', b', c', d', e', f', g', h'* and *i'* are the expansion coefficients. When evaluating the aforementioned coefficients with equation (3.22), the following is observed

$$a' = 0; \quad b' = 0; \quad c' = 0; \quad d' = a; \quad e' = b; \quad f' = c; \quad g' = d; \quad h' = e; \quad i' = f \tag{3.24}$$

Dropping the higher order terms, *a', b'* and *c'*, of equation (3.23) yields the exact second order expansion of equation (3.20). This implies that this scheme can be used to reduce the number of response functions by truncating the higher order cross terms of the tensor product presented in equation (3.6) while still conserving a second order expansion.

3.11.3 Odd Order Polar Angle in 2-D

In two-dimensional calculations, an additional response function reduction technique can be introduced. Recalling the axis reference scheme introduced in Figure 3.1, in a 2-D problem, the azimuthal angle (φ) is chosen to be in the 2-D plane, while the polar angle (θ) is a measure of the complimentary angle from that plane. Since a two-dimensional problem can be seen as a three-dimensional problem with an infinite component in the third dimension, the polar angle distribution of the angular current in the interval [0, π/2] must be symmetric to the distribution in the interval [π/2, π]. When the Legendre polynomial expansion of the cosine of the polar angle is performed, this symmetry requirement alleviates the need of performing the odd-order expansions which are not symmetrical over these intervals.

3.12 COMET

The coarse mesh transport method was implemented in a computer code called COMET (Coarse Mesh Transport) written in Fortran 95. The code used to perform the

calculations of the ensuing chapters was compiled using Compaq Visual Fortran Professional Edition 6.6C under the Windows 2000 operating system. This code is separated into three main functions: 1) an automated response function generator, 2) a response function post-processing/database program and 3) a coarse mesh transport simulator.

3.12.1 Response Function Generator

The response function generator is an automated way of generating all the input files needed to perform the Monte Carlo calculations with the modified MCNP code. It also creates an execution batch file. There is also the option of separating all the calculations in as many folders as allowed on available computer system.

3.12.2 Post-Processing/Database

The post-processing of the data takes place upon the completion of the calculations of all the response functions. The Legendre polynomial scaling illustrated in Figure 3.5 is undone (unfolded) to obtain the true Legendre expansions. The collected data is then stored in a database. The CDF database format (NSSDC, 2006) was chosen because of its capabilities and ease of implementation. Common Data Format (CDF) was developed by the National Space Science Data Center (NSSDC) at NASA and is freely available and portable to many platforms. It is used widely by many universities and government agencies and is continuously supported.

3.12.3 Coarse Mesh Transport Simulator

The coarse mesh transport simulator performs the transport calculations in a system built from different user defined unique meshes, whose properties (response functions) can be found in the database. Calculations can be performed to any order combination up to the maximum orders of the different variables as stored in the database. The simulator can perform both two and three dimensional calculations. The

allowed system boundary conditions are vacuum, specular reflection and periodic. The sweeping order from mesh to mesh is also user defined.

CHAPTER 4

2-D RESULTS

In this chapter, we determine the accuracy and efficiency of the coarse mesh method in 2-D configurations using several benchmark problems We first include a description of the notations used in this chapter and then present the methods used for analyzing the results. Results are presented for a small pressurized water reactor benchmark problem followed by a few CANDU problems. The 2-D MOX C5G7 benchmark problem is presented in Section 4.6. This section is followed by a full core extension of the C5G7 problem and a ¼ core update of the HAFAS benchmark problem. It should also be noted that initially the coarse mesh method was tested using the cosine-current approximation and that this approximation was later replaced by the Legendre polynomial expansion of the interface currents.

4.1 Analysis Method and Notation

Different benchmarks will be used to evaluate the accuracy of the coarse mesh transport method. In all cases, a highly accurate reference solution is obtained from a Monte Carlo simulation which yields the reference eigenvalue and the reference fission densities. The relative error (*RE*) of all the measures is defined by

$$RE_Z = \frac{\left(Z_{COMET} - Z_{referemce}\right)}{Z_{reference}} \times 100 \tag{4.1}$$

where Z_{COMET} is the coarse mesh result and $Z_{reference}$ is the reference solution. The relative error will be used as a method of comparison for the eigenvalue as well as the fission density in individual fuel pins. The terms fission density and pin power are used interchangeably and are meant to refer to the fission reaction rate within a given pin. For the fission densities, a comparison is established using the following error measurements:

the average relative error, the root mean square error, the mean relative error and the maximum error.

4.1.1 Average Relative Error

The average relative error (*AVG*) is a measure of the central tendency of the fission densities. It is thus an indicator of the overall accuracy of the power distribution of the coarse mesh solution. It is evaluated using the following formula:

$$AVG = \frac{\sum_{N} |RE_n|}{N} \tag{4.2}$$

where N is the number of fuel pins and RE_n is the relative error of pin n.

4.1.2 Root Mean Square Error

The root mean square error (*RMS*) measures the magnitude of the variations of the fission density relative errors. Larger errors weigh more than smaller errors in this measurement. It is evaluated from the following formula:

$$RMS = \sqrt{\frac{\sum_{N} RE_n^2}{N}} \tag{4.3}$$

4.1.3 Mean Relative Error

The mean relative error (*MRE*) is an average error in which the relative errors are weighed by the pin powers. This measurement thus gives greater importance to high power pins rather than low power pins. This choice is justifiable considering that in nuclear power reactors, the importance is given to high power pins because they are more likely to suffer failures. The mean relative error is evaluated using the following formula:

$$MRE = \frac{\sum_{N} |RE_n| \cdot p_n}{N.p_{avg}} \tag{4.4}$$

where p_n is the power in pin n and p_{avg} is the average power of all pins.

4.1.4 Notation

In this sub-section, the most common notations and acronyms used in the results tables are explained below.

k: core eigenvalue or core multiplication factor

RE: Relative Error

AVG: Average Relative Pin Power Error

UNC: Statistical Uncertainty in %

RMS: Root Mean Square Pin Power Error

MRE: Mean Relative Pin Power Error

MAX: Maximum Pin Power Error

CPU Time: Computational Time

RF: Number of Response Functions computed

{a,b,c}: Angular current expansion orders used in 2-D coarse mesh calculations:

- a^{th} order in space
- b^{th} order in the cosine of the polar angle
- c^{th} order in the azimuthal angle

$\{a,b,c\}^{\{a',b',c'\}}$: The subscript indicates that the {a,b,c} coarse mesh calculation was accelerated using a {a',b',c'} coarse mesh calculation

$\{a^S,b,c\}$: The subscript indicates that variable a was divided in S equal length segments on which a^{th} order expansions were performed

$\{a_1,a_2,b,c\}$: Angular current expansion orders used in 3-D coarse mesh calculations:

SFCC: Spatially flat cosine current approximation

$SFCC^S$: The subscript indicates that S equal length spatial segments are used on each face of a coarse mesh

PWR: Pressurized Water Reactor

BWR: Boiling Water Reactor

UO_2: Uranium oxyde

MOX: Mixed-oxyde

CANDU: Pressurized Heavy Water Reactor (Canada Deuterium Uranium)

Reference PC: The reference PC is a personal computer for which the computational time was evaluated. This PC is powered by an Intel Pentium 4 processor of 2.8 GHz with 1GB of RAM.

4.2 Small PWR

The first problem that was solved with the coarse mesh code was a small eigenvalue problem shown in Figure A.1. The problem is composed of four fuel assemblies, each with 8 fuel rods arranged in a 3 by 3 array, of two distinct types with light water coolant. The Type 1 assemblies contain 2% enriched UO_2 fuel, while the Type 2 assemblies contain 1% enriched UO_2 fuel. The diameter of each fuel rod is 0.82 cm and the rod pitch is 1.26 cm, which is representative of a PWR design. Specular reflective boundary conditions are imposed on all external surfaces of the problem. This problem was solved with a one energy group library and a continuous energy group library. The one group cross-sections and the material number densities are presented in Appendix A.

4.2.1 Continuous Energy

The initial work on the coarse mesh transport method was tested on the continuous energy version of the test problem.

4.2.1.1 Reference Solution

The MCNP4B2 code was used to perform a reference calculation of the core problem. Fifty million histories were simulated to estimate the eigenvalue and rod fission densities. The eigenvalue was found to be 1.17406 ± 0.00006, and the relative uncertainties in the rod fission density results were less than 0.1%. Continuous energy cross-sections at 300K from the ENDF/B-VI library were used in the Monte Carlo simulations of this problem.

4.2.1.2 COMET Solution and Analysis

The angular variables are approximated using the cosine-current approximation. Two representations of the spatial and energy dependence of the partial currents on the coarse mesh boundaries were considered. First, one and two equal-width spatial segments per coarse mesh edge were treated. In addition, both 12 and 45 energy bins were considered. The 12 bin set, which is specified in Table A.1, was chosen based on the coolant flux spectra in the Type 1 assemblies from a reference calculation. The 45 bin boundaries correspond to those of the 45-group production library of the lattice depletion code HELIOS (Casal *et al.*, 1991) version 1.6 (Guist, 2000) code. A modified version of the MCNP code was used to perform the response function calculations with two million histories in each simulation. It should also be noted that the coarse mesh results were obtained without performing any outer iterations. They were omitted to reduce the pre-computational time and remove the eigenvalue residual errors in the solutions. The fission source in the response function calculations was thus scaled using the reference eigenvalue. The convergence criterion of the iteration process on the pin

powers is 10^{-4}. The differences between the coarse mesh method and reference results, for each possible current representation, are summarized in Table 4.1.

Table 4.1: COMET Results for the Continuous-Energy Benchmark Problem

	SFCC / EB12 (%)	**SFCC^2 / EB12 (%)**	**SFCC / EB45 (%)**	**SFCC^2 / EB45 (%)**
RE k	-0.99	-1.03	-0.69	-0.57
AVG	1.27	1.09	0.81	0.33
RMS	1.55	1.34	1.03	0.43
MAX	2.79	2.26	2.58	0.88
# RF	24	24	90	90

EB: Number of Energy Bins

It can be seen that both the energy and spatial representation of the currents have a significant impact on the results. With 12 energy bins, increasing the number of spatial segments has no effect on the eigenvalue accuracy, but leads to a slight improvement in the fission densities. The accuracy of the results improves with the 45 bin approximation. The most detailed representation leads to highly accurate fission density results, however the error in the eigenvalue remains significant.

4.2.2 One Energy Group

The eigenvalue results for the continuous energy form of the small 2-D problem are much less accurate than those obtained in 1-D discrete ordinates problems, even without the application of variational techniques. It was conjectured that the simplistic treatment of the complex energy dependence was the cause of the error in the eigenvalue results. A one-group version of this problem was posed using cross-sections generated by a HELIOS calculation of the system. The actual values defining this benchmark can be found in the appendix.

4.2.2.1 Reference Solution

A reference calculation was performed on a quarter model of the system with five million histories to estimate the eigenvalue and fission density results. The eigenvalue was found to be 1.18471 ± 0.00021, and the relative uncertainties in the rod fission density results were less than 0.1%.

4.2.2.2 COMET Solution and Analysis

Initially, the cosine current approximation was again used to represent the angular variables. The current interface was later improved using a tensor product of Legendre polynomials. The results are also obtained without any outer iteration, which indicates that the fission source of the response functions was scaled using the reference eigenvalue. The pin powers were converged to a criterion of 10^{-4}. The differences between the coarse mesh and reference results for this problem are presented in Table 2 with one segment per coarse mesh edge and in Table 3 with two segments per coarse mesh edge.

Table 4.2: COMET Results for the One Group Problem (one segment per edge)

	{0,0,0} (%)	**{0,1,1} (%)**	**{0,2,2} (%)**	**{1,2,2} (%)**	**{2,2,2} (%)**	**SFCC (%)**
RE k	-0.89	-0.89	0.21	0.22	0.22	-0.16
AVG	1.04	1.04	0.28	0.12	0.13	0.27
RMS	1.08	1.09	0.35	0.16	0.15	0.32
MAX	1.60	1.64	0.67	0.35	0.31	0.66
# RF	2	8	18	36	54	2

For this problem, the coarse mesh results are in excellent agreement with the reference calculation. Therefore, it appears that a more sophisticated treatment of the

energy dependence of the partial currents is required to achieve highly accurate results in continuous energy problems. A great improvement in the fission densities is also observed by replacing the cosine-current approximation by the tensor product of Legendre polynomials. Second order expansions in both angles, {0,2,2}, are fairly equivalent to the cosine-current approximation. Adding the linear spatial expansion reduces considerably the fission density average error (from 0.28% to 0.12%) and the maximum error (from 0.67% to 0.35%). The second order spatial term adds very little to the solution. The following table illustrates the effect of further spatial refinement by segmenting the coarse mesh edge in two equal width segments.

Table 4.3: COMET Results for the One Group Problem (two segments per edge)

	$\{0^2,0,0\}$ (%)	**$\{0^2,1,1\}$ (%)**	**$\{0^2,2,2\}$ (%)**	**$\{1^2,2,2\}$ (%)**	**$\{2^2,2,2\}$ (%)**	**$SFCC^2$ (%)**
RE k	-0.97	-0.98	-0.07	-0.06	-0.06	-0.16
AVG	0.91	0.82	0.13	0.09	0.09	0.12
RMS	0.95	0.84	0.15	0.10	0.11	0.14
MAX	1.25	1.18	0.28	0.16	0.18	0.26
# RF	4	16	36	72	108	2

The addition of spatial segments improves greatly the accuracy of the eigenvalue for the cases with second order angular expansions. The fission density accuracy is also improved considerably. The average error of the linear spatial expansion is reduced from 0.12% to 0.09% and the maximum error is reduced even more significantly going from 0.35% to 0.16%. Once again, the addition of second order spatial expansion has little to no effect on the results. However, it should be noted given a larger core, the second order spatial term might become much more important.

4.2.3 Spectral Mapping

Comparing the results of Sections 4.1.1 and 4.1.2, it is obvious how important the energy variable is in obtaining an accurate coarse mesh solution. The one-group approximation was shown to work considerably well, and later on the multigroup approximation will be shown to be as effective. However, when trying to approximate the continuous-energy calculation with equally distributed energy bins, a great number of response functions must be used. In Section 4.1.1, 45 energy bins were used to attempt to reproduce the continuous-energy results with limited success on the eigenvalue. In the next section, this method will be pushed even further on a more realistic benchmark. In this section, the spectral mapping method discussed in Section 3.8.1 is tested on the small PWR benchmark.

4.2.3.1 COMET Solutions and Analysis

The initial spectral map was computed by averaging the surface current obtained from infinite lattice calculations performed on each assembly type. This initial spectrum corresponds to the 0^{th} order energy expansion. The spectral map was then shifted up to Legendre polynomials of 3^{rd} order. The spatial and angular variables were all expanded up to 2^{nd} order. The results are presented in Table 4.4.

Table 4.4: Spectral Mapping Results with {2,2,2} Expansion

	SM 0^{th} (%)	**SM 1^{st} (%)**	**SM 2^{nd} (%)**	**SM 3^{rd} (%)**
RE k	-0.25	-1.04	-1.18	-0.42
AVG	3.63	1.71	1.50	0.81
RMS	4.92	2.26	1.86	0.98
MAX	10.67	5.32	4.21	1.91
# RF	54	108	162	216

SM: Spectral Mapping Expansion Order

The coarse mesh calculation with the initial spectrum improves the eigenvalue greatly but worsens the fission densities considerably. The fission densities are greatly improved by increasing the spectral map order, however the eigenvalue result tends to oscillate. The spectral mapping method shows some potential. However, significant work is required to achieve acceptable accuracy. The choice of the initial spectrum seems to be of utmost importance. It is well known that infinite lattice calculations do not produce the correct energy spectrum (Stamm'ler and Abbate, 1983). The spectral map should thus be representative of the core by a buckling correction or a leakage adjustment. The scope of this work goes beyond the objectives of this thesis, In the next two sections, we present the continuous energy results for the case in which response functions are generated by sampling from a unit surface source that is distributed uniformly over each energy bin. This section is then followed by results based on multigroup response function calculations.

4.3 CANDU-6 - 3 by 4

The benchmark problem consists of 12 standard 37-pin CANDU-6 natural uranium fuel bundles placed in a 3 by 4 arrangement with periodic boundary conditions, as shown in Figure A.2. The geometrical configuration is based on previous work reported in Rahnema *et al* (2000).

The test cores are made up of three unique coarse meshes that are either voided or cooled. Each mesh is represented by the fuel bundle at a given average fuel burnup. The three levels of burnup considered are denoted by high (H), mid (M) and low (L) and correspond to 8737.19 MWd/t, 4086.27 MWd/t and 1465.36 MWd/t, respectively. They were arbitrarily chosen as being the midpoints among the 12 fuel bundles over different burnup ranges at the third axial plane of a reference reactor core (Rahnema *et al*, 2000). Considering the emphasis attributed to the analysis of the loss of coolant scenarios for the CANDU-6 reactors, three different coolant states were simulated: the cooled (non-

voided) checkerboard voided and fully voided configurations. The material temperature and densities in the cooled case corresponds to those for the hot operating condition in CANDU-6 core as specified in Rahnema *et al* (2000). The checkerboard voided configuration corresponds to voiding the odd-numbered cells in rows J and L and the even-numbered cells in row K. The fully voided case corresponds to voiding all of the channels. The material densities and temperatures remain the same as the cooled case.

4.3.1 Reference Solution

The reference solutions were computed using MCNP-4B2 with the ENDF/B-VI continuous-energy library developed at the hot operating temperatures. The solutions consist of the eigenvalue and the fuel rod fission densities, which are normalized to the total number of pins. Our convergence criterion for the reference solutions was to obtain a relative standard deviation of less than 0.1% for all rod fission densities. This required simulating 120 million active particles using a converged source distribution. The cooled case eigenvalue is 1.01800 ± 0.00004, the voided case eigenvalue is 1.02418 ± 0.00004 and the checkerboard case eigenvalue is 1.03334 ± 0.00004.

4.3.2 COMET Solutions and Analysis

The response function calculations for all of the cases were performed with half a million particles. These response functions were obtained using the 45 and 190 energy bin structures that correspond to the ones used by the lattice depletion code HELIOS. Outer iterations were omitted from these calculations to reduce the number of response functions. The reference eigenvalue was thus used to scale the fission source in the fixed source calculations. The convergence criterion of the pin powers was set to 10^{-4}. Each response function calculation requires 2-3 minutes of computational time on the reference PC. The 45 energy bin structure for the cooled configuration required 270 response

functions, while the 190 structure needed 1140 response functions. The results are presented in Table 4.5.

Table 4.5: COMET Results for the 3 by 4 CANDU-6 Benchmark

	Cooled		**Voided**		**Checkerboard**
	SFCC[2] / EB45 (%)	**SFCC[2] / EB190 (%)**	**SFCC[2] / EB45 (%)**	**SFCC[2] / EB190 (%)**	**SFCC[2] / EB45 (%)**
RE k	-0.66	-0.28	-0.75	-0.44	-0.70
k UNC	0.05	0.04	0.05	0.04	0.05
AVG	0.48	0.45	0.48	0.45	0.51
RMS	0.61	0.57	0.59	0.56	0.63
MAX	1.68	1.58	1.65	1.55	1.79

For the 45 energy bin structure, in the cooled case, the eigenvalue relative error between MCNP and the coarse mesh method is -0.66% with a standard deviation of 0.05%. The pin power average error is 0.48%, and the maximum error is 1.68%. The pin power uncertainty ranged from 0.18% (outer pins) to 0.20% (inner pins). The maximum relative errors occur near the center of the fuel assemblies. However, the absolute errors in the pins in this region are comparable to all the others. The checkerboard voided configuration corresponds to the case when one of the two primary coolant loops is ruptured. The eigenvalue error in this scenario is -0.70% with a one-sigma uncertainty of 0.05%. Once again, the pin power errors are small, with an average of 0.51% and a maximum error of 1.79%, with a pin fission density uncertainty ranging from 0.17% to 0.20%. The error distribution in this configuration is very similar to that of the cooled configuration, indicating that the presence of void does not affect the accuracy of the method. The fully voided configuration is attributed to a rupture of both coolant loops. The results indicate that the method remains very accurate for the individual pin fission density but the eigenvalue accuracy deteriorates slightly to -0.75%. As seen from Table

4.5, the root mean square errors are around 0.6%. The average error of around 0.5% is very close to the root mean square error indicating a smooth distribution of errors centered about the mean value. The mean relative error, which is a pin power weighted, is also close to the average error indicating a uniform pin error distribution across the entire configuration.

The eigenvalue errors observed in Table I with the 45 bins energy structure seem quite large for a transport calculation. A great deal of the eigenvalue error can be once again attributed to the selection of the energy structure of bins (45) used in this study. In order to support this claim, calculations involving a greater number of energy bins (190) were performed. We see a much better agreement between the reference solution and the coarse mesh solution when the 190 bin energy structure is used. The eigenvalue error has dropped to -0.27% with a one-sigma statistical uncertainty of 0.04% for the cooled case. For the voided case the error is reduced to $-0.44\% \pm 0.04\%$. Even though better accuracy is obtained for the eigenvalue, the accuracy gain in the pin power distribution is minimal. The errors are slightly reduced but not enough to justify using more energy bins. The one-sigma statistical uncertainties range from 0.14% to 0.16%. The reduction in the statistical uncertainties is simply due to the presence of more response functions representing a larger number of simulated particles.

The coarse mesh calculation for the 45 energy bin structure took 26 seconds while the 190 energy bin structure needed 450 seconds to converge the pin power distribution to 10^{-5} on the reference PC. As mentioned previously, the outer iterations were avoided, thus removing the residual eigenvalue errors, in order to isolate as best as possible the impact of the partial current representation on the solution accuracy.

4.4 CANDU-6 - 4 x 4

This benchmark is a one row extension of the previous 3 by 4 CANDU6 benchmark problem as illustrated by Figure A.3. It is composed of 16 fuel assemblies of

three varying burnups in a 4 by 4 lattice with periodic boundary conditions. This configuration is more representative of the CANDU-6 reactor when performing coolant voiding analysis. The cooled and fully voided configurations were simulated.

4.4.1 Reference Solution

As with the prior benchmark, reference solutions were obtained using MCNP4B2 with the hot operating temperature continuous-energy cross-section files. The simulation required 160 million active particles on a converge source to obtain fission densities results with an uncertainty below 0.1%. The cooled case eigenvalue is 1.01833 ± 0.00004 and the voided case eigenvalue is 1.03377 ± 0.00004.

4.4.2 COMET Solutions and Analysis

Response functions were generated with a modified version of MCNP using ½ million and 5 million particles to study the effect of the statistical uncertainty on the void reactivity coefficient, eigenvalue and fission densities. Once again, the outer iterations were omitted and the reference eigenvalue was used to scale the fission source of the response function calculations. Also, a 10^{-4} convergence criterion was used on the pin powers. The following table summarizes the results obtained with the coarse mesh method.

Table 4.6: COMET Results for the 4 by 4 CANDU-6 Benchmark

	SFCC[2] / EB45 ½ million particles		**SFCC[2] / EB45 5 million particles**	
	Cooled (%)	**Voided (%)**	**Cooled (%)**	**Voided (%)**
RE k	-0.63	-0.70	-0.68	-0.73
k UNC	0.05	0.05	0.02	0.02
AVG	0.7	0.7	0.7	0.7
RMS	0.8	0.8	0.8	0.8
MAX	2.5	2.4	2.3	2.1

When comparing the cases with ½ million particles and 5 million particles, very little to no difference exists in the fission densities average errors and root mean square errors. However, a noticeable change is observed in the maximum errors, which drop from 2.5% to 2.3% in the cooled case and from 2.4% to 2.1% in the voided case. The individual pin power uncertainties range from 0.17% to 0.21% for the ½ million particle cases and from 0.10% to 0.12% for the 5 million particle cases, thus indicating that all variations are within the one standard deviation statistical uncertainties. Small variations are also observed for the eigenvalues but these are well within the 95% confidence interval ensuing from the statistical uncertainty.

The 4 by 4 CANDU-6 benchmark problem can also be used to estimate the reactors void reactivity coefficient which is evaluated by the following formula:

$$\rho_{void} = \left(\frac{1}{k_{cooled}} - \frac{1}{k_{voided}} \right) \cdot 1000 \tag{4.5}$$

where ρ_{void} is the void reactivity coefficient in mk, k_{cooled} is the eigenvalue of the cooled case and k_{voided} is the eigenvalue of the voided case. The results of the coarse mesh calculations are compared to the result obtained from the MCNP reference results and are presented in Table 4.7.

Table 4.7: Void Reactivity Coefficient Results

	Reference (mk)	**Coarse Mesh (mk)**	**Absolute Error (mk)**
SFCC[2] / EB45 ½ million particles	14.6 ± 0.1	14.1 ± 0.7	0.5 ± 0.7
SFCC[2] / EB45 5 million particles		14.5 ± 0.2	0.1 ± 0.2

In Table 4.7, the results showed no indications for the need of using more particles, however when computing the void reactivity coefficients, the importance of

low statistical uncertainty is highlighted. With ½ million particles per response function, the void reactivity coefficient is found to be 0.5 m*k* off the reference solution with a standard deviation of 0.7 m*k*. Using 5 million particles, the absolute error is reduced to 0.1 m*k* with a one-sigma uncertainty of 0.2 m*k*. Since the void reactivity calculation is based on a difference between the un-voided (cooled) and voided eigenvalue results, good results can still be obtained even thought the eigenvalues themselves are not very accurate. The important thing is that the method is consistent. The nature of the void reactivity coefficient expressed in equation (4.5) necessitates very good accuracy on the eigenvalue, because it is comparing very small changes in reactivity. It is thus imperative that the amount of particles used in the response function calculation be taken into account when performing this type of calculation.

When the previous results were computed, the Legendre polynomial expansion of the interface current was not yet available. In an attempt to once again prove the gain obtained by replacing the cosine-current approximation, the cooled case with ½ million particles was reevaluated. Table 4.8 presents results with second order expansions in space and angles.

Table 4.8: COMET Results for the CANDU-6 Benchmark with Legendre Expansion

	SFCC^2 / EB45* (%)	**{0^2,2,2} (%)**	**{2^2,2,2} (%)**
RE k	-0.63	-0.63	-0.64
k UNC	0.05	0.05	0.05
AVG	0.7	0.3	0.3
RMS	0.8	0.4	0.4
MAX	2.5	1.1	1.2

*These results are reinserted from Table 4.6 to facilitate comparison.

A second order expansion in angle with two spatial segments is more than sufficient to greatly improve the fission densities of the 4 by 4 CANDU-6 benchmark problem but has no effect on the eigenvalue. The average error is reduced from 0.7% to 0.3% and the maximum error goes from 2.5% to 1.1%. The additional spatial expansions have no effect on the results. The fission densities uncertainties range from 0.18% to 0.21% in all cases.

4.5 CANDU-6 - ¼ Core

The 2-D quarter core CANDU-6 benchmark problem is representative of a simplified upper right hand corner of an operating CANDU-6 reactor as shown in Figure A.4. The 95 fuel assemblies are exact representations of 37 fuel elements CANDU-6 bundles shown in Figure A.5. Reflective boundary conditions are used on the west and south surfaces and vacuum elsewhere. The author is well aware that rotational periodic boundary conditions would have been more appropriate for an accurate representation of the reactor. However the code (MCNP) used to perform the reference solution did not readily permit such a calculation. Four different burnups (800 kWd/t, 2700kWd/t, 5000 kWd/t, 7000 kWd/t) were chosen and distributed according to an operating core burnup map as illustrated by Figure A.4 and Table A.4. Depletion calculations were performed on a single bundle infinite lattice calculation using the lattice depletion code HELIOS from which two group cross-sections were obtained. All fuel elements are represented by a single set of cross-sections for each burnup. A separate set of cross-sections is also used for the moderator, the coolant and the cladding. The gap normally filled with gas was considered to be a void in the HELIOS calculation.

4.5.1 Reference Solution

A two group MCNP reference solution was obtained using 2.1 billion active particles on a previously well converge source. The core has an eigenvalue of 1.01943 ±

0.00001 with average and maximum pin power uncertainties of 0.06% and 0.10%, respectively.

4.5.2 COMET Solutions and Analysis

Low-order response functions were computed using a modified version of MCNP. Each response function was computed using 3 million particles which took about 6 minutes for fuel assemblies and 1 minute for moderator assemblies. Three different fission source scaling values were used to generate response functions: 0.9, 1.0 and 1.1. The eigenvalues were computed using the neutron balance method, presented in Section 2.2.3.1, with an initial guess of 1.0. The pin powers convergence criterion was set to 10^{-4}. The results of the coarse mesh method are shown in Table 4.9.

Table 4.9: COMET Results for the ¼ Core CANDU-6 Benchmark

	{0,0,0} (%)	**{1,0,0} (%)**	**{2,2,2} (%)**
RE k	-0.60	0.41	0.09
AVG	3.0	0.5	0.5
RMS	3.6	0.7	0.6
MRE	2.8	0.5	0.4
MAX	9.2	2.4	2.0
CPU time (s)	2.0	2.9	31.7

With low-order expansion of the angular current at the interface of the fuel cells, very good accuracy is obtained in the ¼ core benchmark problem. The eigenvalue error is 0.09% with a standard deviation of about 0.03%. The pin power average error is 0.5% with a maximum error of 2.0%. The uncertainties associated with the pin power are all around 0.3%. It is also interesting to notice that the 0^{th} order expansion in angles with 1^{st} order expansion in space yields a very accurate power map. The average pin power error for that case is 0.5% with a maximum pin error of 2.4%. The computational time of the

2^{nd} order calculation (last column) is around 32 seconds. However, the coarse mesh method also allows for seamless low-order acceleration from low-order solutions. The results of this acceleration are presented in Table 4.10.

Table 4.10: Low-Order Acceleration on the ¼ Core CANDU-6 Benchmark

	$\{2,2,2\}^{\{0,0,0\}}$	$\{2,2,2\}^{\{1,0,0\}}$
CPU time (s)	16.4	18.3

By using the 0^{th} order, the 2^{nd} order results are greatly accelerated. The solution converges to the same eigenvalue and pin power results that were presented in Table 4.9 but in half the time. The acceleration with the {1,0,0} expansion order does not offer any gain over the 0^{th} order expansion.

4.6 2-D C5G7 MOX Benchmark

This benchmark problem was described in Chapter 1. Lewis et al (2003) published a reference solution using the Monte Carlo code MCNP with many million particles with the ensuing seven group cross-sections that were used. This reference solution will be used to compare the coarse mesh results. This section is separated in two parts: first, a spatial analysis is performed to determine which of segmentation and polynomial expansion is the way to go for the spatial variable and second, the two methods for evaluating the eigenvalue presented in Chapter 2 are compared. All results presented in this section used convergence criteria of 10^{-4} for both the eigenvalue and the pin powers.

4.6.1 Spatial Analysis

The spatial analysis consists of comparing segmentation, high order expansion and a mix of both methods. In this analysis, the angular expansion was kept fixed to 2nd order in both the cosine of the polar angle and the azimuthal angle (Forget and Rahnema, 2005d).

4.6.1.1 COMET Solutions and Analysis

Response functions were generated with 3 million particles per calculation up to 6th order in space. The reference eigenvalue was used to scale the fission source in an effort to eliminate the residual eigenvalue uncertainty and reduce the number of pre-computations. Each fuel assembly was considered to be a coarse mesh. There are thus three unique coarse meshes, namely: the UO2 assembly, the MOX assembly and the moderator assembly, each of size 21.42 cm by 21.42 cm. Each fuel assembly calculation took about 12 minutes on the reference PC, while each moderator assembly calculation took about 3 minutes. Table 4.11 summarizes the results obtained with increasing spatial order.

Table 4.11: High Order Spatial Expansion on the 2-D C5G7 MOX Benchmark

	{0,2,2} (%)	**{1,2,2} (%)**	**{2,2,2} (%)**	**{3,2,2} (%)**	**{4,2,2} (%)**	**{6,2,2} (%)**
RE k	-2.79	-0.04	0.05	0.05	0.05	0.05
AVG	12.0	1.1	0.7	0.6	0.5	0.4
RMS	17.3	2.3	2.1	0.9	0.6	0.5
MAX	107.9	12.1	7.3	6.9	2.8	2.2
# RF	189	378	567	756	945	1323

Increasing the spatial order beyond second order has little to no effect on the eigenvalue results. However, a constant diminishing trend can be observed in the fission

densities results. With a 6th order spatial expansion, the average error is 0.4%, the root mean square error is 0.5% and the maximum error is 2.2%. In all cases, the pin power average uncertainties were around 0.5%.

Table 4.12 compares the results obtained for a given number of response functions with a different number of segments per edge. The total number of response functions is fixed at 756. For one segment per edge, this number corresponds to a third order spatial expansion. Once again the angular expansions are held fixed at quadratic. For two segments per edge, the spatial expansion is limited to 1st order and for the four segments per edge case, the spatial expansion is of 0th order. It should also be noted that taking full advantage of the symmetry of the fuel assembly would reduce the total number of response functions required to 630 for the calculation for the cases where segmentation is used. However, the added complexity in dealing with these response functions is very error prone and was omitted in this analysis.

Table 4.12: Spatial Analysis on the 2-D C5G7 MOX Benchmark

	{3^1,2,2} (%)	**{1^2,2,2} (%)**	**{0^4,2,2} (%)**
RE k	0.05	0.05	-0.25
AVG	0.6	0.6	1.3
RMS	0.9	1.1	1.9
MAX	6.9	8.4	12.0
# RF	756	756*	756*

*Could be reduced to 630 if one takes into account all possibilities of symmetry. The complexity is however much greater.

The results in Table 4.12 show once again the importance of the method in which the spatial variable is treated. All three approximations have a dimension of 4 along each segment; the difference thus relies on the quality of the approximation. A piecewise

approximation on uniform segments, $\{0^4,2,2\}$, is not sufficient to obtain accurate results with the least pre-computation time. The best results are obtained for higher order spatial expansion with no segmentation. The average pin power error in this case is 0.6%, the root mean square error is 0.9% and the maximum error is 6.9%. The piecewise linear approximation, $\{1^2,2,2\}$, also has a average fission density error of 0.6%, but its maximum and root mean square error is a bit larger. The approach of combining both segmentation and polynomial expansion yields good results, but uniform segmentation may not be the best approximation; one might consider segmenting at the zeros of the Legendre polynomial of appropriate degree. Determining the appropriate segmentation may require some analysis by the user as is the case with any numerical transport meshing scheme.

However, this analysis was performed in hopes that it would be shown that segmentation could be replaced entirely by a higher order spatial expansion, which was the case. The complexity of using spatial segmentation in three dimensions with the additional spatial variable would have been reason enough to consider high order spatial expansion sufficient. Spatial segmentation will thus be omitted from the three dimensional results in the next chapter.

4.6.2 Eigenvalue Method

In this section, the two eigenvalue evaluation techniques discussed in Chapter 2 are compared.

4.6.2.1 COMET Solutions and Analysis

A response function database was generated for the 7-group PWR assemblies found in the MOX benchmark for three different values of k (1.0, 1.1 and 1.2). The response functions, generated with a modified version of MCNP4C using 1.5 million particles, on two segments per edge have Legendre polynomial expansion orders of 3, 2,

and 4 for the spatial variable, polar angle and azimuthal angle, respectively. Once again, the same three unique coarse meshes were defined as in the previous analysis. Table 4.13 presents the results comparing both eigenvalue evaluation method with interface current expansions of $\{3^2,2,4\}$. Since the neutron balance method (NBM) only requires a single initial guess, while the discontinuous normalization method (DNM) requires two, the initial guess of the NBM technique was chosen as the average of the two points of the DNM to ensure a consistent comparison. The initial guess for the NBM was chosen to be 1.15, while the bounds of the DNM were chosen to be 1.1 and 1.2.

Table 4.13: Eigenvalue Method Comparison with $\{3^2,2,4\}$ Expansion

	NBM (%)	**DNM (%)**
RE k	-0.03	0.05
AVG	0.4	0.4
RMS	0.5	0.5
MAX	1.8	1.5
Norm. Cst	1.0003	1.0000
CPU time (s)	149	146

NBM: Neutron Balance Method (Section 2.2.3.1)
DNM: Discontinuous Normalization Method (Section 2.2.3.2)
Norm. Cst: Normalization Constant of equation 2.17

Both eigenvalue estimates (via NBM and DNM) are in close agreement with the reference MCNP results. The difference in the pin power distribution between the two methods is within one-sigma of the statistical uncertainty of about 0.25% on the average. The corresponding statistical uncertainty in the eigenvalue is of the order of 0.04% and 0.01% for the NBM and DNM, respectively. The computational times for the two methods are comparable as seen from the table. However, the new method eliminates the need for tallying (pre-computing) the production response function and the ensuing calculation of the absorption response functions. Therefore the new method requires less

pre-computation time and storage than the NBM. However, the acceleration technique presented in Chapter 3, makes the NBM method substantially faster as can be seen in Table 4.14.

Table 4.14: Low-Order Acceleration of the NBM

	$\{2^2,2,2\}^{\{0,0,0\}}$	$\{3^2,2,4\}^{\{0,0,0\}}$	$\{3^2,2,4\}^{a}$
CPU time (s)	27.1	89.9	67.9

a: $\{2^2,2,2\}^{\{0,0,0\}}$ (incremental acceleration)

By adding the 0^{th} order acceleration to the $\{3^2,2,4\}$ calculation, the coarse mesh calculation takes only 90 seconds. Incremental acceleration from 0^{th} order to 2^{nd} order to $\{3^2,2,4\}$ cuts the computational time to 68 seconds on the reference PC. Implementing this acceleration scheme in the discontinuous normalization method is not as trivial as in the neutron balance method. Many variations have been implemented, but none that are as successful.

4.7 Full Core PWR

A PWR full core was constructed using the uranium oxide (UO_2) and mixed oxide fuel assemblies (MOX) of the C5G7 problem. The core is composed of 48 uncontrolled UO_2 assemblies, 21 controlled UO_2 assemblies, 28 uncontrolled MOX assemblies and 24 controlled MOX assemblies. The core geometry is presented in Figure A.6. The core was deliberately build with 1/8 symmetry to minimize the time requirement for the Monte Carlo reference solution. The purpose of this benchmark is to determine the efficiency of the coarse mesh method for solving a full-core problem. The results presented in this section used convergence criteria of 10^{-5} for both the eigenvalue and the pin powers.

4.7.1 Reference Solution

The same 7-group cross section library as in the C5G7 problem was used to perform the reference MCNP and COMET calculations. The reference solution was obtained by performing MCNP5 calculation in $1/8^{th}$ of the core using 1.6 billion active particles with a converge source. As an illustration of this solution, a quarter-core representation of the pin power distribution is presented in Figure A.7. The reference eigenvalue of the core is 1.12623 ± 0.00002. The average pin power uncertainty is 0.11% with a maximum uncertainty of 0.23%.

4.7.2 COMET Solutions and Analysis

Since this problem is an extension of the C5G7 benchmark, the response functions used previously in Section 4.4.2.1 can be used once again for this problem. However, two additional coarse mesh types were added to the database. These two additional coarse meshes represent the addition of control rods in the two distinct fuel assemblies. Table 4.15 summarizes the results for the full 2-D core (see Figure A.6 for the core configuration). The eigenvalue was computed using the neutron balance method with an initial guess of 1.0.

Table 4.15: COMET Results for the Full Core PWR Benchmark

	$\{2^2,2,2\}$ (%)	**$\{3^2,2,4\}$ (%)**
RE k	-0.01	-0.01
AVG	0.5	0.4
RMS	0.4	0.4
MAX	4.1	1.7
CPU time (min)	23.0	112.3

The COMET eigenvalue is very accurate as seen from Table 4.15. With both interface current expansion order, the eigenvalue error is -0.01% with an uncertainty of 0.01%. The pin power uncertainty associated with the coarse mesh calculations is roughly 0.25%. Increasing the expansion order has little effect on the average and root mean square errors, however the maximum error is reduced from 4.1% to 1.7%. This gain in accuracy always comes with a price; the higher order calculation takes approximately five times longer than the second order calculation. Both calculations can be accelerated by using low-order solutions as the initial guess. The results of this acceleration are presented in Table 4.16.

Table 4.16: Low-Order Acceleration Results on the Full Core PWR

	$\{2^2,2,2\}^{\{0,0,0\}}$	$\{3^2,2,4\}^{\{0,0,0\}}$	$\{3^2,2,4\}^{a}$
CPU time (min)	13.6	62.7	37.7

a: $\{2^2,2,2\}^{\{0,0,0\}}$ (incremental acceleration)

By performing a 0^{th} order calculation beforehand, both interface current representation of Table 4.16 are accelerated substantially. The computational time for the {2,2,2} case is reduced from 23 minutes to 13.6 minutes, while the {3,2,4} case goes from 112.3 minutes to 62.7 minutes. Incremental acceleration reduces the high order calculation even more requiring only 37.7 minutes to converge to the same solution.

4.8 Updated HAFAS Benchmark

An extended version of the BWR HAFAS diffusion benchmark mentioned in Section 1.2.3.4 and shown in Figure A.8 was proposed (Breen and Forget, 2005). The fuel assemblies of the original benchmark were composed of 16 homogeneous regions and the control blade was modeled as a homogenous entity. The fuel assembly was replaced by an exact representation of the GE9 fuel assembly (Kelly, 1995) and a heterogeneous

control blade model was developed. Both fuel assemblies are shown in Figures A.9 and A.11.

HELIOS (Casal *et al*, 1991) calculations were performed on the GE9 assembly to generate three energy group cross sections for the 12 fuel types, the control rods, the control sheath, the coolant, the moderator and the cladding. Cross sections were obtained at three different void levels (0%, 40% and 70%) and two different burnups (A: 0.1 MWd/t and B: 17 MWd/t).

4.8.1 Reference Solution

A multi-group MCNP calculation was performed to serve as a reference solution for the core configuration illustrated in Figure A.10. A simulation on half the problem (diagonal symmetry) was performed using 230 000 particles per cycle over 6000 active cycles (500 cycles were skipped to converge fission source). The reference core eigenvalue is 1.03592 ± 0.00002. Fission densities in all fuel pins were also tallied. The average fission density uncertainty is 0.09% with a maximum uncertainty of 0.18%.

4.8.2 COMET Solutions and Analysis

Response functions were generated for each unique coarse mesh for an angular current expansion of fourth order in space, second order in the cosine of the polar angle and third order in azimuthal angle. Each simulation was performed using 5 million particles. New features were added to COMET to reduce the number of response functions needed to represent the problem: 1) a new axis system was introduced to take full advantage of the diagonal symmetry of the GE9 fuel assembly (Figure A.12), 2) a coarse mesh rotation feature was added to position the fuel assemblies correctly in the core, and 3) the odd order moments of the cosine of the polar angle were dropped. The polar angle was chosen as coming out of the 2-D plane, thus in a 2-D problem its shape must be symmetric. The total number of pre-computations is 5760 response functions for

the fuel meshes and 240 response functions for the reflector mesh, which take approximately 15 minutes and 5 minutes each on the reference PC, respectively. The COMET results obtained from an initial eigenvalue guess of 1.0 are presented in Table 4.17.

Table 4.17: COMET Results for the Updated HAFAS Benchmark Problem

	{2,2,2} (%)	**{3,2,2} (%)**	**{4,2,2} (%)**	**{3,2,3} (%)**	**{4,2,3} (%)**
RE k	-0.21	-0.12	-0.12	-0.13	-0.13
AVG	3.0	2.0	2.0	1.8	1.7
RMS	3.5	2.3	2.3	2.1	2.0
MRE	3.0	2.0	1.9	1.7	1.7
MAX	10.3	7.4	7.0	7.1	6.5
CPU Time (s)	151	238	375	394	593

The results of Table 4.17 with low-order expansion are not nearly as good as with the other two types of reactors. The fission density errors for PWR (Table 4.15) and CANDU (Table 4.9) calculations were always around 0.5 % with a maximum error around 2.0% for low-order angular current expansions. However, the higher discrepancy of the BWR results was to be expected when one considers the high level of heterogeneity that is present in the BWR. The GE9 bundle of Figure A.11 is composed of 10 different enrichments of the fuel pins and two different types of enrichment in the gadolinium pins in comparison to 3 or 4 different fuel types for the other reactors. The presence of the control blade is also a major hinder on accuracy. The meshes are defined in such a way that the control blade lies on the outer surface of a mesh, thus influencing greatly the surface angular current on which Legendre polynomial expansions are performed. With an expansion order of {4,2,3}, the eigenvalue differed from the reference solution by 0.13% with a statistical uncertainty of 0.01%. The fission density

errors differed on average by 1.7% with a maximum of 6.5%. The statistical uncertainties of the pins were on average 0.2% with a maximum of 0.4%. The larger errors are all found in pins in close vicinity to the control blades. Higher order expansions might be necessary to correctly represent the surface current along the edge of the controlled meshes. The clever use of segmentation at the edge of the blade might also prove to be a valid option. With no acceleration, the {4,2,3} expansion took 593 seconds to converge to a criterion of 10^{-4} on both the eigenvalue and the surface currents. Using the incremental acceleration obtained by performing a {0,0,0} expansion followed by a {2,2,2} expansion and finally followed by the {4,2,3} expansion, the computational time is reduced to 250 seconds.

CHAPTER 5

3-D RESULTS

Three dimensional results are presented in this section. The first 3-D test problem is an extension of the small PWR benchmark presented in Section 4.2 (Forget and Rahnema, 2005b). Two distinct configurations were developed. The method is then tested on the more rigorous 3-D C5G7 MOX benchmark problem that was described in Chapter 1. Supplemental information on the benchmarks and the results is included in Appendix B.

5.1 Small PWR

5.1.1 Configuration 1

This is a one-group problem with specular reflective boundary condition on five of the six surfaces and vacuum on the other as illustrated in Figures B.1 and B.2. The one-group cross-sections are the same as those of the 2-D benchmark problem described in Section 4 and can be found in appendix A. The benchmark problem is composed of nine fuel assemblies, each with 8 fuel rods arranged in a 3 by 3 array, of two distinct types with light water coolant. The first type contains 2% enriched UO_2 fuel, while the second type contains 1% enriched fuel. The remaining assemblies contain light water and act as a reflector. The system is a cube measuring 11.34 cm per side.

5.1.1.1 Reference Solution

The reference solution was generated with a one-group MCNP simulation. The reference solution was obtained using five million histories, which yielded an eigenvalue of 0.9255 ± 0.0002. Individual pin fission densities were also tallied, all with relative errors smaller than 0.15%. The reference solution took 27 minutes on the reference PC.

5.1.1.2 COMET Solutions

Each coarse mesh was chosen as being a cube of 3.78 cm per side (1/27 of the system). Initially the code was tested using a spatially flat cosine current approximation (SFCC), but eventually the polynomial expansion of the surface currents was implemented using continuous Legendre polynomials. The results of both phase space representation are found in Table 5.1.

Table 5.1: COMET Results for Configuration 1

	SFCC (%)	**{2,2,2,2} (%)**
RE k	0.3	0.3
AVG	0.6	0.3
RMS	0.8	0.4
MAX	2.9	0.9

As expected, replacing the SFCC by the orthogonal expansion reduces the pin power errors. However, the approximation of the eigenvalue remains unchanged. The cosine-current distribution is a good approximation in the presence of water gaps, which is usually the case in 2-D for conventional fuel assemblies. However, the addition of the third dimension leads to also assuming that the current is cosine distributed along the coarse-mesh edge that cuts through the fuel pins. Using a 2^{nd} order Legendre polynomial expansion reduces the pin power average error to 0.3% from 0.6%. The root mean square error is also reduced from 0.8% to 0.4%. The greatest improvement is in the maximum pin power error which dropped from 2.9% to 0.9%. When this problem was solved, the propagation of statistical uncertainty was omitted from the 3-D code to facilitate the development work. Given the pre-computed response functions, the 2^{nd} order expansion results were obtained in 20 seconds on the reference PC. The inner convergence criterion

on the fission densities was 10^{-4}. No outer iterations were performed in this case, meaning that the response functions were generated using the reference eigenvalue. Each response function calculation took roughly 3 minutes.

5.1.2 Configuration 2

The second configuration is once again based on the 1 group cross-sections of Section 4. This benchmark, illustrated in Figures B.3 and B.4, has specular reflective boundaries on three of the six surfaces and vacuum elsewhere. It is composed of 16 fuel assemblies, each with 8 fuel rods arranged in a 3 by 3 array, of the same two distinct fuel types as previously. The entire system forms a cube of 22.68 cm per side.

5.1.2.1 Reference Solution

The reference solution was generated with a one-group MCNP simulation. The reference solution was obtained using 22 million histories, which yielded an eigenvalue of 0.9469 ± 0.0001. Individual pin fission densities were also tallied, all with relative errors smaller than 0.4%. The reference solution took about a day on the reference PC.

5.1.2.2 COMET Solutions

Once again, the coarse meshes were chosen to be cubes of 3.78 cm per side. The system is composed of three unique coarse meshes for which response functions were generated with 2 million particles. The response functions of the fuel assemblies were evaluated for three different fission scaling factors (0.9, 1.0, 1.1) and took on average 2 minutes each on the reference PC. The coarse mesh results are presented in Table 5.2.

The second order calculation of the second configuration yielded an eigenvalue error of -0.16% with an average pin power error of 0.3%. The maximum error was 1.3%. The coarse mesh calculation took 160 seconds with a convergence criterion of 10^{-4} for both the inner and outer iterations. The average pin power uncertainty was 0.2%.

Table 5.2: COMET Results for Configuration 2

	{2,2,2,2} (%)
RE k	-0.16
AVG	0.3
RMS	0.4
MAX	1.3

5.2 3-D C5G7 MOX Benchmark

5.2.1 One Energy Group

To facilitate the phase-space variable analysis of the C5G7 benchmark problem and reduce the pre-computational downtime, a one-group version of the unrodded benchmark was developed (Section 1.2.3.1). A seven group MCNP calculation was performed in the 2-D problem to obtain the 7-group flux distribution. These fluxes were then used to collapse the material dependent cross sections to one group. The one energy group cross-sections are given in the appendix.

5.2.1.1 Reference Solution

The reference solution was generated with a one-group MCNP calculation using 750 million particles. The obtained reference eigenvalue was 1.17544 ± 0.00002. Individual pin fission densities were also tallied over three axial slices of 14.28 cm (one third of the fuel assembly), all with relative errors smaller than 0.1%. The pin powers were normalized over the entire length of the fuel assemblies for comparison to the COMET solution in the next section.

5.2.1.2 COMET Solution – Unrodded Configuration

The unrodded configuration requires response functions for the five unique coarse meshes. Two of these meshes are for the fuel assemblies and the other three are needed

to represent the moderator regions of varying sizes and composition (*e.g.* presence of control rods). Response functions were generated with a modified version of MCNP4C using 3 million particles. The fission source scaling factors were chosen to be (1.0, 1.1, 1.2). To perform this analysis, the interface currents were expanded up to 5^{th} order in both spatial and angular variables. In this section, results with the most importance to this analysis will be presented. A summary of the results is presented in appendix B. Table 5.3 shows the importance of the azimuthal expansion in the coarse mesh calculation.

Table 5.3: COMET Results for the One Group 3-D C5G7 Benchmark

	{2,2,2,2} (%)	**{2,2,2,3} (%)**	**{2,2,2,4} (%)**	**{2,2,2,5} (%)**
RE k	0.10	0.07	0.06	0.06
AVG	0.8	0.6	0.6	0.6
RMS	0.9	0.8	0.8	0.8
MRE	0.7	0.6	0.5	0.5
MAX	3.2	2.8	2.6	2.7
# RF*	81	108	135	162
CPU Time (s)	107	137	179	227

*: Represents only the phase-space response functions for a unique node

Increasing the expansion order of the azimuthal variable has a positive effect on the coarse mesh results. The eigenvalue error is reduced from 0.1% to 0.06% and the average pin power error is reduced from 0.8% to 0.6%. Similar trends are also observed for the root mean square, mean relative error and maximum errors. The eigenvalue uncertainty is of the order of 0.05% and the pin power uncertainties are roughly 0.4%. The impact of using higher than third order is more or less lost in the statistical noise. From this analysis we can conclude that the seven group calculation should at the very least have a third order expansion in the azimuthal angle.

Another aspect tested in the one group problem is the order reduction technique proposed in Section 3.10. The following table presents coarse mesh results to a 4th order expansion in all variables with different order reduction schemes.

Table 5.4: Order Reduction of a {4,4,4,4} Expansion

Maximum Order	4[a] (%)	8[b] (%)	12[c] (%)	16[d] (%)
RE k	0.08	0.07	0.04	-0.02
k UNC	0.05	0.05	0.08	0.21
AVG	0.6	0.6	0.6	0.7
RMS	0.8	0.8	0.7	0.9
MRE	0.6	0.6	0.6	0.7
MAX	2.8	3.1	2.6	3.7
AVG UNC	0.4	0.5	0.7	2.0
# RF*	70	225	375	625
CPU Time (s)	344	966	1571	2598

[a]: 4th order maximum for all variables
[b]: 4th order maximum in angle and 4th order maximum in space
[c]: 4th order maximum in space
[d]: no order reduction
*: Represents only the phase-space response functions for a unique node

The most noticeable effect of the order reduction is on the eigenvalue and pin power uncertainties. The high order terms tallied in the response functions carry a very large statistical uncertainty that would require many millions more particle to reduce. By simply dropping these high order terms, the statistical uncertainty of the results becomes more reasonable. Another interesting aspect from the order reduction is that the pin power results remain almost the same. This indicates that the dropped terms had very little influence on the pin power distribution and only a slight effect on the eigenvalue.

Results in Tables 5.3, 5.4 and B.1 indicate that the azimuthal angle has a greater importance than the polar. Also reducing the spatial expansion order has little effect on

the accuracy. Therefore, it can be concluded that a spatial expansion order reduction should be employed. Table 5.5 presents various coarse mesh results using spatial order reductions.

Table 5.5: COMET Results with Spatial Order Reductions

	{3,3,2,3} (%)	**{3,3,2,4} (%)**	**{4,4,2,3} (%)**	**{4,4,2,4} (%)**
Maximum Order	**8**	**9**	**9**	**10**
RE k	0.09	0.08	0.08	0.05
AVG	0.6	0.6	0.6	0.6
RMS	0.7	0.7	0.8	0.7
MRE	0.5	0.5	0.6	0.6
MAX	3.0	2.7	3.2	3.0
# RF*	120	150	180	225
CPU Time (s)	198	278	391	577

*: Represents only the phase-space response functions for a unique node

Once again these results are all very similar and the variations are within the statistical uncertainties. However, it can be seen that a 3rd order expansion in space with order reduction leads to sufficient accuracy. Note that reducing the order decreases the total number of response functions needed to perform the COMET calculations. Therefore, the order reduction improves COMETs computational efficiency and the memory requirement (response function library size). Based on the one-group results, it seems that a {3,3,2,4} expansion order with 3rd order spatial reduction should lead to reasonable accuracy in the 7-group problem.

5.2.2 Seven Energy Group

This benchmark problem was described in Chapter 1. Reference solutions for all three configurations were published by Lewis *et al* (2005) and these were used to establish a comparison with the COMET coarse mesh solutions.

5.2.2.1 Unrodded Configuration

5.2.2.1.1 Reference Solution

The reference eigenvalue published by Lewis *et al* (2005) is 1.14308 with a standard deviation of 0.00003. The pin power results are presented over three axial slices of 14.28 cm. The average uncertainty of the pin power (1/3 length) is 0.20% with a maximum uncertainty of 0.43%.

5.2.2.1.2 COMET Solution

Based on the one energy group analysis of this configuration, response functions were generated with a phase space expansion of {3,3,2,4} with 3rd order spatial reduction with a fission scaling factor grid of 1.0, 1.1 and 1.2. Each response function was computed using a modified version of MCNP4C with 5 millions particles per calculation. Each calculation for a fuel mesh took roughly 10-15 minutes on the reference PC, while reflector meshes took on average 3 minutes. The pre-computational phase required a total of 28,350 response functions of which 18,900 were for the fuel meshes. Table 5.6 presents a summary of the errors for the eigenvalue and the pin power distribution.

The eigenvalue uncertainty of these calculations is 0.02% indicating that the {2,2,2,2} and the {3,3,2,2} results are within a two standard deviation interval and the other three calculations are within a one standard deviation interval. The average pin power uncertainty of these calculations is about 0.3 % with a maximum of 0.7%. As the spatial expansion is increased ({3,3,2,2} case), the average error is reduced to 0.7%, the

root mean square error drops to 1.1% and the mean relative error to 0.6%. The maximum error is also reduced slightly to 9.8%.

Table 5.6: COMET Results for Total Pin Power– Unrodded Configuration

	{2,2,2,2} (%)	**{2,2,2,4} (%)**	**{3,3,2,2} (%)**	**{3,3,2,3} (%)**	**{3,3,2,4} (%)**
Maximum Order	**7**	**9**	**7**	**8**	**9**
RE k	0.04	0.00	0.04	-0.01	0.00
AVG	1.0	1.0	0.7	0.8	0.8
RMS	1.5	1.6	1.1	1.2	1.2
MRE	0.7	0.8	0.6	0.6	0.6
MAX	10.6	10.8	9.8	10.0	10.0

Increasing the azimuthal expansion has no positive effect on the pin power results but gives a more accurate representation of the eigenvalue. The pin power variations are attributed to slightly larger uncertainties that appear in the higher order terms. Another interesting aspect caused by the large uncertainties is the asymmetrical nature of the solution along the diagonal symmetry axis. The reference solution does not show any sign of asymmetry since it was unfolded from a simulation in half of the core. However, the coarse mesh calculations were performed in the entire geometry. This asymmetry is best illustrated when comparing the two MOX fuel assemblies that should ideally be mirror reflections of each other. In the {3,3,2,2} case, the maximum error in both assemblies is 9.8% and 8.0%. Interestingly, these errors occur in the same location (in reference to the symmetry axis) and both in the same direction to the reference pin power (both overestimated). Tighter convergence (10^{-6}) of the eigenvalue and pin powers had little effect on this asymmetry. Resolving this issue would require using a much larger number of particles per response function, thus reducing the pin power and surface

angular current uncertainties. However, such calculations would require much more computational power.

The calculations presented here achieved a pin power average error of less than 1% and an eigenvalue error of less than 0.05%. However, when comparing to other transport methods (Lewis *et al*, 2006), it is desirable to reduce the maximum error substantially. It seems that higher spatial expansion order should reduce the maximum error. Response functions are thus generated for a {4,4,2,2} expansion with a 4^{th} order spatial reduction. The range for the fission source scaling factor is chosen to include the eigenvalue of all three configurations while minimizing the amount of pre-computations (i.e., 1.05 and 1.15). The response function calculations were once again performed using 5 million particles. The results of the unrodded configuration for the eigenvalue and the total pin powers are presented in Table 5.7. The results for the three fuel slices are presented in Appendix B. The eigenvalue was evaluated using the neutron balance method with an initial guess of 1.14.

Table 5.7: COMET Results for Total Pin Power– Unrodded Configuration

	{3,3,2,2} (%)	**{4,4,2,2} (%)**
Maximum Order	**8**	**8**
RE k	0.05	0.03
AVG	0.7	0.5
RMS	1.1	0.7
MRE	0.6	0.4
MAX	9.7	3.3
CPU Time (s)	2273	3248

The eigenvalue statistical uncertainty for these cases is 0.02%. Therefore, the eigenvalue error is well within a 95% confidence interval. The pin power average

uncertainty is 0.3% with a maximum of 0.7%. Using a {4,4,2,2} expansion with 4^{th} order spatial reduction reduces the pin power errors. The average error drops to 0.5% with a maximum of 3.3%. The computational times presented for this surface angular current expansion could be accelerated quite easily by simply adding more random access memory (RAM) to the reference PC. When using such a high order expansion in 3D, the size of the variables becomes larger than the available RAM thus making the computer swap data to the hard disk. This swapping of the data out of the memory makes the code much slower than the case where the RAM is sufficient to contain the entire response function data. Obviously, adding RAM is a short term solution because at some point bigger problems with even higher order expansions will exceed the maximum memory currently available. More efficient memory management within the COMET code must be considered in the future. The same memory problem is also encountered in solving the next two configurations. The lack of RAM also makes the acceleration procedure impractical because this technique requires even more memory.

Response functions for the fuel assemblies with control elements were generated using the same expansion order and added to the database. The pin power and the eigenvalue results of the rodded A configuration are presented in Table 5.8. The initial eigenvalue guess used in the neutron balance method was 1.13. Pin power results for the three selected slices are given in Appendix B.

Once again, the eigenvalue uncertainty is 0.02%, while the pin power uncertainties have an average of 0.3% and a maximum of 0.7%. With the {4,4,2,2} expansion of the surface angular current, the eigenvalue error is 0.04%. Similar to the unrodded configuration, the pin power errors are on average 0.5% with a maximum of 3.8%. The results of the rodded B configuration for the eigenvalue and the pin powers are presented in Table 5.9, while the pin power errors on the three slices are given in Appendix B. The neutron balance method was used to compute the eigenvalue with an initial guess of 1.08.

Table 5.8: COMET Results for Total Pin Power– Rodded A Configuration

	{3,3,2,2} (%)	**{4,4,2,2} (%)**
Maximum Order	**8**	**8**
RE k	0.06	0.04
AVG	0.7	0.5
RMS	1.1	0.7
MRE	0.6	0.4
MAX	9.4	3.8
CPU Time (s)	2013	3521

Table 5.9: COMET Results for Total Pin Power– Rodded B Configuration

	{3,3,2,2} (%)	**{4,4,2,2} (%)**
Maximum Order	**8**	**8**
RE k	0.05	0.03
AVG	0.7	0.5
RMS	1.1	0.7
MRE	0.6	0.4
MAX	9.0	3.7
CPU Time (s)	2207	3652

The uncertainties on the eigenvalue and pin powers are the same as with the previous two configurations. The eigenvalue differs from the reference solution by 0.03%, while the pin power errors are 0.5% on average when using the {4,4,2,2} expansion order. Increasing the expansion order from {3,3,2,2} to {4,4,2,2} has a very visible effect on the maximum pin power error and also has a noticeable effect on the pin power error distribution.

CHAPTER 6

CONCLUSION

The desire to increase fuel utilization and optimization of parameters related to other economic and safety factors have led to reactor core designs that are substantially more heterogeneous than the current designs. It is anticipated that the trend in increased heterogeneity in fuel assembly and core designs will continue with the advanced and Generation IV reactors. The new designs are pushing the validity of the approximations made in the current state-of-the-art methods. The need to maintain or improve the solution accuracy has led researchers to consider the use of pure transport theory in favor of the current two step methodology in which transport theory is used at the lattice level to generate homogenized cross section for diffusion theory calculations at the core level.

Unfortunately, the current available transport codes and methods are mostly impractical or require significant amount of memory and computational resources to perform accurate core calculations. Most researchers are developing new acceleration and parallelization techniques to overcome these difficulties. In this dissertation, a new method has been developed for performing highly accurate and efficient reactor core calculations in highly heterogeneous core configurations.

In this work, a heterogeneous coarse mesh transport method has been extended to three-dimensional Cartesian geometry. The high efficiency of the method is achieved by decoupling the problem into smaller sub-volume elements (*e.g*. coarse meshes) and shifting the computation time to a priori calculations of response functions for the unique sub-volumes in the system. That is, the method takes advantage of the repeated structure found frequently in large reactor problems. Previously, a deterministic method was used to generate the response functions when the surface angular current is represented by an expansion in discrete Legendre polynomials that are orthogonal on uniform intervals.

The complexity of nuclear reactor designs makes uniform intervals highly impractical and inaccurate. Also, the discrete spatial representation along the coarse mesh edge leads to the need for a significant number of pre-computed response function data. It was found that the size of this data can be greatly reduce if continuous Legendre polynomials are used. The deterministic method was thus replaced by a stochastic response function generator making this transition fairly simple.

Initially, the method was implemented in two dimensions and tested on many benchmark problems representative of various reactor types and sizes. With low-order expansion of the surface angular currents ($\{3^2,2,4\}$), a full core PWR reactor was modeled using seven energy groups. When comparing to the full core Monte Carlo reference calculation, the core eigenvalue differed by only 0.01% while the average and maximum pin power errors were 0.4% and 1.7%, respectively. A two-group quarter core CANDU-6 benchmark was also simulated using 2^{nd} order polynomial expansion in space and angle. In just over 18 seconds (not including the pre-computation time) the coarse mesh method achieved a solution accuracy of 0.09% in the eigenvalue. The corresponding errors in the average and maximum pin power were 0.5% and 2.0%, respectively. A BWR benchmark problem was also simulated using three group cross sections. For this problem, using a {4,2,3} expansion, the eigenvalue of the coarse mesh transport method differed from the reference Monte Carlo solution by 0.13%. The average and maximum pin power errors were 1.7% and 6.5%, respectively. For all three types of reactor simulated in two dimensions, very accurate results were obtained using low order approximation in space and angle.

The method was then implemented in three dimensions and tested on the C5G7 MOX Benchmark problem. Through a series of calculations, it was observed that the spatial variables have a strong influence on the accuracy of the results. With an expansion order of {4,4,2,2} in conjunction with a 4^{th} order spatial reduction, the core

eigenvalue of all three configurations differed by less than 0.05%. The pin power errors averaged 0.5% with a maximum error of less than 4% for all three configurations

6.1 Recommendations for Future Work

In 2-D, the addition of spatial segmentation was presented as a way of gaining some accuracy with low-order expansions. Since segmentation becomes complicated in 3D, this feature was not retained when the coarse mesh method was extended to 3-D. However, surface segmentation might be useful for reactors that would otherwise require very high expansion orders. In this thesis, segmentation was only tested using uniform segments. An additional possibility would be to consider variable length segmentation. For example, segments might be chosen as a function of the zeros of the orthogonal polynomials.

The spectral mapping idea presented in Section 3.8.1 was barely explored and could lead to significant improvements in reproducing continuous energy results. One should explore higher order methods as well as improved ways to find a more suitable spectral map that is representative of the core (e.g. critical spectrum). The idea of spectral mapping could also be extended to other variables of the phase space. For example, both angular variables could be mapped such that their 0^{th} order would represent the cosine-current approximation.

In the concepts considered for the next generation nuclear reactors, the use of a hexagonal lattice is a strong possibility. The coarse mesh method could easily be extended to such geometry. Another possible addition to the coarse mesh method would be the coupling of neutron, photon and electron transport. This coupling is essentially straightforward except for the energy variable.

In order for the coarse mesh methodology to become practical for core monitoring and follow-up, better memory management techniques must be investigated to accelerate the coarse mesh solution and reduce the strain on the computer resources. Parallelization

of the coarse mesh algorithm is a definite possibility. Also, grid computing should be explored for response functions calculations.

Another interesting idea is to use triangular meshes at the reflector edge. This would allow for a better representation of the outer reflector without the problem of re-entering boundaries of the staircase approximation. Another possibility is to represent the outer core as a single coarse mesh and linking it to the rest of the core in the sweeping process.

APPENDIX A

COMPLEMENT TO CHAPTER 4

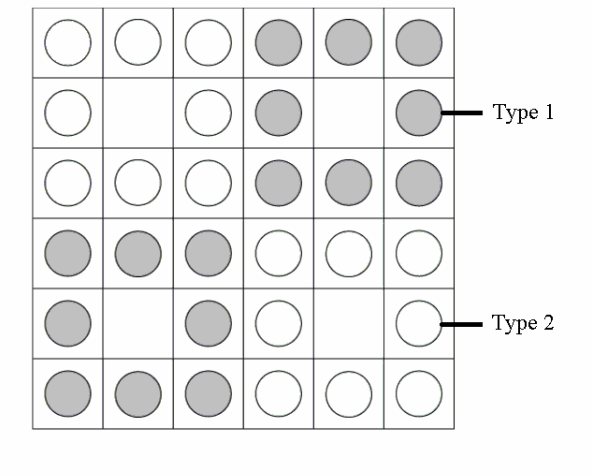

Figure A.1: Geometrical Configuration of the Benchmark Problem

The structure of the 12 energy bin approximation that was used to solve the problem in Section 4.2.1 is given in Table A.1.

Table A.1: Twelve Energy Bin Limits (MeV)

Bin	Lower Energy Bound	Upper Energy Bound
1	6.0653	20.0
2	3.6788	6.0653
3	1.8316e-01	3.6788
4	6.7379e-02	1.8316e-01
5	9.1188e-03	6.7379e-02
6	2.0347e-03	9.1188e-03
7	1.3007e-04	2.0347e-03
8	2.3824e-06	1.3007e-04
9	6.2506e-07	2.3824e-06
10	8.1968e-08	6.2506e-07
11	1.2396e-08	8.1968e-08
12	1.0e-10	1.2396e-08

The material properties used in the continuous-energy benchmark are presented in Table A.2 and the cross-sections of the one-group version are found in Table A.3.

Table A.2: Material Number Densities for Continuous-Energy Benchmark

	U-234	U-235	U-238	O-16	H	Total
1% enriched fuel	1.8491E-06	2.2732E-04	2.2218E-02	4.4894E-02		6.734151E-02
2% enriched fuel	4.0177E-06	4.5461E-04	2.1991E-02	4.4899E-02		6.734888E-02
Moderator (@300K)				3.3338E-02	6.6676E-02	1.00014E-01

Table A.3: Cross-sections for one-group problem

	Coolant (2%)	Fuel (2%)	Coolant (1%)	Fuel (1%)
Σ_{tr}	9.6691584E-01	4.3288590E-01	1.0522071E+00	4.1543850E-01
Σ_{ab}	5.3858400E-03	3.4606100E-02	6.0670900E-03	3.2901800E-02
Σ_{s}	9.6153000E-01	3.4354800E-01	1.0461400E+00	3.4915900E-01
Σ_{f}		5.4731800E-02		3.3377700E-02
ν		2.44844861671		2.45482762443
χ		1.		1.

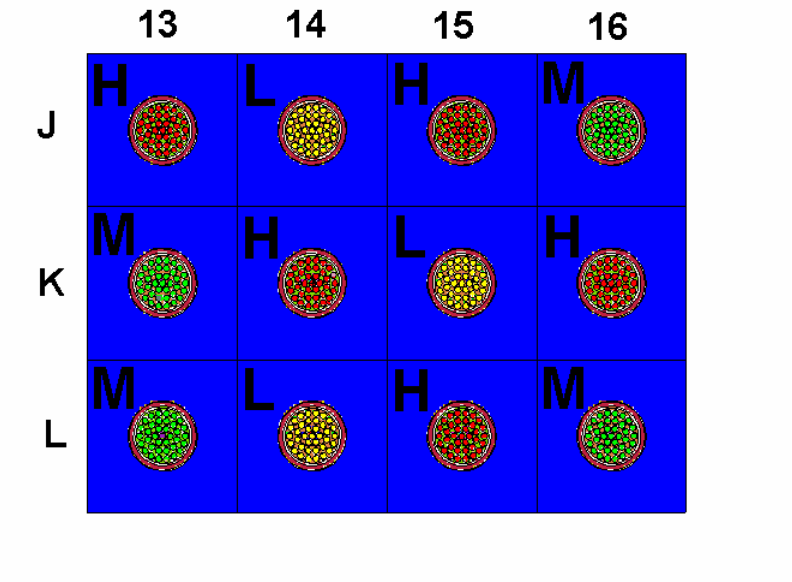

Figure A.2: Core Configuration of the 3 by 4 CANDU-6 Benchmark

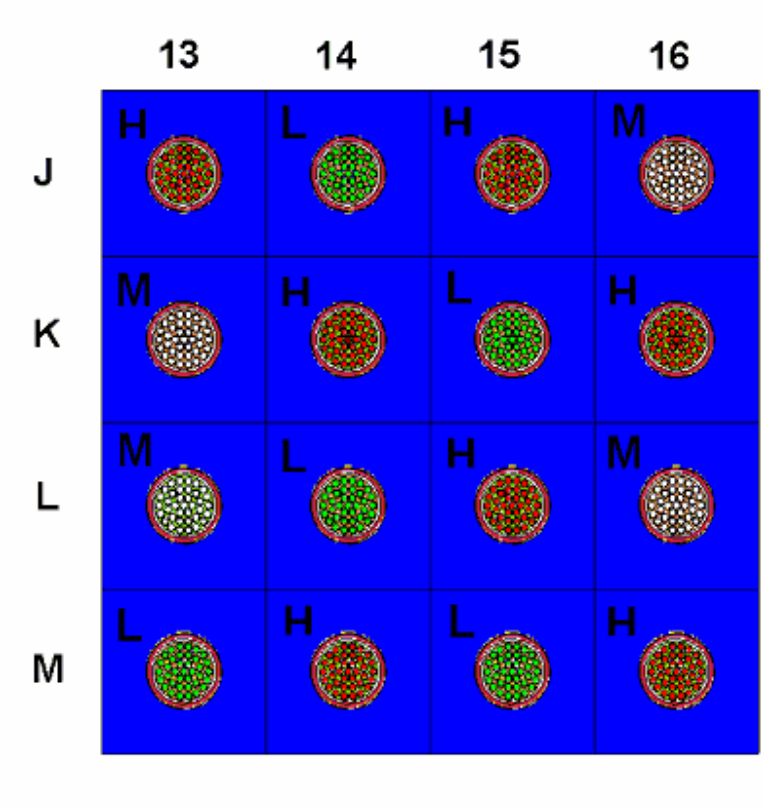

Figure A.3: Core Configuration of the 4 by 4 CANDU-6 Benchmark

Table A.4: Burnup Distribution for ¼ Core CANDU-6 Benchmark

Color Scheme	Burnup (kWd/t)
Green	800
Yellow	2700
Orange	5000
Red	7000

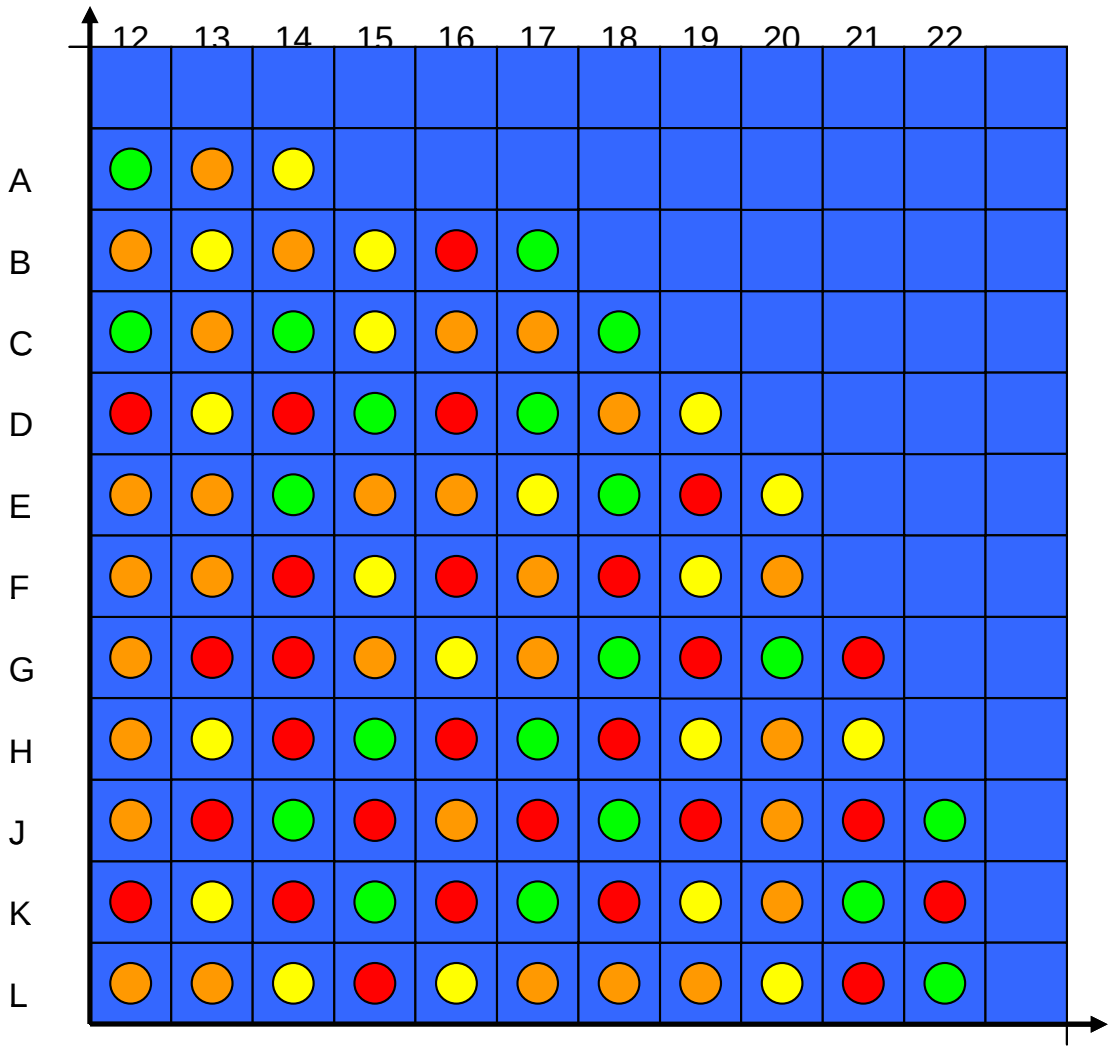

Figure A.4: Core Configuration of the ¼ Core CANDU-6 Benchmark

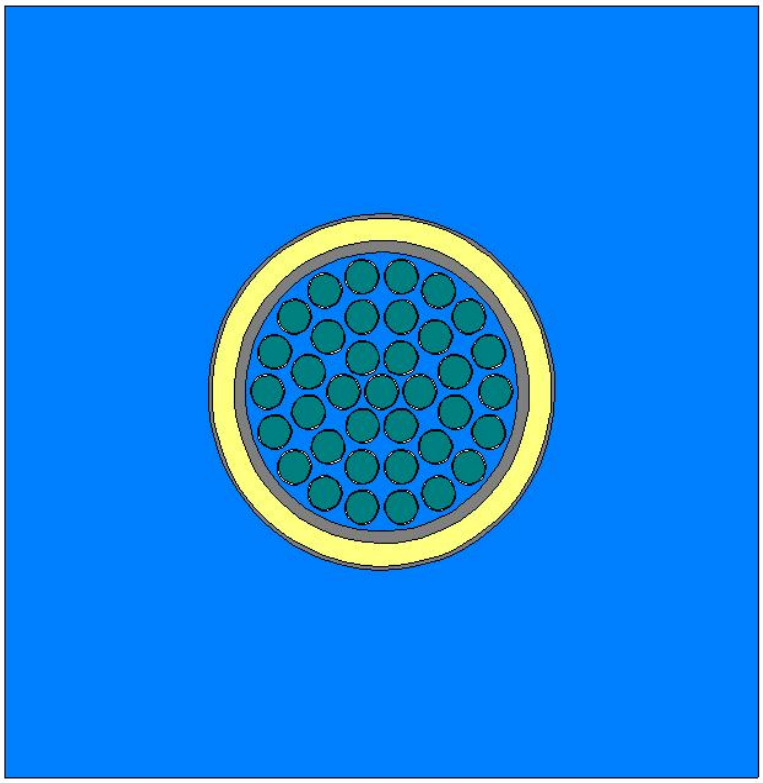

Figure A.5: CANDU-6 Cell Geometry

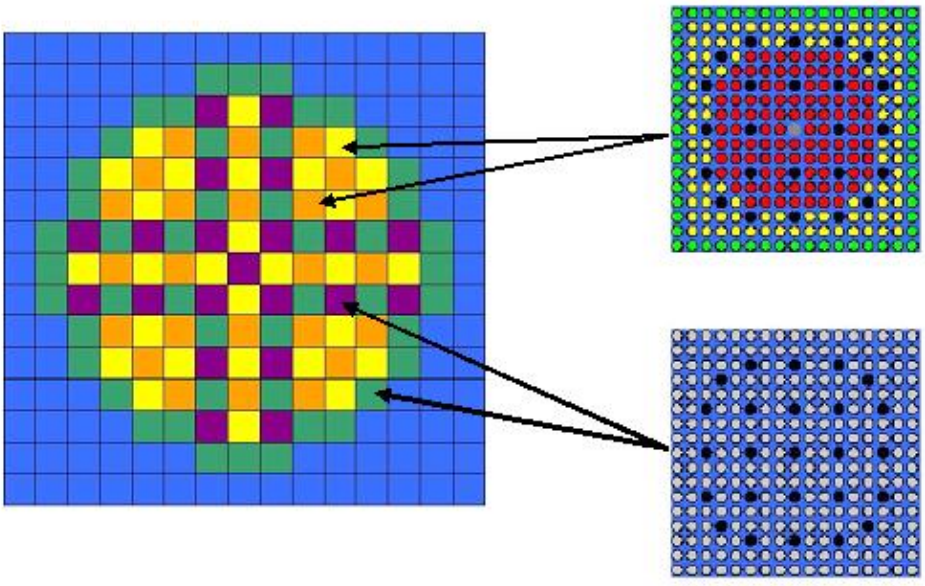

Figure A.6: Core Configuration of the Full Core PWR Benchmark

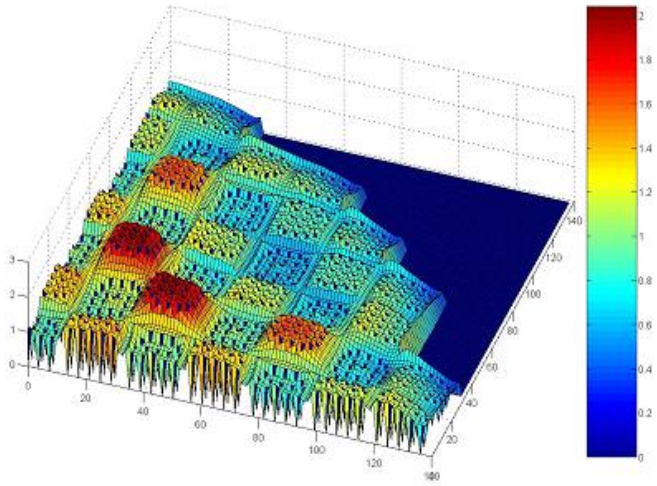

Figure A.7: Pin Power Distribution of the Full Core PWR Benchmark

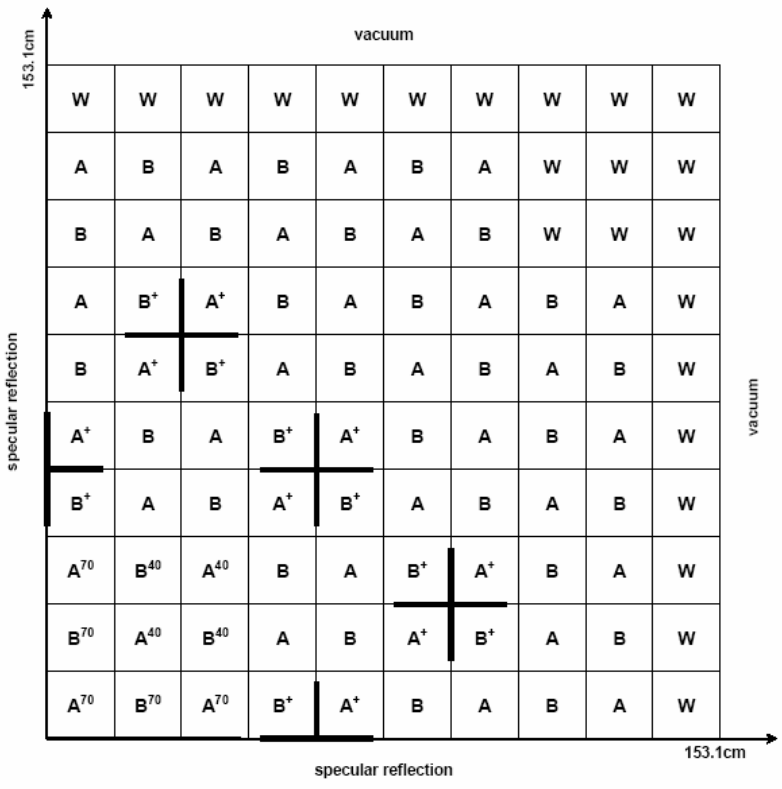

Figure A.8: Core Configuration of the Original HAFAS Benchmark

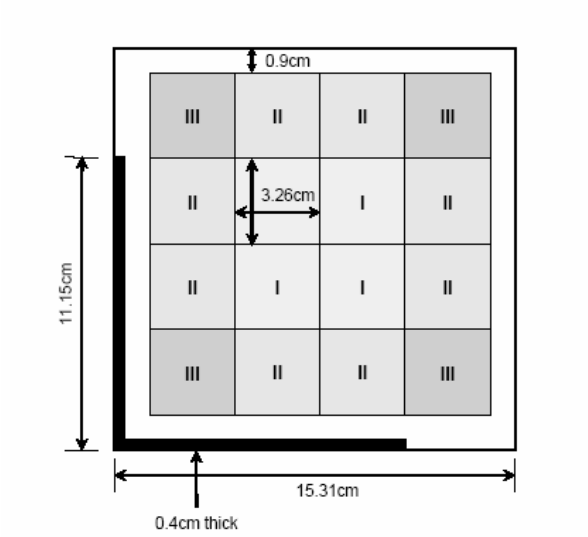

Figure A.9: Bundle Configuration of the Original HAFAS Benchmark

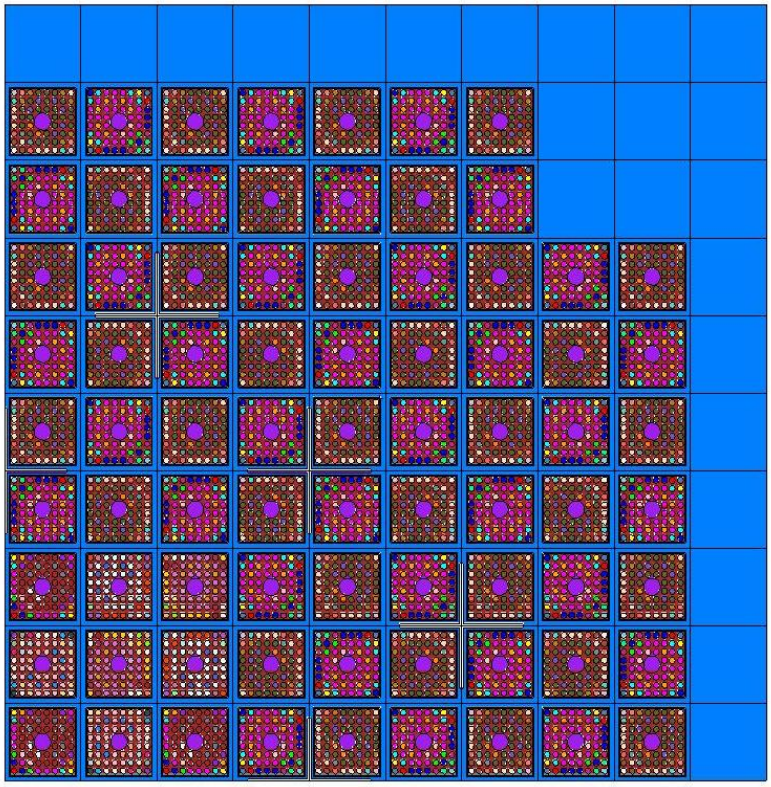

Figure A.10: Core Configuration of the Updated HAFAS Benchmark

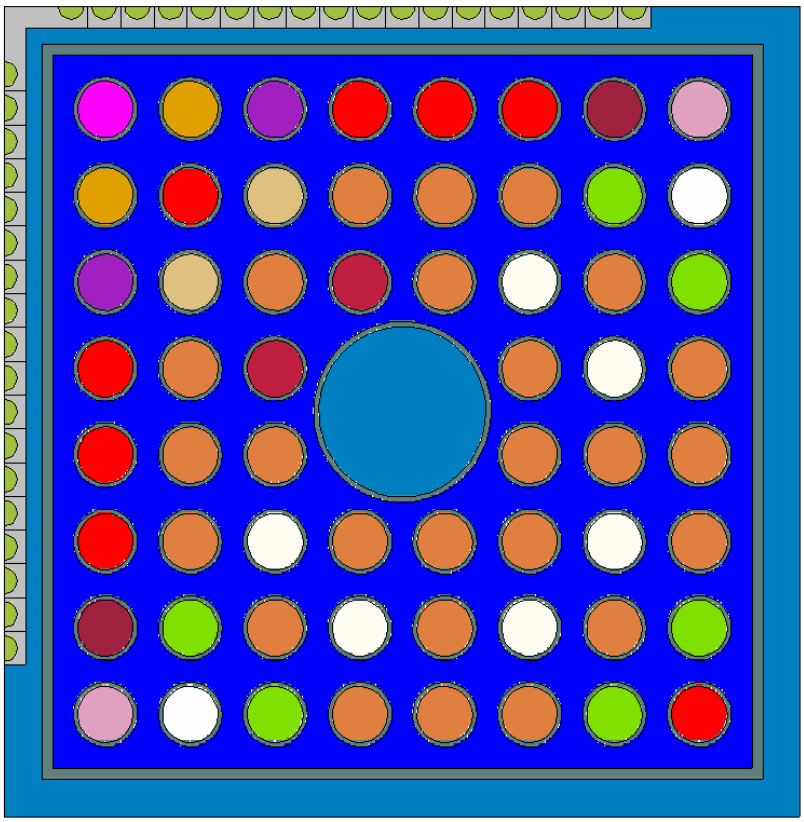

Figure A.11: GE9 Cell Geometry

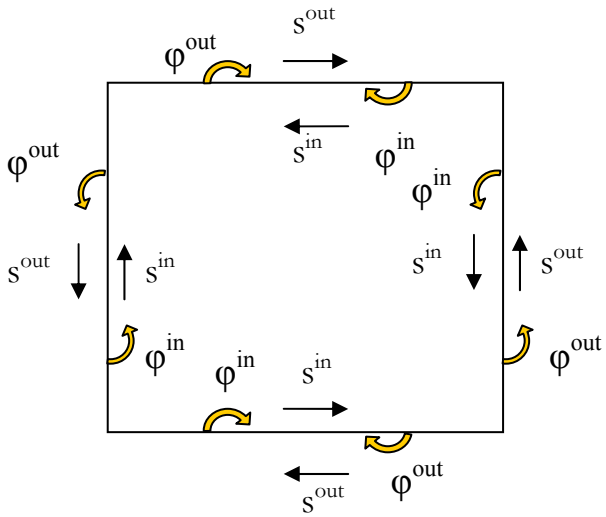

Figure A.12: Reference System for Diagonal Symmetry

APPENDIX B

COMPLEMENT TO CHAPTER 5

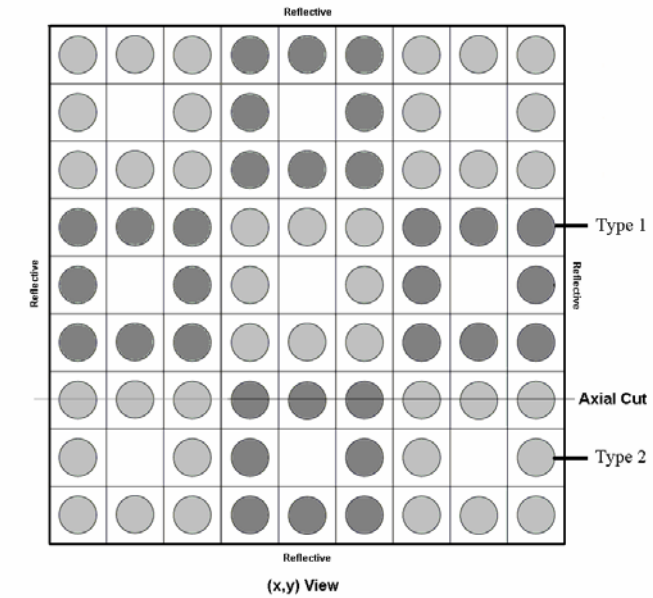

Figure B.1: Configuration 1 – Radial View

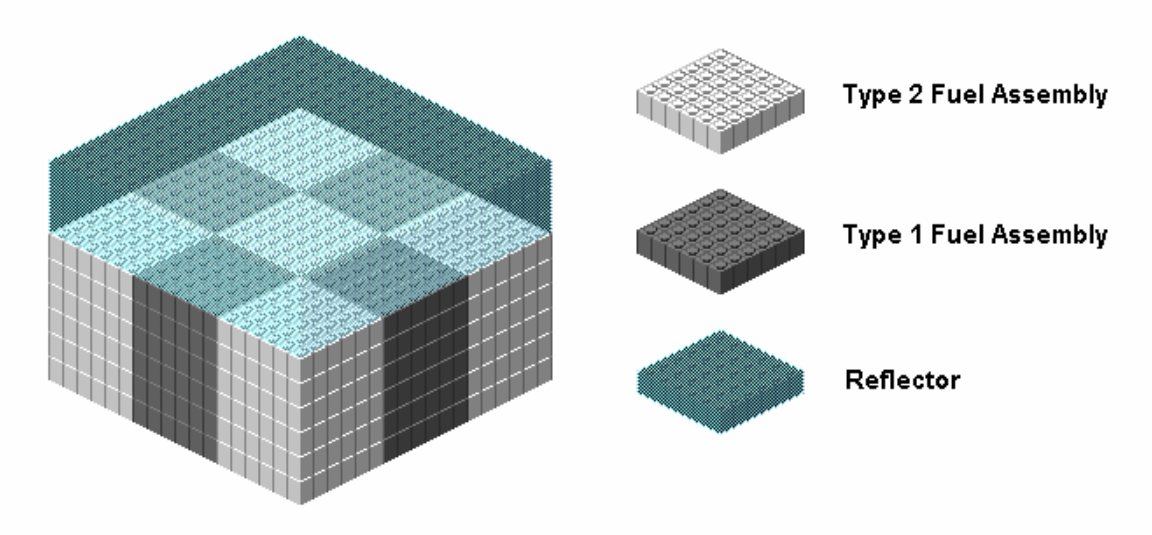

Figure B.2: Configuration 1 – Simplified 3-D

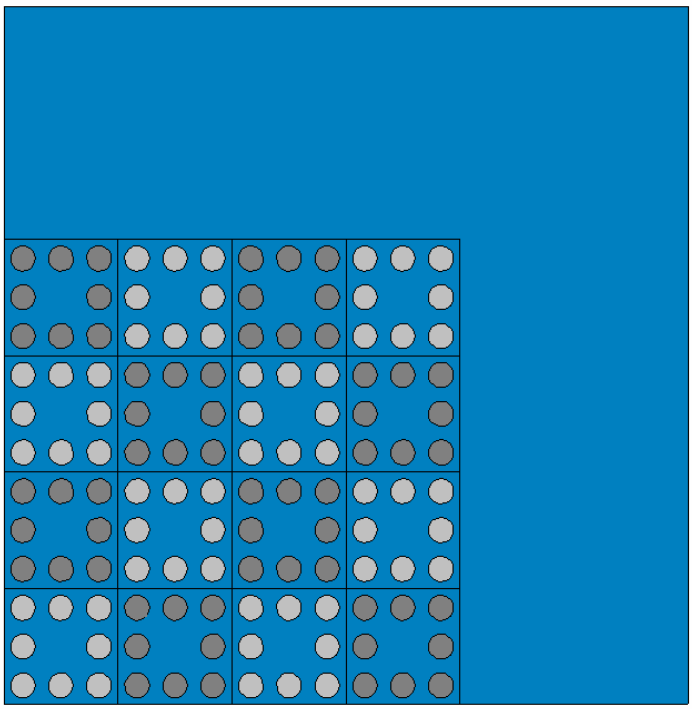

Figure B.3: Configuration 2 – Radial View

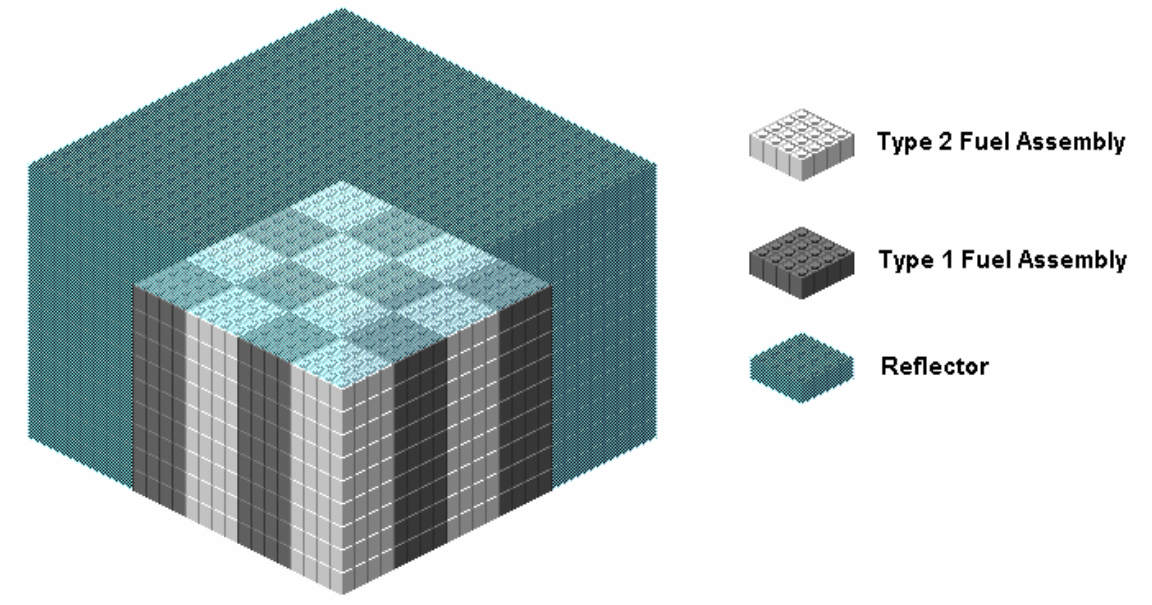

Figure B.4: Configuration 2 – Simplified 3-D

Table B.1: One Group C5G7 Cross-sections – Non Fissionable Materials

	Water	**GT**	**CR**
Σ_{tr}	6.83673E-1	3.43076E-1	6.99624E-1
Σ_{ab}	4.94752E-3	2.66447E-3	2.18095E-1
Σ_{s}	6.78725E-1	3.40412E-1	4.81530E-1

Table B.2: One Group C5G7 Cross-sections – Fissionable Materials

	Fuel I	**Fuel II**	**Fuel III**	**Fuel IV**
Σ_{tr}	3.59815E-1	3.72108E-1	3.79763E-1	3.82151E-1
Σ_{ab}	4.02914E-2	5.00665E-2	5.38881E-2	5.37404E-2
Σ_{s}	3.19524E-1	3.22042E-1	3.25875E-1	3.2841E-1
Σ_{f}	2.2072815E-2	2.19634E-2	2.3546655E-2	2.3146111E-2
ν	2.65494	2.86813	2.89563	2.90991
χ	1.0	1.0	1.0	1.0

Table B.3: One Group C5G7 Results – Unrodded Configuration

	Maximum Order	***RE k* (%)**	***AVG* (%)**	***RMS* (%)**	***MRE* (%)**	***MAX* (%)**	***AVG UNC* (%)**	**Time(s)**
{1,1,1,3}	6	-0.01	2.3	2.9	2.1	10.4	0.4	70
{1,1,2,3}	7	-0.11	1.9	2.4	1.7	8.2	0.4	76
{1,2,1,3}	7	0.04	2.0	2.5	1.8	10.0	0.4	76
{2,1,1,3}	7	0.06	2.0	2.5	1.8	8.1	0.4	75
{2,2,2,2}	8	0.10	0.8	0.9	0.7	3.2	0.4	107
{2,2,1,3}	8	0.13	1.9	2.2	1.7	7.6	0.4	101
{2,2,2,3}	9	0.07	0.6	0.8	0.6	2.8	0.4	137
{2,2,3,2}	9	0.10	0.8	1.0	0.7	3.1	0.4	138
{2,3,2,2}	9	0.11	0.7	0.9	0.6	3.3	0.4	139
{3,2,2,2}	9	0.10	0.7	0.9	0.6	3.4	0.4	140
{3,3,2,2}	10	0.10	0.7	0.9	0.6	3.4	0.4	189
{2,2,3,3}	10	0.07	0.6	0.8	0.6	2.8	0.4	189
{2,2,2,4}	10	0.06	0.6	0.8	0.5	2.6	0.4	179
{2,2,2,5}	11	0.06	0.6	0.8	0.5	2.7	0.4	227
{3,3,2,3}	8[1]	0.09	0.6	0.7	0.5	3.0	0.4	198
{3,3,2,4}	9[1]	0.08	0.6	0.7	0.5	2.7	0.4	278
{3,3,2,5}	10[1]	0.07	0.6	0.7	0.5	2.7	0.4	374
{3,3,3,3}	3[3]	0.10	0.7	0.9	0.7	2.9	0.4	187
{3,3,3,3}	6[1,2]	0.10	0.7	0.9	0.7	2.9	0.4	456
{3,3,3,3}	12	0.08	0.6	0.7	0.5	2.9	0.6	1043
{4,4,2,3}	9[1]	0.08	0.6	0.8	0.6	3.2	0.4	391
{4,4,2,4}	10[1]	0.05	0.6	0.7	0.6	3.0	0.5	577
{4,4,3,3}	10[1]	0.08	0.6	0.8	0.6	3.1	0.5	667
{4,4,3,3}	14	0.06	0.6	0.7	0.5	2.8	0.9	1054
{4,4,4,4}	4[3]	0.08	0.6	0.8	0.6	2.8	0.4	344
{4,4,4,4}	8[1,2]	0.07	0.6	0.8	0.6	3.1	0.5	966
{4,4,4,4}	12[1]	0.04	0.6	0.7	0.6	2.6	0.7	1571
{4,4,4,4}	16	-0.02	0.7	0.9	0.7	3.7	2.00	2598

[1] Spatial Reduction
[2] Angular Reduction
[3] All Variable Reduction

Table B.4: COMET Results for Pin Powers in Slice 1 – Unrodded Configuration

	{3,3,2,2}	**{4,4,2,2}**
Maximum Order	**8**	**8**
AVG	0.7	0.5
RMS	1.1	0.7
MRE	0.6	0.5
MAX	9.2	3.2

Table B.5: COMET Results for Pin Powers in Slice 2 – Unrodded Configuration

	{3,3,2,2}	**{4,4,2,2}**
Maximum Order	**8**	**8**
AVG	0.7	0.5
RMS	1.1	0.7
MRE	0.6	0.4
MAX	9.7	3.7

Table B.6: COMET Results for Pin Powers in Slice 3 – Unrodded Configuration

	{3,3,2,2}	**{4,4,2,2}**
Maximum Order	**8**	**8**
AVG	1.0	0.7
RMS	1.4	0.9
MRE	8.4	0.7
MAX	10.6	4.0

Table B.7: COMET Results for Pin Powers in Slice 1 – Rodded A Configuration

	{3,3,2,2}	**{4,4,2,2}**
Maximum Order	**8**	**8**
AVG	0.7	0.5
RMS	1.1	0.7
MRE	0.6	0.5
MAX	9.2	3.4

Table B.8: COMET Results for Pin Powers in Slice 2 – Rodded A Configuration

	{3,3,2,2}	**{4,4,2,2}**
Maximum Order	**8**	**8**
AVG	0.7	0.5
RMS	1.1	0.7
MRE	0.6	0.4
MAX	9.3	4.2

Table B.9: COMET Results for Pin Powers in Slice 3 – Rodded A Configuration

	{3,3,2,2}	**{4,4,2,2}**
Maximum Order	**8**	**8**
AVG	0.9	0.6
RMS	1.3	0.8
MRE	0.8	0.6
MAX	10.0	4.0

Table B.10: COMET Results for Pin Powers in Slice 1 – Rodded B Configuration

	{3,3,2,2}	**{4,4,2,2}**
Maximum Order	**8**	**8**
AVG	0.7	0.5
RMS	1.1	0.7
MRE	0.6	0.4
MAX	8.8	3.5

Table B.11: COMET Results for Pin Powers in Slice 2 – Rodded B Configuration

	{3,3,2,2}	**{4,4,2,2}**
Maximum Order	**8**	**8**
AVG	0.8	0.6
RMS	1.2	0.7
MRE	0.7	0.5
MAX	9.1	3.7

Table B.12: COMET Results for Pin Powers in Slice 3 – Rodded B Configuration

	{3,3,2,2}	**{4,4,2,2}**
Maximum Order	**8**	**8**
AVG	1.2	0.7
RMS	1.6	1.0
MRE	1.1	0.7
MAX	9.1	4.6

REFERENCES

Anderson, M.M. and Honeck, H.C. (1973), "An Interface Current Technique for Two-Dimensional Cell Calculations," CONF-730414 – P1, p. I-53.

Bell, G.I. and Glasstone, S. (1970), "Nuclear Reactor Theory," *Van Nostrand Reinhold Company*, New York.

Bevington, P.R. (1969), Data Reduction and Error Analysis of the Physical Sciences, *McGraw-Hill Book Company*, New York.

Breen, J. and Forget, B. (2004) "An updated HAFAS BWR benchmark", *ANS Student Conference*, Ohio State.

Briesmeister, J.F. (1997), "MCNP – A General Monte Carlo N-Particle Transport Code, Version 4B," *Los Alamos National Laboratory*, LA-12625-M.

Briesmeister, J.F. (2000), "MCNP – A General Monte Carlo N-Particle Transport Code, Version 4C," *Los Alamos National Laboratory*, LA-13709-M.

Burden, R.L. and Faires, J.D. (1997), "Numerical Analysis," *Brooks/Cole Publishing Company*, 6th edition, New York.

Casal, J.J., Stamm'ler, R.J.J., Villarino, E.A. and Ferri, A.A. (1991), HELIOS: Geometric Capabilities of a New Fuel-Assembly Program, *Intl. Topical Meeting on Advances in Mathematics, Computations, and Reactor Physics*, Pittsburgh, Pennsylvania, April 28-May 2, **2**, 10.2.1 1-13.

Forget, B., Rahnema, F. (2006), "COMET Solution to the 3-D C5G7 MOX Benchmark Problem," *Progress in Nuclear Energy*, submitted (January 2006).

Forget, B. and Rahnema, F. (2005a), "Improved Monte Carlo Adaptation of the Heterogeneous Coarse Mesh Transport Method," *Monte Carlo 2005 Topical Meeting – The Monte Carlo Method: Versatility Unbounded in a Dynamic Computing World*, Chattanooga, Tennessee, April 17-21.

Forget, B. and Rahnema, F. (2005b), "3-D Heterogeneous Coarse Mesh Transport Method," *International Topical Meeting on Mathematics and Computations, Supercomputing, Reactor Physics and Nuclear and Biological Applications*, Avignon, France, September 12-15.

Forget, B. and Rahnema, F. (2005c), "New Eigenvalue Evaluation Technique in the Heterogeneous Coarse Mesh Transport Method," *Transactions of the American Nuclear Society*, **93**, 511.

Forget, B. and Rahnema, F. (2005d), "High Order Spatial Expansion of the Incident Current in the Heterogeneous Coarse Mesh Transport Method", *Transactions of the American Nuclear Society*, **92**, 725.

Forget, B., Rahnema, F. and Mosher, S.W. (2004a), "A Heterogeneous Coarse Mesh Solution for the 2-D NEA C5G7 MOX Benchmark Problem," *Progress in Nuclear Energy*, **45**, 2-4, 233-254.

Forget, B., Ilas, G. and Rahnema, F. (2004b), "A Heterogeneous Coarse Mesh Transport Solution for a 2-D CANDU-6 Benchmark Problem", *Sixth International Conference on Simulation Methods in Nuclear Engineering*, Montreal, Canada, October 12-15.

Forget, B., Rahnema, F. and Mosher, S.W. (2004c), "Application of A Heterogeneous Coarse Mesh Transport Method to a MOX Benchmark Problem," *PHYSOR-2004 The Physics of Fuel Cycles and Advanced Nuclear Systems: Global Developments*, April 25-29, Chicago, Illinois.

Gheorghiu, H.N.M., and Rahnema, F. (1998), "Variational Principles for Steady-State Neutron Flux Functionals," *Transport Theory and Statistical Physics*, **27**, 67.

Giust, F.D. (2000), Release Notes for Helios System 1.6, *Studsvik Scandpower Report*, SSP-00/205, January 03.

Griesheimer, D.P. and Martin, W.R. (2003), "Monte-Carlo Based Angular Flux Response Functions," *Transactions of the American Nuclear Society*, **89**, 370 (2003).

Hines, W.W., Montgomery, D.C., Goldsman, D.M. and Borror, C.M. (2003), "Probability and Statistics in Engineering," 4th edition, *John Wiley & Sons, Inc.*, New York.

Honeck, H.C. (1971), "Integral Transport Theory Methods in the JOSHUA System," *Transactions of the American Nuclear Society*, **14**, 224.

Ilas, D. and Rahnema, F. (2003), "A Heterogeneous Coarse Mesh Transport Method," *Transport Theory and Statistical Physics*, **32**, 441-467.

Ilas, D. (2001), "Coarse Mesh Transport Theory Model for Heterogeneous Systems," Ph.D. Thesis, Georgia Institute of Technology.

Kelly, D.J. (1995), "Depletion of a BWR Lattice Using the RACER Continuous Energy Monte Carlo Code," *Proceedings of the International Conference on Mathematics and Computations, Reactor Physics and Environmental Analyses*, Portland, Oregon, April 30-May 4, Vol. 2, p. 1011, American Nuclear Society.

Larsen, E.W. (1975), "Neutron Transport and Diffusion in Inhomogeneous Media. I," *Journal of Mathematical Physics*, **16**, 1421-1427.

Larsen, E.W. (1976), "Neutron Transport and Diffusion in Inhomogeneous Media. II," *Nuclear Science and Engineering*, **60**, 357-368.
Lawrence, R.D. (1986), "Progress in Nodal Methods for the Solution of the Neutron Diffusion and Transport Equations," *Progress in Nuclear Energy*, **17**, 271-301.

Leonard, A. (1975), "Collision Probabilities and Response Matrices: An Overview," *Proc. Conf. Computational Methods in Nuclear Engineering*, CONF-750413, III-15, U.S. Atomic Energy Commission.

Leonard, A., McDaniel, C.T. and Petrick, W.P. (1971), "A Modified Collision Probability Method for Non-Uniform Lattices," CONF-710302, **1**, 644.

Lewis, E.E., Palmiotti, G., Taiwo, T.A., Blomquist, R.N., Smith, M.A. and Tsoulfanidis, N. (2005), "Benchmark Specifications for Deterministic MOX Fuel Assembly Transport Calculations Without Spatial Homogenization (3-D Extension C5G7 MOX)," *Nuclear Energy Agency*.

Lewis, E.E., Palmiotti, G., Taiwo, T.A., Blomquist, R.N., Smith, M.A. and Tsoulfanidis, N. (2003), "Benchmark Specifications for Deterministic MOX Fuel Assembly Transport Calculations Without Spatial Homogenization," *Nuclear Energy Agency*.

Lewis, E.E. and Miller, W.F., Jr. (1993), "Computational Methods of Neutron Transport, *American Nuclear Society*, La Grange Park, Illinois.

McDaniel, C.T. (1975), "A Two Dimensional Few Group Response Matrix Calculation Method for Flux and Reactivity," *Proc. Conf. Computational Methods in Nuclear Engineering*, CONF-750413, V-111, U.S. Atomic Energy Commission.

Misfeldt, I., (1975), "2D IAEA Benchmark Problem", *Danish Atomic Energy Commission*, Research Establishment Riso, Department of Reactor Technology, Reactor Physics Section.

Misfeldt, I., (1975), "3D IAEA Benchmark Problem, 2^{nd} order FEM Calculations", *Danish Atomic Energy Commission*, Research Establishment Riso, Department of Reactor Technology, Reactor Physics Section.

Mohanakrishnan, P. (1981), "Angular Current Approximations in Neutron Transport Calculations using Interface Currents – A Review", *Progress in Nuclear Energy*, **7**, 1-10.

Moriwaki, M., Ishii, K., Maruyama, H. and Aoyama, M. (1999), "A New Direct Calculation Method of Response Matrices Using Monte Carlo Calculation," *J.Nucl.Sci.Technol.*, **36**, 877.

Mosher, S.W. and Rahnema, F. (2005), "The Incident Flux Response Expansion Method for Heterogeneous Coarse Mesh Transport Problems," *Transport Theory and Statistical Physics*, **34**, No. 6, in press.

Mosher, S.W. (2004), "A Variational Transport Theory Method for Two-Dimensional Reactor Core Calculations," Ph.D. Thesis, Georgia Institute of Technology.

Mosher, S.W., Rahnema, F. and Forget, B. (2003), "Monte Carlo Adaptation of a Heterogeneous Coarse Mesh Transport Method," *Transactions of the American Nuclear Society*, **89**, 310 see also erratum, **90**, 601, (2004).

Mosher, S.W. and Rahnema, F. (2003), "An Intra-Nodal Flux Expansion for a Heterogeneous Coarse Mesh Discrete Ordinates Method," *Proc. of ANS Nuclear Mathematical and Computational Sciences: A Century in Review, A Century Anew*, April 6-10, Gatlinburg, Tennessee.

Mueller, A. and Wagner, M.R. (1972), "Use of Collision Probability Methods for Multidimensional Neutron Flux Calculations," *Transactions of the American Nuclear Society*, **15**, 280.

NSSDC: National Space Science Data Center (2006), "Common Data Format (CDF)," http://cdf.gsfc.nasa.gov/, last accessed on March 29th, 2006.

Neuman, C.P. and Schonbach, D.I. (1974), "Discrete (Legendre) Orthogonal Polynomials - A Survey," *International Journal of Numerical Methods in Engineering*, **8**, 743-770.

Palmiotti, G., Lewis, E.E. and Carrico, C.B. (1995), "VARIANT: VARIational Anisotropic Nodal Transport for Multidimensional Cartesian and Hexagonal Geometry Calculation," ANL-95/40, Argonne National Laboratory.

Pomraning, G.C. (1990), "Near-Infinite-Medium Solutions of the Equation of Transfer," *J. Quant. Spectrosc. Radiat. Transfer*, **44**, 317-338.

Pryor, R.J. and Graves, W.E. (1973), "Response Matrix Method for Treating Reactor Calculations," CONF-730414 – P2, p. VII-179.

Rahnema, F. (2002), "Nuclear Energy Research Initiative Report: Innovative Transport Theory Method for Efficient Design, Analysis and Monitoring of Generation IV Reactor Cores," Project DE-FG03-02SF226199, No. 2002-081.

Rahnema, F., Mosher, S.W., and Pitts, M. (2000), "Void Reactivity Calculations-Phase 2," *Final Report to the Atomic Energy Control Board of Canada*, FR2-AECB-0100R, March 15.

Rathkopf, J.A. and Martin, W.R. (1986), "The Finite Element Response Matrix Method for the Solution of the Neutron Transport Equation," *Progress in Nuclear Energy*, **18**, 237-250.

Sanchez, R. and McCormick, N.J. (1972), "A Review of Neutron Transport Approximations," Sec. II.C.3, *Nuclear Science and Engineering*, **80**, 481-535.

Satterfield, M., Forget, B., Rahnema, F., Fox, T. and Wang, C. (2005), "Application of a Heterogeneous Coarse Mesh Transport Method to a Radiation Therapy Benchmark Problem," *American Association of Physicist in Medicine (AAPM) – Annual Meeting*, Seattle, WA, July 24-28.

Suetin, P.K. (1999), "Orthogonal Polynomials in Two Variables," *Gordon and Breach Science Publishers*, Amsterdam.

Smith, K.S. (1980), "Spatial Homogenization Methods for Light Water Reactor Analysis," Ph.D. Thesis, Massachusetts Institute of Technology.

Smith, K.S. (1986), "Assembly Homogenization Techniques for Light Water Reactor Analysis," *Progress in Nuclear Energy*, **17**, 303-335.

Smith, M.A., Tsoulfanidis, N., Lewis, E.E., Palmiotti, G. and Taiwo, T.A. (2003), "A Finite Subelement Generalization of the Variational Nodal Method," *Nuclear Science and Engineering*., **144**, 36-46.

Stamm'ler, R.J.J. and Abbate, M.J. (1983), "Methods of Steady-State Reactor Physics in Nuclear Design," *Academic Press*, London.

Takeda, T. and Ikeda, H. (1991), "3-D Neutron Transport Benchmarks" *Nuclear Energy Agency*.

Villarino, E.A. and Stamm'ler, R.J.J. (1984), "The Heterogeneous Response Method in Slab Geometry," *Annals of Nuclear Energy*, **11**, 429-440.

Zhang, H., Rizwan-uddin, and Dorning, J.J. (1995), "Systematic Homogenization and Self-Consistent Flux and Pin Power Reconstruction for Nodal Diffusion Methods - I: Diffusion Equation-Based Theory," *Nuclear Science and Engineering*, **121**, 226-244.

Zhang, H., Rizwan-uddin, and Dorning, J.J. (1997), "Systematic Homogenization and Self-Consistent Flux and Pin Power Reconstruction for Nodal Diffusion Methods. Part II: Transport Equation Based Theory," *Transport Theory and Statistical Physics*, **26**, 433 468.

VITA

Benoit Forget was born in Canada in the city of North Bay, Ontario on June 13th, 1979 to Robert and Louise Forget. He grew up in the neighboring town of Temiscaming, Quebec with his parents and his older brother François. Benoit attended Gilbert-Theberge High School and graduated in 1996. He then moved to Montreal, Quebec to attend Ahuntsic College were he graduated from in 1998. Through a five-year program offered by Ecole Polytechnique de Montreal, he received in 2003 a Bachelors degree and a Master's degree in Chemical and Energy Engineering respectively. Upon graduation, Benoit moved to Atlanta, Georgia to pursue his Doctoral studies in Nuclear Engineering at the Georgia Institute of Technology.